The microbial impact on Fe & S cycling at oxic-anoxic interfaces: a single-cell view

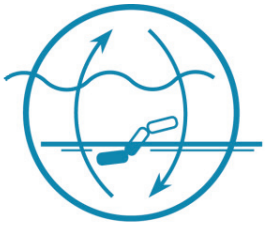

Dissertation

zur Erlangung des Doktorgrades der Naturwissenschaften

Dr. rer. nat.

Dem Fachbereich der Geowissenschaften der Universität Bremen vorgelegt von

Jasmine Berg

Bremen, September 2016

Universität Bremen

Die vorliegende Arbeit wurde in der Zeit vom Mai 2013 bis September 2016 am Max Planck Institut für Marine Mikrobiologie in Bremen angefertigt

Autor: **Jasmine Berg**
Universität Bremen
Max Planck Institut für Marine Mikrobiologie

Gutachter: **Prof. Dr. Marcel MM Kuypers**
Universität Bremen
Max Planck Institut für Marine Mikrobiologie

Zweitgutachter**: Prof Dr. Bo Barker Jørgensen**
Center for Geomicrobiology
Aarhus University

Abstract

At oxic-anoxic interfaces, competing biotic and abiotic reactions drive the rapid turnover of elements involved in biogeochemical cycles. As a result of the complexity of interactions between biological and chemical processes, the contribution of microorganisms to biogeochemical element cycling is still poorly constrained. Understanding the role of microorganisms at oxic-anoxic interfaces is important because they link the carbon cycle to other element cycles via carbon fixation and degradation using inorganic electron donors and acceptors, respectively. The aim of this thesis was to elucidate the microbial impact on the cycling of two of these elements – Fe and S – at oxic-anoxic interfaces. In combination with conventional analytical techniques in biogeochemistry, state-of-the-art single-cell instruments were used to investigate biogeochemical cycling on the level of single microbial cells, enabling novel insights into extremely rapid, even cryptic, microbial processes with transient intermediates.

This approach was first applied to laboratory cultures to investigate sulfur metabolism in large, colorless sulfur bacteria under controlled laboratory conditions. Confocal Raman spectroscopy of living *Beggiatoa* sp. cells revealed that the chemical nature of stored zero valent sulfur reflects the physiological state of the bacteria. Zero-valent sulfur was present in the form of both cyclooctasulfur rings (S_8) and inorganic polysulfide chains (S_x^{2-}), the latter appearing to serve as intermediates during both the accumulation and the breakdown of sulfur storage globules.

In the environment, the factors controlling the speciation of iron and sulfur were investigated in Lake Cadagno, a stratified lake in Switzerland. Despite low, 1-2 $\mu mol \cdot l^{-1}$ iron concentrations, significant rates of microbially-driven iron turnover were measured within the chemocline. The oxidation of iron by anoxygenic phototrophic bacteria could potentially contribute to up to 10% of primary production in this anoxic zone. The coupling of iron oxidation to iron reduction by heterotrophic bacteria generated a closed, “cryptic” iron cycle. These results suggest that rapid microbial redox cycling of iron may thus far have been overlooked in shallow, low-iron redoxclines which are globally widespread.

Although sulfur cycling in Lake Cadagno has already been extensively studied, our high resolution time profiles combined with single-cell analyses revealed surprising insights into the metabolism of the sulfide oxidizing bacteria there. Anoxygenic phototrophic purple sulfur bacteria were actually highly active in the dark and respired sulfur aerobically under both light and dark conditions. To bridge spatially separated gradients of electron donors and acceptors, these bacteria utilized a novel mechanism of storage and transport that is not yet fully understood. Because we could not completely close the sulfur budget in the Lake Cadagno chemocline, the existence of yet-unknown sulfide oxidation mechanisms could not be excluded, presenting exciting possibilities for future research.

In the course of these studies, the challenge of linking microbial identity with function using non-fluorescent-based, single-cell instruments led to the development of a new method (silver-DISH) for the targeted identification of environmental bacteria with nanometer secondary ion mass spectrometry (nanoSIMS), scanning electron microscopy energy-dispersive X-ray

spectroscopy (SEM-EDS), and confocal Raman spectroscopy. This technique may be extremely useful for future environmental microbiology studies, especially for correlative imaging.

Microorganisms evidently play an important role in biogeochemical cycling at oxic-anoxic interfaces in spite of competition with spontaneous chemical reactions. Overall, the results presented in this thesis may help to constrain and quantify the impact of microbes on carbon fixation and degradation processes in such environments.

Zusammenfassung

An oxisch-anoxischen Grenzschichten führen konkurrierende abiotische und biotische Reaktionen zur raschen und kontinuierlichen Umwandlung von Elementen, die in biogeochemischen Kreisläufen involviert sind. Die Wechselwirkung zwischen diesen biotischen und abiotischen Vorgängen ist komplex, weshalb der Beitrag, den Mikroorganismen in diesen biogeochemischen Stoffkreisläufen leisten, oft nur unzulänglich erfasst ist. Ein umfassendes Verständnis des Beitrags von Mikroorganismen in biogeochemischen Kreisläufen ist allerdings essentiell, da Mikroorganismen durch ihren Metabolismus einen Schnittpunkt zwischen Kohlenstoffkreislauf und anderen Stoffkreisläufen darstellen, indem sie Kohlenstoffeinbau und -abbau an die Oxidation bzw. Reduktion anorganischer Elektronendonatoren bzw. –akzeptoren koppeln. Das Ziel der vorgelegten Dissertation war es aufzuklären inwieweit Mikroorganismen den Stoffkreislauf zweier dieser Elemente, nämlich Eisen (Fe) und Schwefel (S), an oxisch-anoxischen Grenzschichten beeinflussen. Im Rahmen dieser Dissertation wurde eine Kombination aus konventionellen analytischen Methoden der Biogeochemie und hochmodernen Techniken zur Untersuchung auf Einzelzellebene angewandt um anhand einzelner Zellen biogeochemische Stoffumwandlungen zu untersuchen. Dies hat neue Einblicke in extrem schnelle und teils kryptische mikrobielle Vorgänge mit kurzlebigen Zwischenprodukten ermöglicht.

Die Methodik, die im Rahmen dieser Doktorarbeit angewandt wurde, wurde zuerst an Kulturen getestet, um den Schwefel-Metabolismus von nicht-phototrophen (“farblosen”) Schwefelbakterien unter kontrollierten Laborbedingungen zu untersuchen. Mithilfe konfokaler

Raman Spektroskopie wurde an lebenden Zellen der Gattung *Beggiatoa* gezeigt, dass die chemische Zusammensetzung des intrazellulär gespeicherten nullwertigen Schwefels den physiologischen Zustand der Bakterien wiederspiegelt. Dieser nullwertige Schwefel lag sowohl als Cyclooctaschwefel (S_8) als auch als anorganische Polysulfidketten (S_x^{2-}) vor, wobei letztere als Zwischenprodukt im Auf- und Abbau von intrazellulären Schwefelkügelchen zu dienen scheinen.

Um die chemischen Umwandlungen von Fe und S auch in der Umwelt besser zu verstehen, wurde der Schweizer Cadagnosee, ein ständig stratifizierter See, untersucht. Trotz der vorgefundenen niedrigen Eisenkonzentration von 1-2 µmol/l, konnten in der Chemokline signifikante mikrobiell-gesteuerte Eisen-Umsatzraten nachgewiesen werden. Die Ergebnisse dieser Dissertation zeigen, dass die Eisenoxidation durch anoxygene phototrophe Bakterien bis zu 10 % der Primärproduktion in der anoxischen Zone des Sees ausmachen kann. Die enge Kopplung von Eisenoxidation und -reduktion durch heterotrophe Bakterien führte zu einem geschlossenen, “kryptischen” Eisenkreislauf. Diese Ergebnisse zeigen auf, dass die von Mikroorganismen katalysierte Umwandlung der Redox-Zustände von Eisen in flachen Chemoklinen mit niedrigem Eisengehalt, welche global weitverbreitet sind, von großer Bedeutung sein können, obwohl sie bislang kaum Beachtung erhielten.

Obwohl der Schwefelkreislauf im Cadagnosee bereits in früheren Studien untersucht wurde, ermöglichten hochauflösende Zeitprofile in Kombination mit Einzelzellanalysen neue Einblicke in den Metabolismus von Sulfid-oxidierenden Bakterien. Überraschenderweise waren anoxygene phototrophe Schwefelpurpurbakterien auch im Dunklen hochaktiv und veratmeten Schwefel aerob sowohl unter Licht- als auch Dunkelbedingungen. Um die räumlich getrennten Gradienten von Elektronendonatoren und -akzeptoren zu überbrücken, setzen diese Bakterien einen

neuartigen Mechanismus von Einbau und Transport ein, welcher jedoch noch nicht restlos aufgeklärt werden konnte. Da wir die Schwefelbilanz der Chemokline des Cadagnosees durch unsere Untersuchungen nicht gänzlich aufklären konnten, kann ein bislang unbekannter Mechanismus der Sulfidoxidation nicht ausgeschlossen werden, was spannende Möglichkeiten für zukünftige Forschung darstellt.

Abgesehen von Fluoreszenz-basierten Einzelzell-Methoden gibt es kaum Möglichkeiten, mikrobielle Identität direkt mit ihrer Funktion in der Umwelt zu verbinden. Im Laufe dieser Dissertation entwickelten wir eine neue Methode (silver-DISH), welche die gezielte Identifikation von Organismen in der Umwelt durch den Einsatz von Nanometer Sekundärionen-Massenspektrometrie (nanoSIMS), Rasterelektronenmikroskopie-Energiedispersive Röntgenspektroskopie (SEM-EDS) und konfokaler Raman-Spektroskopie erlaubt. Diese Technik wird bei zukünftigen Untersuchungen von Mikroorganismen in der Umwelt äußerst hilfreich sein, besonders in Hinsicht auf korrelative Bildgebung.

Die Ergebnisse dieser Dissertation belegen und quantifizieren den Einfluss von Mikroorganismen auf den Kohlenstoff-, Eisen- und Schwefelkreislauf in oxisch-anoxischen Grenzschichten und zeigen, dass Mikroorganismen, obwohl sie mit spontanen chemischen Reaktionen konkurrieren, in biogeochemischen Kreisläufen an oxisch-anoxischen Grenzschichten nichtsdestotrotz eine äußerst wichtige Rolle spielen.

Table of Contents

INTRODUCTION

1.1.1 *Biogeochemical cycling and the redox tower of electron acceptors*

Up to half of the yearly global primary production is performed by microorganisms fixing CO_2 and consuming nutrients in the illuminated surface ocean (Field et al., 1998). The majority of this newly produced organic matter is then degraded by microorganisms as it sinks through the water column and after it is buried in sediments, recycling essential nutrients and trace elements. Organic matter is preferentially respired with molecular oxygen (O_2), followed by a host of alternative terminal electron acceptors after O_2 depletion. In diffusion-limited environments such as muddy sediments, a vertical chemical zonation of these electron acceptors is generally observed in the same recurring sequence (Fig 1). This stratification reflects the microbial consumption of electron acceptors in order of decreasing energy yield (Froelich et al., 1979; Emerson et al., 1980).

The dogma that a thermodynamic hierarchy can be used to predict respiratory pathways has been increasingly challenged in recent years. A growing number of exceptions to this rule have been observed in nature such as aerobic denitrification (Gao et al., 2010), aerobic sulfate reduction (Canfield and Des Marais, 1991) and iron cycling driven by sulfate reduction (Hansel et al., 2015b). Some of these processes are difficult to detect because reaction products are consumed as rapidly as they are produced. For example, (Canfield et al., 2010) proposed the existence of a cryptic sulfur cycle in the suboxic surface ocean, where the tight coupling of sulfate reduction and sulfur oxidation processes makes transient reaction intermediates

undetectable. Instead, cryptic sulfur cycling was inferred from metagenomic libraries containing a prevalence of genes for sulfide oxidation and sulfate reduction (Canfield et al., 2010).

The degradation of organic matter by microorganisms is not the only important process linking the carbon cycle to other element cycles. Autotrophic organisms can also harness redox reactions between different inorganic electron donors and acceptors to drive CO_2 assimilation into biomass. In redox transition zones, microbes compete with many spontaneous abiotic reactions (Fig 1), making it difficult to disentangle the microbial from the abiotic contribution to

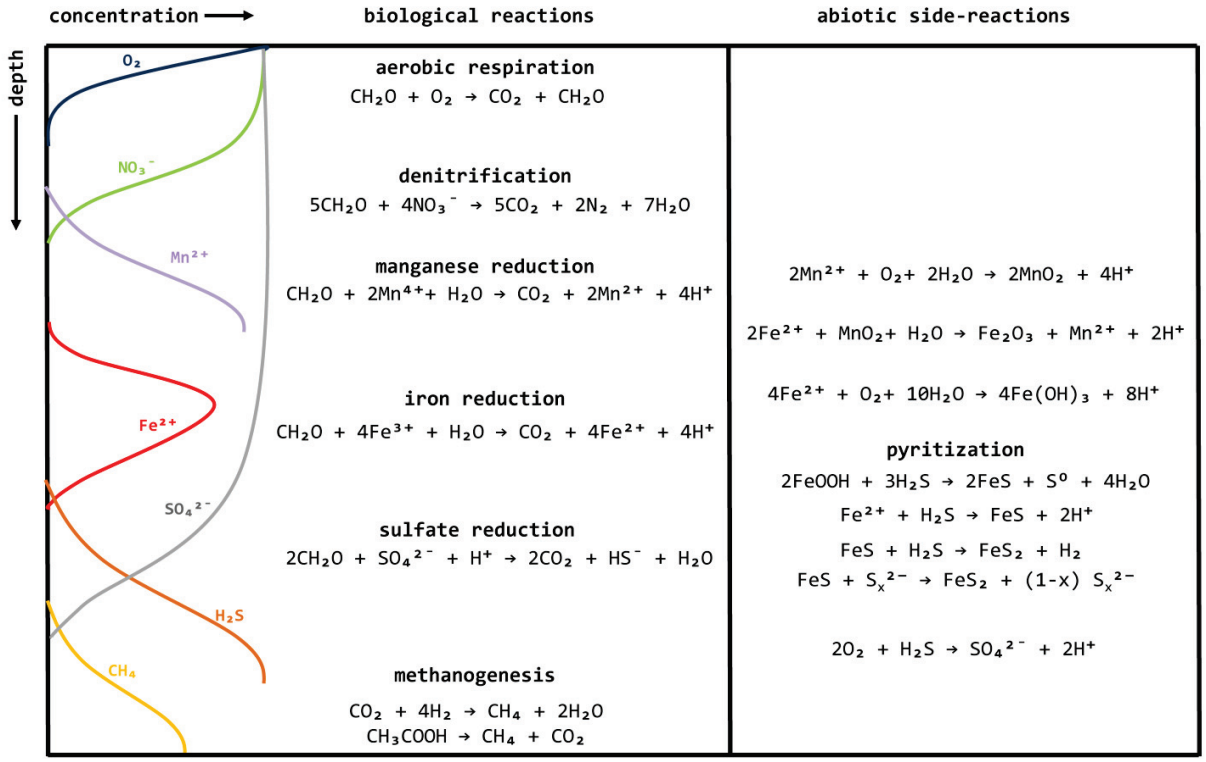

Figure 1: Schematic representation of the succession of terminal electron accepting pathways in marine sediment (modified from Millero and Sohn, 1996). Aerobic respiration of organic matter yields the most energy, followed by denitrification, manganese and iron reduction, sulfate reduction, and finally methanogenesis. The corresponding biological reactions are shown next to the concentrations of dissolved oxidants/reductants. Organic matter is simplified with the general formula “CH2O”.

redox element cycling. Intense biogeochemical cycling occurs at oxic-anoxic interfaces where intersecting gradients of oxidants and reductants, and in some cases sunlight, fuel high microbial activity and abiotic reaction rates. In particular, the abiotic oxidation of ferrous iron (Fe^{2+}) and reduced sulfur (S^{-II} as H_2S, HS^-, and S_x^{2-}) with O_2 in circumneutral environments proceeds on the order of minutes to hours (Morgan and Lahav, 2007; Buisman et al., 1990) and abiotic reduction of ferric iron (Fe^{3+}) with HS^- is almost instantaneous (Pyzik and Sommer, 1981). Microorganisms also influence the cycling of these elements, but dynamics of these biotic and abiotic redox processes is much more complicated and variable than originally imagined. More recent studies have highlighted the role of reactive intermediates, of both chemical and biological origin, linking these element cycles (reviewed in Hansel et al., 2015a). However, studying these short-lived intermediates of generally low concentration in a sea of less reactive Fe and S species is a challenge. In this thesis, state-of-the-art single-cell methods were used to investigate the microbial impact on both Fe and S cycling and the coupling of these intricately linked cycles via transient intermediates.

1.1.2 *Iron biogeochemistry*

Iron is the fourth most abundant element in the Earth's crust, but in large parts of the open ocean, dissolved Fe is depleted due to its low solubility and short supply – mainly from atmospheric dust deposition and hydrothermal activity (Mahowald et al., 2005; Tagliabue et al., 2010). The restricted availability of iron in the open ocean limits the growth of phytoplankton and other microorganisms (Martin, 1992; Moore et al., 2001). In these regions called High Nutrient Low Chlorophyll (HNLC) zones, iron concentrations are in the pico- to nanomolar range (Nolting et al., 1998).

The scarcity of iron in the oceans is related to its extremely low solubility in oxygenated seawater. Iron principally exists in two oxidation states in the marine environment, Fe^{2+} and Fe^{3+}, and its speciation is governed by physicochemical parameters including pH, oxygen concentration and redox potential (Stumm and Morgan, 1996). In seawater, iron is mainly present in the form of Fe^{3+}, whose determined solubility (as ferric hydroxide) is as low as 0.01 $nmol \cdot l^{-1}$ (Liu and Millero, 2002). Nevertheless, complexation by organic ligands such as siderophores or humic substances helps to maintain more Fe^{3+} in solution than would be expected (e.g. Rue and Bruland, 1995). Fe^{2+} is much more soluble than Fe^{3+} and thus the most biologically available form of iron, but it can be rapidly and spontaneously oxidized by O_2 at a rate dependent on temperature, pH, and dissolved O_2 and Fe^{2+} concentrations. Under surface ocean conditions, Fe^{2+} is oxidized almost instantaneously (Millero et al., 1987), but under

Abiotic reactions	Biotic reactions
oxygen $4Fe^{2+} + O_2 + 6H_2O \rightarrow 4FeOOH + 8H^+$	**microaerophiles** $4Fe^{2+} + O_2 + 10H_2O \rightarrow 4Fe(OH)_3 + 8H^+$
light reactions $L\text{-}Fe^{3+} \xrightarrow{hv} L\text{-}Fe^{2+}$	**photoferrotrophs** $HCO_3^- + Fe^{2+} + 10H_2O \xrightarrow{hv} (CH_2O) + 4Fe(OH)_3 + 7H^+$
nitrogen species $4Fe^{2+} + 2NO_2^- + 5H_2O \rightarrow 4FeOOH + N_2O + 6H^+$	**Fe-oxidizing denitrifiers** $10Fe^{2+} + 2NO_3^- + 24H_2O \rightarrow 10Fe(OH)_3 + N_2 + 18H^+$ $6Fe^{2+} + 2NO_2^- + 14H_2O \rightarrow 6Fe(OH)_3 + N_2 + 10H^+$ $2Fe^{2+} + N_2O + 6H_2O \rightarrow 2Fe(OH)_3 + N_2 + 4H^+$
manganese oxides $2Fe^{2+} + MnO_2 + 2H_2O \rightarrow 2FeOOH + Mn^{2+} + 2H^+$	
humic acids $Fe^{3+} + HumAc^- \rightarrow HumAc + Fe^{2+}$ **reduced sulfur** $2FeO0H + 3H_2S \rightarrow 2FeS + S^0 + 4H_2O$	**Fe-reducers** $8FeO0H + CH_3COO^- + 15H^+ \rightarrow 8Fe^{2+} + 2HCO_3^- + 12H_2O$ $2FeO0H + H_2 \rightarrow 2Fe^{2+} + 4OH^-$

Figure 2: List of relevant abiotic and biotic reactions cycling iron. L-Fe = organically liganded iron. HumAc = humic acid.

microoxic conditions or at pH < 4, spontaneous oxidation of Fe^{2+} proceeds extremely slowly (Morgan and Lahav, 2007). Other environmentally relevant abiotic reactions of iron (Fig 2) include spontaneous reduction by sulfide and some organic acids (Szilagyi, 1971; Pyzik and Sommer, 1981) and oxidation by O_2 and manganese oxides or even nitrite at low pH (Chao and Kroontje, 1966; Postma, 1985; Morgan and Lahav, 2007).

Taxonomically, all of the microbes capable of cycling iron are extremely diverse, distributed across the Archaeal and Bacterial branches of the phylogenetic tree (Fig 3). This reflects their

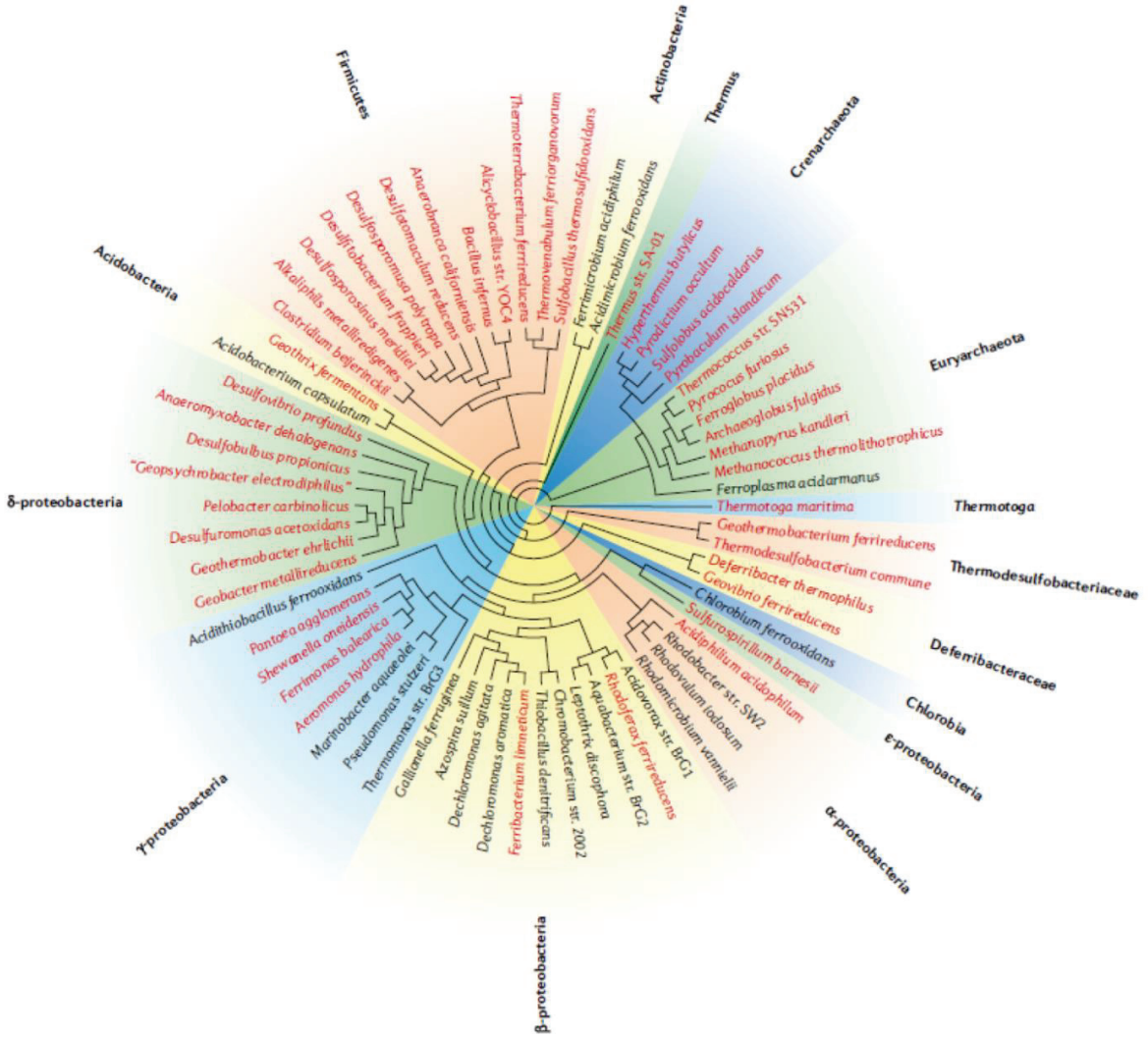

Figure 3: A phylogenetic tree showing the diversity of iron oxidizing microorganisms in black and iron reducing microorganisms in red (from Weber et al., 2006).

long evolutionary history, as microbial iron oxidation/reduction processes are considered some of the most ancient metabolisms on Earth (Emerson et al., 2010). Time has allowed for the diversification of microbial iron-utilizing metabolisms and the colonization of a wide variety of environments, ranging from brackish ponds to highly acidic hot springs (e.g. Johnson et al., 2003; Straub et al., 2005). It is this lack of any specific phylogenetic affiliation, and the absence of any known iron oxidation or reduction genes, that makes the identification of iron oxidizers and reducers in the environment a challenge.

Many microorganisms can also harness the oxidation and reduction of iron for energy gain (Fig 2). Microbial iron oxidation can be coupled to O_2, NO_3^-, NO_2^-, and N_2O reduction (Straub et al., 1996; Emerson and Moyer, 1997; Benz et al., 1998). Some well-studied iron-oxidizing microaerophiles include *Gallionella* spp. (Hanert, 2006), *Siderooxydans* spp. (Weiss et al., 2007) and *Leptothrix* spp. (Van Veen et al., 1978), whereas denitrifying iron reducers include *Thiobacillus denitrificans* (Straub et al., 1996) and *Acidovorax* spp. (Byrne-Bailey et al., 2010; Pantke et al., 2012) Fe^{2+} can also be utilized instead of H_2O as the electron source during photosynthetic CO_2 reduction by some specialized anaerobic bacteria (Widdel et al., 1993). Thus far, a handful of so-called photoferrotrophs have been described: the green sulfur bacterium *Chlorobium ferrooxidans* (Heising et al., 1999), the purple sulfur bacterium *Thiodictyon* sp. (Croal et al., 2004), and several purple non-sulfur bacteria (e.g. (Ehrenreich and Widdel, 1994; Straub et al., 1999). Certain microorganisms can also utilize simple organic compounds or H_2 to reduce iron (Lovley and Phillips, 1986). These microorganisms must overcome the challenge of transferring electrons to solid ferric iron, a mechanism which has been well-studied among

several species of *Geobacter, Shewanella,* and *Geothrix* (Lovley et al., 1993; Myers and Myers, 1994; Coates et al., 1999).

The activity of these iron-metabolizing microorganisms has been reported to play an important role in biogeochemical cycling. This is because iron redox reactions involve the transfer of a single electron, and large amounts of iron must be oxidized or reduced to generate sufficient energy for microbial growth. Significant microbial iron cycling is therefore expected to occur where substantial pools of iron are available. In sediments, for example, large amounts of iron oxide fuel microbial organic matter degradation processes (e.g. Canfield et al., 1993; Thamdrup et al., 1994). In some sediments, especially in freshwater systems, iron reduction accounts for more of the total anaerobic carbon respiration than manganese or sulfate reduction (Canfield et al., 1993). Iron may be intensively recycled at sediment redox transition zones because of iron re-oxidation which is especially stimulated by bioturbation and bioirrigation (Thamdrup et al., 1994; Thamdrup, 2000). The importance of microbial iron cycling has also been demonstrated in ferruginous lakes such as Lake Matano, Indonesia and Lake La Cruz, Spain where hundreds of micromolar of dissolved Fe^{2+} sustain large populations of photoferrotrophic bacteria in the anoxic bottom waters (Crowe et al., 2008; Walter et al., 2014). Most natural waters actually contain comparably low concentrations of reactive iron, but microbial iron cycling has largely been ignored in stratified aquatic environments with low iron concentrations, such as anoxic lakes and basins, which are globally widespread.

1.1.3 Sulfur biogeochemistry

Sulfur is an extremely versatile element, existing in a total of 8 oxidation states from -2 to +6. The biogeochemical sulfur cycle is therefore extremely complex. The most reduced form of

sulfur is sulfide, which can take the form of gaseous H_2S or sulfide minerals (e.g. FeS_2, PbS, ZnS). The most oxidized form of sulfur is sulfate (SO_4^{2-}), a major ion in the world's oceans and also a major component of ocean sediments in the form of barite ($BaSO_4$) or gypsum ($CaSO_4 \cdot H_2O$) (Sievert et al., 2007). Sulfur exists in many intermediate states including zero-valent sulfur (S^0), of which more than 30 allotropes have been described (Meyer, 1964). These S^0 species include the most stable and hydrophobic species, cyclooctasulfur (S_8) as well as highly reactive hydrophilic polysulfide chains (S^{x-}) and polythionates ($S_xO_6^{2-}$) among others. Reduced sulfur species other than S_8 are extremely reactive, and O_2, iron oxide and manganese oxide may rapidly oxidize them under various pH- and redox conditions (Chen and Morris, 1972; Druschel et al., 2003; Kleinjan et al., 2005). Measuring some of these reduced sulfur species can therefore be extremely challenging.

The complexity of sulfur chemistry is reflected in the biological pathways that have evolved to utilize it (Fig 4). Sulfur disproportionation is the inorganic fermentation of S^0, thiosulfate ($S_2O_3^{2-}$), sulfite (SO_3^{2-}), or tetrathionate ($S_4O_6^{2-}$), where a single sulfur compound simultaneously serves as the electron acceptor and donor for microbial energy generation (Bak and Cypionka, 1987; Bak and Pfennig, 1987). Disproportionation is especially relevant to the sulfur cycle in sediments containing sulfide scavengers such as iron or manganese because it was

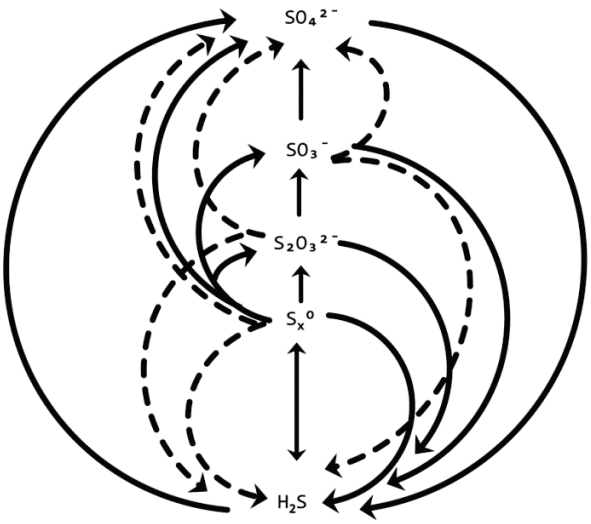

Figure 4: A comprehensive overview of the biogeochemical sulfur cycle. Dashed lines represent disproportionation reactions (adapted from Zopfi et

believed for a long time to be thermodynamically inhibited by high sulfide concentrations (Thamdrup et al., 1993) although recent evidence suggests this is not necessarily true (Milucka et al., 2012). Sulfate reduction is performed for assimilatory purposes by many prokaryotes and plants during the biosynthesis of organic sulfur compounds (Takahashi et al., 2011). Anaerobic, mostly heterotrophic bacteria principally affiliated with the *Deltaproteobacteria* perform dissimilatory sulfate reduction utilizing the Dsr pathway, releasing sulfide as an end product (Rabus et al., 2013). The oxidative side of the biological sulfur cycle is driven by both phototrophic and chemotrophic microorganisms using O_2 or NO_x^- (nitrate and nitrite). The sulfide oxidizing microbes are diverse and belong to the *Alphaproteobacteria, Betaproteobacteria*, *Gammaproteobacteria*, *Epsilonproteo-bacteria, Aquaficales, Chlorobiaceae*, and Archaea (reviewed in (Dahl et al., 2008)).

On a biochemical level, sulfur undergoes many complex transformations via transient intermediates. Several major sulfur oxidation pathways have been described for bacteria, of which three major ones are mentioned here. The canonical Sox pathway of sulfur oxidation (Fig 5) is the most widely distributed across the bacteria and encodes Sox proteins that form a closed reaction cycle (Dahl et al., 2008). The Sox enzyme system has been shown to oxidize not only thiosulfate but also reduced sulfur species such as sulfide, elemental sulfur, sulfite, and tetrathionate, which can be fed into the pathway at appropriate intermediate stages (Dahl et al., 2008). Some organisms possess only a partial Sox pathway, and it has been observed that the lack of a *soxCD* gene is correlated with the obligate production of S^0 storage granules either intra- or extracellularly (Friedrich et al., 2005). The form in which this sulfur is stored has been a matter of long-standing debate and has important implications for the utilization of this storage

Figure 5: Two of the major enzymatic pathways of microbial sulfur oxidation (based on Friedrich et al., 2000; Friedrich et al., 2001; Frigaard and Dahl, 2008). (top) The complete sox pathway as described in *Paracoccus pantotrophus*) which contains the entire set of sox enzyme genes. (bottom) The reverse Dsr pathway composed of dissimilatory sulfite reductase *dsr*, APS reductase *apr*, and sulfate adenylyltransferase/ATP sulfurylase *sat*.

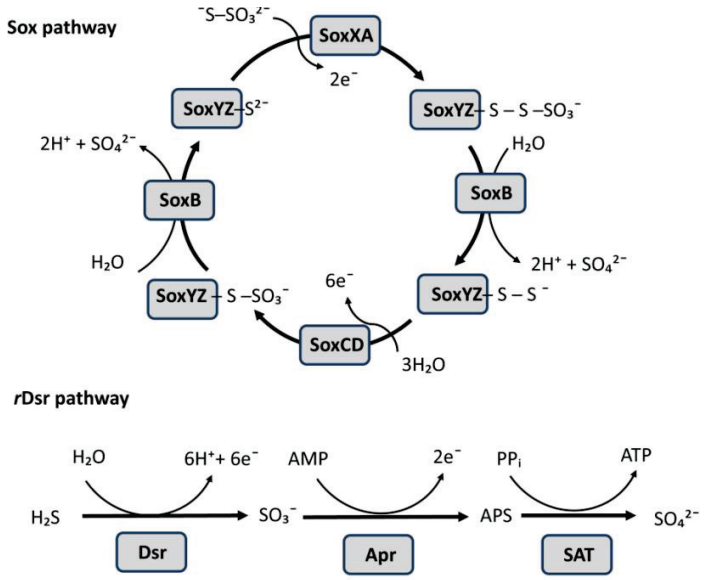

compound by biological enzymes. Bacteria can further oxidize this stored sulfur via the *r*Dsr pathway (Fig 5) which proceeds in reverse of the Dsr sulfate reduction pathway. Many acidophilic bacteria oxidize thiosulfate via the tetrathionate intermediate (S_4I) pathway which involves the intermediate formation of tetrathionate, a much more stable intermediate under acidic conditions (Trudinger, 1964). The end products are sulfate and disulfane monosulfonic acid ($HS_2SO_3^-$), a highly reactive compound which immediately decomposes leading to the formation of elemental sulfur and sulfite (Kelly et al., 1997). In these biological reactions involving sulfur, the speciation of sulfur is evidently governed by both biotic and abiotic mechanisms. Characterizing the sulfur intermediates in these pathways is key to understanding the biochemistry of sulfur.

These sulfur oxidation pathways confer extreme metabolic flexibility to the sulfur bacteria. A single species, i.e. *Allochromatium vinosum* can often grow on a multitude of sulfur substrates H_2S, S^0, SO_3^- and $S_2O_3^-$ (Hensen et al., 2006; Dahl et al., 2013). Moreover, like many other purple bacteria, *Allochromatium* can switch to chemolithotrophic respiration with O_2 as an electron acceptor in the dark (Kämpf and Pfennig, 1986; Imhoff et al., 1998). Even anaerobic sulfate-

reducing bacteria have been reported to utilize various sulfur compounds for microaerophilic respiration (Dannenberg et al., 1992).

On a global scale, sulfur-utilizing microorganisms cycle sulfur between the large pool of sulfate in the oceans and reduced sulfur bound in pyrite, thus contributing to the redox balance of the ocean and atmosphere. Sulfate reduction is the dominant anaerobic carbon degradation process in marine sediments (Jørgensen, 1982), but only about 10-20% of the sulfide produced is buried as metal sulfides, i.e. pyrite (Ferdelman et al., 1999). The remaining fraction is recycled abiotically by reaction with iron oxide, manganese oxide, and O_2, or biotically by sulfide-oxidizing microorganisms. Sulfide-oxidizing microbes are responsible for much of the sulfide detoxification in oxygen minimum zones, sulfidic sediments, and euxinic lakes and marine basins (Jørgensen et al., 1991; Kühl and Jørgensen, 1992; Overmann, 1997; Lavik et al., 2009). However, our understanding of the microbial sulfur cycle is far from complete, as recent evidence suggests that alternative electron acceptors and sulfide oxidation pathways remain to be discovered. Already the discovery of cable bacteria transferring electrons along filaments or "nanowires" over centimeter distances has helped to resolve the question of how oxygen consumption can be coupled to sulfide oxidation in deeper, anoxic sediment layers (Pfeffer et al., 2012). Some observations of sulfide oxidation and carbon fixation in stratified environments such as the Chesapeake Bay (Findlay et al., 2015), the Black Sea (Jørgensen et al., 1991), and Lake Cadagno (Musat et al., 2008; Halm et al., 2009), can still not be explain explained by any known oxidation processes. Elucidating these unexplained dark sulfur and carbon cycling mechanisms is essential to closing the global S budget and understanding the impact of S on other biogeochemical cycles.

1.1.4 Coupling of the Fe & S cycles

The biogeochemical sulfur cycle is inextricably linked to the iron cycle via reaction with sulfide produced by sulfate reducing bacteria (Fig 1). Sulfide can reduce Fe^{3+} minerals generating S^0, $S_2O_3^{2-}$, Fe^{2+}, and FeS, and also reacts with Fe^{2+} forming FeS and FeS_2 (Pyzik and Sommer, 1981). The reduction of iron with sulfide may be the major pathway for dissolution of iron oxides in sulfidic sediments and euxinic basins (Canfield, 1989; Kostka and Luther III, 1995; Krom et al., 2002). Sulfur cycling is even postulated to drive iron cycling in low-sulfate freshwater environments (Hansel et al., 2015b). Iron monosulfide (FeS) is a precursor to pyrite (FeS_2) which is the major end product of sulfate reduction and an important sink for both iron and sulfide (Berner, 1970, 1984). Pyrite formation is generally controlled by the availability of organic matter in marine sediments, and sulfate availability in freshwater sediments, but reactive iron becomes limiting in euxinic systems (Berner, 1984). Current conceptual models emphasize the removal of Fe and S via pyritization on geological timescales, but FeS could also be recycled by oxidative processes bypassing the burial of insoluble minerals. Unlike pyrite which is extremely insoluble and very slowly oxidized (Fowler et al., 2001), FeS is a highly reactive and bioavailable compound oxidized by chemotrophic and anoxygenic phototrophic microorganisms (e.g. Kappler and Newman, 2004; Senko et al., 2005).

1.2 OUTLINE AND OBJECTIVES

A combination of abiotic and biotic redox reactions cycle Fe and S at oxic-anoxic interfaces, but the dynamics of these competing reactions are still unknown. Evaluating which reactions are dominant under different environmental conditions is key to understanding the network of reactions within the biogeochemical Fe and S cycles. The aim of this thesis was to combine conventional chemical analyses with various state-of-the-art single-cell imaging techniques to elucidate the microbial role in Fe and S cycling. The application of single-cell methods allowed us not only to gain new insights into biogeochemical processes that are often overlooked by bulk analytical methods but also to identify the bacteria responsible for them.

We first applied single-cell analyses to bacteria in culture to investigate microbial sulfur cycling under controlled conditions. Many sulfide-oxidizing bacteria store S^0 sulfur as an obligate intermediate during the oxidation of reduced sulfur to sulfate. Because most of these S^0 species are unstable, the form in which this sulfur is stored is still a matter of debate. In **chapter 1**, confocal Raman spectroscopy was used to investigate the speciation of stored sulfur in cultures of *Beggiatoa* sp. under regulated physiological conditions. Characterizing this stored sulfur could provide key insights into the biochemistry of sulfur bacteria.

To investigate Fe and S cycling at oxic-anoxic interfaces in the environment, we selected Lake Cadagno as a model stratified system with measureable (1-2 $\mu mol \cdot l^{-1}$) Fe and high (1-2 $mmol \cdot l^{-1}$) sulfate concentrations. Microbial Fe cycling has largely been ignored in such waters where low Fe concentrations imply low Fe cycling activity. Furthermore, it has recently been suggested that contrary to our thermodynamic predictions, Fe reduction is driven by S cycling as long as sulfate is present (Hansel et al., 2015b). In **chapter 2** we addressed this assumption and revealed that

intensive microbial Fe cycling may occur despite low Fe concentrations. We attempted to disentangle the microbial from the abiotic processes cycling iron to show that microbial iron cycling could substantially impact both carbon fixation and respiration in this high sulfate environment.

The sulfur cycle in Lake Cadagno has been comparatively well described. Sulfate reducers in the anoxic sediments and monolimnion produce large amounts of sulfide which diffuse upwards in the water column. Anoxygenic phototrophs at the oxycline are responsible for most of the sulfide removal before it reaches oxic, overlying waters. However, it is not known how sulfide and carbon in this environment are cycled in the dark. Our understanding of the ecophysiology of anoxygenic phototrophs comes mostly from laboratory cultures, but bacteria may utilize different survival mechanisms in culture than in highly dynamic environments. In **chapter 3** we show that the ecophysiology of purple sulfur bacteria *in situ* is much more complex than previously thought. We found that anoxygenic phototrophs may oxidize sulfide with oxygen in the dark by actively transporting an unknown intermediate between sulfide and oxygen gradients.

Our investigations using single-cell techniques enabled surprising insights into the ecophysiology of uncultured bacteria. They also highlight the need for new methods of phylogenetic identification compatible with these emerging technologies. In **chapter 4** we developed a method for microbial identification compatible with nanoSIMS, SEM-EDS, and Raman spectroscopy. The potential of this labeling method for environmental microbiological applications was demonstrated by targeting the large purple sulfur bacteria *Chromatium* sp. in a

complex environmental sample. This method is promising for the analysis of intracellular compounds via cell-specific SERS enhancement.

REFERENCES

Bak, F., and Pfennig, N. (1987) Chemolithotrophic growth of Desulfovibrio sulfodismutans sp. nov. by disproportionation of inorganic sulfur compounds. *Archives of Microbiology* **147**: 184-189.

Bak, F., and Cypionka, H. (1987) A novel type of energy metabolism involving fermentation of inorganic sulphur compounds. *Nature* **326**: 891-892.

Benz, M., Brune, A., and Schink, B. (1998) Anaerobic and aerobic oxidation of ferrous iron at neutral pH by chemoheterotrophic nitrate-reducing bacteria. *Archives of Microbiology* **169**: 159-165.

Berner, R.A. (1970) Sedimentary pyrite formation. *American Journal of Science* **268**: 1-23.

Berner, R.A. (1984) Sedimentary pyrite formation: an update. *Geochimica et Cosmochimica Acta* **48**: 605-615.

Buisman, C., Uspeert, P., Janssen, A., and Lettinga, G. (1990) Kinetics of chemical and biological sulphide oxidation in aqueous solutions. *Water Research* **24**: 667-671.

Byrne-Bailey, K.G., Weber, K.A., Bose, S., Knox, T., Spanbauer, T.L., Chertkov, O., and Coates, J.D. (2010) Completed genome sequence of the anaerobic iron-oxidizing bacterium Acidovorax ebreus strain TPSY. *Journal of Bacteriology* **192**: 1475-1476.

Canfield, D.E. (1989) Reactive iron in marine sediments. *Geochimica et Cosmochimica Acta* **53**: 619-632.

Canfield, D.E., and Des Marais, D.J. (1991) Aerobic sulfate reduction in microbial mats. *Science* **251**: 1471-1473.

Canfield, D.E., Thamdrup, B., and Hansen, J.W. (1993) The anaerobic degradation of organic matter in Danish coastal sediments: iron reduction, manganese reduction, and sulfate reduction. *Geochimica et Cosmochimica Acta* **57**: 3867-3883.

Canfield, D.E., Stewart, F.J., Thamdrup, B., De Brabandere, L., Dalsgaard, T., Delong, E.F. et al. (2010) A cryptic sulfur cycle in oxygen-minimum–zone waters off the Chilean coast. *Science* **330**: 1375-1378.

Chao, T.-T., and Kroontje, W. (1966) Inorganic nitrogen transformations through the oxidation and reduction of iron. *Soil Science Society of America Journal* **30**: 193-196.

Chen, K.Y., and Morris, J.C. (1972) Kinetics of oxidation of aqueous sulfide by oxygen. *Environmental Science & Technology* **6**: 529-537.

Coates, J.D., Ellis, D.J., Gaw, C.V., and Lovley, D.R. (1999) Geothrix fermentans gen. nov., sp. nov., a novel Fe (III)-reducing bacterium from a hydrocarbon-contaminated aquifer. *International Journal of Systematic and Evolutionary Microbiology* **49**: 1615-1622.

Croal, L.R., Johnson, C.M., Beard, B.L., and Newman, D.K. (2004) Iron isotope fractionation by Fe (II)-oxidizing photoautotrophic bacteria. *Geochimica et Cosmochimica Acta* **68**: 1227-1242.

Crowe, S.A., Jones, C., Katsev, S., Magen, C., O'Neill, A.H., Sturm, A. et al. (2008) Photoferrotrophs thrive in an Archean Ocean analogue. *Proceedings of the National Academy of Sciences* **105**: 15938-15943.

Dahl, C., Friedrich, C., and Kletzin, A. (2008) Sulfur oxidation in prokaryotes. *eLS*.

Dahl, C., Franz, B., Hensen, D., Kesselheim, A., and Zigann, R. (2013) Sulfite oxidation in the purple sulfur bacterium Allochromatium vinosum: identification of SoeABC as a major player and relevance of SoxYZ in the process. *Microbiology* **159**: 2626-2638.

Dannenberg, S., Kroder, M., Dilling, W., and Cypionka, H. (1992) Oxidation of H2, organic compounds and inorganic sulfur compounds coupled to reduction of O2 or nitrate by sulfate-reducing bacteria. *Archives of Microbiology* **158**: 93-99.

Druschel, G.K., Hamers, R.J., and Banfield, J.F. (2003) Kinetics and mechanism of polythionate oxidation to sulfate at low pH by O 2 and Fe 3+. *Geochimica et Cosmochimica Acta* **67**: 4457-4469.

Ehrenreich, A., and Widdel, F. (1994) Anaerobic oxidation of ferrous iron by purple bacteria, a new type of phototrophic metabolism. *Applied and Environmental Microbiology* **60**: 4517-4526.

Emerson, D., and Moyer, C. (1997) Isolation and characterization of novel iron-oxidizing bacteria that grow at circumneutral pH. *Applied and Environmental microbiology* **63**: 4784-4792.

Emerson, D., Fleming, E.J., and McBeth, J.M. (2010) Iron-oxidizing bacteria: an environmental and genomic perspective. *Annual Review of Microbiology* **64**: 561-583.

Emerson, S., Jahnke, R., Bender, M., Froelich, P., Klinkhammer, G., Bowser, C., and Setlock, G. (1980) Early diagenesis in sediments from the eastern equatorial Pacific, I. Pore water nutrient and carbonate results. *Earth and Planetary Science Letters* **49**: 57-80.

Ferdelman, T.G., Fossing, H., Neumann, K., and Schulz, H.D. (1999) Sulfate reduction in surface sediments of the southeast Atlantic continental margin between 15 38'S and 27 57'S (Angola and Namibia). *Limnology and Oceanography* **44**: 650-661.

Field, C.B., Behrenfeld, M.J., Randerson, J.T., and Falkowski, P. (1998) Primary production of the biosphere: integrating terrestrial and oceanic components. *Science* **281**: 237-240.

Findlay, A.J., Bennett, A.J., Hanson, T.E., and Luther, G.W. (2015) Light-dependent sulfide oxidation in the anoxic zone of the Chesapeake Bay can be explained by small populations of phototrophic bacteria. *Applied and Environmental Microbiology* **81**: 7560-7569.

Fowler, T., Holmes, P., and Crundwell, F. (2001) On the kinetics and mechanism of the dissolution of pyrite in the presence of Thiobacillus ferrooxidans. *Hydrometallurgy* **59**: 257-270.

Friedrich, C.G., Rother, D., Bardischewsky, F., Quentmeier, A., and Fischer, J. (2001) Oxidation of reduced inorganic sulfur compounds by bacteria: emergence of a common mechanism? *Applied and Environmental Microbiology* **67**: 2873-2882.

Friedrich, C.G., Bardischewsky, F., Rother, D., Quentmeier, A., and Fischer, J. (2005) Prokaryotic sulfur oxidation. *Current Opinion in Microbiology* **8**: 253-259.

Friedrich, C.G., Quentmeier, A., Bardischewsky, F., Rother, D., Kraft, R., Kostka, S., and Prinz, H. (2000) Novel genes coding for lithotrophic sulfur oxidation of Paracoccus pantotrophus GB17. *Journal of Bacteriology* **182**: 4677-4687.

Frigaard, N.-U., and Dahl, C. (2008) Sulfur metabolism in phototrophic sulfur bacteria. *Advances in Microbial Physiology* **54**: 103-200.

Froelich, P.N., Klinkhammer, G., Bender, M.a.a., Luedtke, N., Heath, G.R., Cullen, D. et al. (1979) Early oxidation of organic matter in pelagic sediments of the eastern equatorial Atlantic: suboxic diagenesis. *Geochimica et Cosmochimica Acta* **43**: 1075-1090.

Gao, H., Schreiber, F., Collins, G., Jensen, M.M., Kostka, J.E., Lavik, G. et al. (2010) Aerobic denitrification in permeable Wadden Sea sediments. *The ISME Journal* **4**: 417-426.

Halm, H., Musat, N., Lam, P., Langlois, R., Musat, F., Peduzzi, S. et al. (2009) Co-occurrence of denitrification and nitrogen fixation in a meromictic lake, Lake Cadagno (Switzerland). *Environmental Microbiology* **11**: 1945-1958.

Hanert, H.H. (2006) The genus Gallionella. In *The Prokaryotes*: Springer, pp. 990-995.

Hansel, C.M., Ferdelman, T.G., and Tebo, B.M. (2015a) Cryptic cross-linkages among biogeochemical cycles: novel insights from reactive intermediates. *Elements* **11**: 409-414.

Hansel, C.M., Lentini, C.J., Tang, Y., Johnston, D.T., Wankel, S.D., and Jardine, P.M. (2015b) Dominance of sulfur-fueled iron oxide reduction in low-sulfate freshwater sediments. *The ISME Journal* **9**: 2400-2412.

Heising, S., Richter, L., Ludwig, W., and Schink, B. (1999) Chlorobium ferrooxidans sp. nov., a phototrophic green sulfur bacterium that oxidizes ferrous iron in coculture with a “Geospirillum” sp. strain. *Archives of Microbiology* **172**: 116-124.

Hensen, D., Sperling, D., Trüper, H.G., Brune, D.C., and Dahl, C. (2006) Thiosulphate oxidation in the phototrophic sulphur bacterium Allochromatium vinosum. *Molecular Microbiology* **62**: 794-810.

Imhoff, J.F., Süling, J., and PETRI, R. (1998) Phylogenetic relationships among the Chromatiaceae, their taxonomic reclassification and description of the new genera Allochromatium, Halochromatium, Isochromatium, Marichromatium, Thiococcus, Thiohalocapsa and Thermochromatium. *International Journal of Systematic and Evolutionary Microbiology* **48**: 1129-1143.

Johnson, D.B., Okibe, N., and Roberto, F.F. (2003) Novel thermo-acidophilic bacteria isolated from geothermal sites in Yellowstone National Park: physiological and phylogenetic characteristics. *Archives of Microbiology* **180**: 60-68.

Jørgensen, B.B. (1982) Mineralization of organic matter in the sea bed-the role of sulphate reduction. *Nature* **296**: 643-645.

Jørgensen, B.B., Fossing, H., Wirsen, C.O., and Jannasch, H.W. (1991) Sulfide oxidation in the anoxic Black Sea chemocline. *Deep Sea Research Part A Oceanographic Research Papers* **38**: S1083-S1103.

Kämpf, C., and Pfennig, N. (1986) Chemoautotrophic growth of Thiocystis violacea, Chromatium gracile and C. vinosum in the dark at various O_2-concentrations. *Journal of basic microbiology* **26**: 517-531.

Kappler, A., and Newman, D.K. (2004) Formation of Fe (III)-minerals by Fe (II)-oxidizing photoautotrophic bacteria. *Geochimica et Cosmochimica Acta* **68**: 1217-1226.

Kelly, D.P., Shergill, J.K., Lu, W.-P., and Wood, A.P. (1997) Oxidative metabolism of inorganic sulfur compounds by bacteria. *Antonie Van Leeuwenhoek* **71**: 95-107.

Kleinjan, W.E., de Keizer, A., and Janssen, A.J. (2005) Kinetics of the chemical oxidation of polysulfide anions in aqueous solution. *Water Research* **39**: 4093-4100.

Kostka, J.E., and Luther III, G.W. (1995) Seasonal cycling of Fe in saltmarsh sediments. *Biogeochemistry* **29**: 159-181.

Krom, M.D., Mortimer, R.J., Poulton, S.W., Hayes, P., Davies, I.M., Davison, W., and Zhang, H. (2002) In-situ determination of dissolved iron production in recent marine sediments. *Aquatic Sciences* **64**: 282-291.

Kühl, M., and Jørgensen, B.B. (1992) Microsensor measurements of sulfate reduction and sulfide oxidation in compact microbial communities of aerobic biofilms. *Applied and Environmental Microbiology* **58**: 1164-1174.

Lavik, G., Stührmann, T., Brüchert, V., Van der Plas, A., Mohrholz, V., Lam, P. et al. (2009) Detoxification of sulphidic African shelf waters by blooming chemolithotrophs. *Nature* **457**: 581-584.

Liu, X., and Millero, F.J. (2002) The solubility of iron in seawater. *Marine Chemistry* **77**: 43-54.

Lovley, D.R., and Phillips, E.J. (1986) Organic matter mineralization with reduction of ferric iron in anaerobic sediments. *Applied and Environmental Microbiology* **51**: 683-689.

Lovley, D.R., Giovannoni, S.J., White, D.C., Champine, J.E., Phillips, E., Gorby, Y.A., and Goodwin, S. (1993) Geobacter metallireducens gen. nov. sp. nov., a microorganism capable of coupling the complete oxidation of organic compounds to the reduction of iron and other metals. *Archives of Microbiology* **159**: 336-344.

Mahowald, N.M., Baker, A.R., Bergametti, G., Brooks, N., Duce, R.A., Jickells, T.D. et al. (2005) Atmospheric global dust cycle and iron inputs to the ocean. *Global Biogeochemical Cycles* **19**.

Martin, J.H. (1992) Iron as a limiting factor in oceanic productivity. In *Primary Productivity and Biogeochemical Cycles in the Sea*: Springer, pp. 123-137.

Meyer, B. (1964) Solid allotropes of sulfur. *Chemical Reviews* **64**: 429-451.

Millero, F., and Sohn, M. (1996) *Chemical Oceanography*, CRC press. *Boca Raton*.

Millero, F.J., Sotolongo, S., and Izaguirre, M. (1987) The oxidation kinetics of Fe (II) in seawater. *Geochimica et Cosmochimica Acta* **51**: 793-801.

Milucka, J., Ferdelman, T.G., Polerecky, L., Franzke, D., Wegener, G., Schmid, M. et al. (2012) Zero-valent sulphur is a key intermediate in marine methane oxidation. *Nature* **491**: 541-546.

Moore, J.K., Doney, S.C., Glover, D.M., and Fung, I.Y. (2001) Iron cycling and nutrient-limitation patterns in surface waters of the World Ocean. *Deep Sea Research Part II: Topical Studies in Oceanography* **49**: 463-507.

Morgan, B., and Lahav, O. (2007) The effect of pH on the kinetics of spontaneous Fe (II) oxidation by O 2 in aqueous solution–basic principles and a simple heuristic description. *Chemosphere* **68**: 2080-2084.

Musat, N., Halm, H., Winterholler, B., Hoppe, P., Peduzzi, S., Hillion, F. et al. (2008) A single-cell view on the ecophysiology of anaerobic phototrophic bacteria. *Proceedings of the National Academy of Sciences* **105**: 17861-17866.

Myers, C., and Myers, J. (1994) Ferric iron reduction-linked growth yields of Shewanella putrefaciens MR-1. *Journal of Applied Bacteriology* **76**: 253-258.

Nolting, R., Gerringa, L., Swagerman, M., Timmermans, K., and De Baar, H. (1998) Fe (III) speciation in the high nutrient, low chlorophyll Pacific region of the Southern Ocean. *Marine Chemistry* **62**: 335-352.

Overmann, J. (1997) Mahoney Lake: a case study of the ecological significance of phototrophic sulfur bacteria. In *Advances in Microbial Ecology*: Springer, pp. 251-288.

Pantke, C., Obst, M., Benzerara, K., Morin, G., Ona-Nguema, G., Dippon, U., and Kappler, A. (2012) Green rust formation during Fe (II) oxidation by the nitrate-reducing Acidovorax sp. strain BoFeN1. *Environmental Science & Technology* **46**: 1439-1446.

Pfeffer, C., Larsen, S., Song, J., Dong, M., Besenbacher, F., Meyer, R.L. et al. (2012) Filamentous bacteria transport electrons over centimetre distances. *Nature* **491**: 218-221.

Postma, D. (1985) Concentration of Mn and separation from Fe in sediments—I. Kinetics and stoichiometry of the reaction between birnessite and dissolved Fe (II) at 10 C. *Geochimica et Cosmochimica Acta* **49**: 1023-1033.

Pyzik, A.J., and Sommer, S.E. (1981) Sedimentary iron monosulfides: kinetics and mechanism of formation. *Geochimica et Cosmochimica Acta* **45**: 687-698.

Rabus, R., Hansen, T.A., and Widdel, F. (2013) Dissimilatory sulfate-and sulfur-reducing prokaryotes. In *The Prokaryotes*: Springer, pp. 309-404.

Rue, E.L., and Bruland, K.W. (1995) Complexation of iron (III) by natural organic ligands in the Central North Pacific as determined by a new competitive ligand equilibration/adsorptive cathodic stripping voltammetric method. *Marine Chemistry* **50**: 117-138.

Senko, J.M., Dewers, T.A., and Krumholz, L.R. (2005) Effect of oxidation rate and Fe (II) state on microbial nitrate-dependent Fe (III) mineral formation. *Applied and Environmental Microbiology* **71**: 7172-7177.

Sievert, S.M., Kiene, R.P., and Schultz-Vogt, H.N. (2007) The sulfur cycle. *Oceanography* **20**: 117-123.

Straub, K.L., Rainey, F.A., and Widdel, F. (1999) Rhodovulum iodosum sp. nov. and Rhodovulum robiginosum sp. nov., two new marine phototrophic ferrous-iron-oxidizing purple bacteria. *International Journal of Systematic and Evolutionary Microbiology* **49**: 729-735.

Straub, K.L., Kappler, A., and Schink, B. (2005) Enrichment and isolation of ferric-iron-and humic-acid-reducing bacteria. *Methods in Enzymology* **397**: 58-77.

Straub, K.L., Benz, M., Schink, B., and Widdel, F. (1996) Anaerobic, nitrate-dependent microbial oxidation of ferrous iron. *Applied and Environmental Microbiology* **62**: 1458-1460.

Stumm, W., and Morgan, J. (1996) Aquatic chemistry, chemical equilibra and rates in natural waters. *Environmental Science and Technology Series*.

Szilagyi, M. (1971) Reduction of Fe3+ ion by humic acid preparations. *Soil Science* **111**: 233-235.

Tagliabue, A., Bopp, L., Dutay, J.-C., Bowie, A.R., Chever, F., Jean-Baptiste, P. et al. (2010) Hydrothermal contribution to the oceanic dissolved iron inventory. *Nature Geoscience* **3**: 252-256.

Takahashi, H., Kopriva, S., Giordano, M., Saito, K., and Hell, R. (2011) Sulfur assimilation in photosynthetic organisms: molecular functions and regulations of transporters and assimilatory enzymes. *Annual Review of Plant Biology* **62**: 157-184.

Thamdrup, B. (2000) Bacterial manganese and iron reduction in aquatic sediments. In *Advances in Microbial Ecology*: Springer, pp. 41-84.

Thamdrup, B., Fossing, H., and Jørgensen, B.B. (1994) Manganese, iron and sulfur cycling in a coastal marine sediment, Aarhus Bay, Denmark. *Geochimica et Cosmochimica Acta* **58**: 5115-5129.

Thamdrup, B., Finster, K., Hansen, J.W., and Bak, F. (1993) Bacterial disproportionation of elemental sulfur coupled to chemical reduction of iron or manganese. *Applied and Environmental Microbiology* **59**: 101-108.

Trudinger, P. (1964) Evidence for a four-sulphur intermediate in thiosulphate oxidation by Thiobacillus X. *Australian Journal of Biological Sciences* **17**: 577-580.

Van Veen, W., Mulder, E., and Deinema, M.H. (1978) The Sphaerotilus-Leptothrix group of bacteria. *Microbiological Reviews* **42**: 329.

Walter, X.A., Picazo, A., Miracle, M.R., Vicente, E., Camacho, A., Aragno, M., and Zopfi, J. (2014) Phototrophic Fe (II)-oxidation in the chemocline of a ferruginous meromictic lake. *Frontiers in Microbiology* **5**.

Weber, K.A., Achenbach, L.A., and Coates, J.D. (2006) Microorganisms pumping iron: anaerobic microbial iron oxidation and reduction. *Nature Reviews Microbiology* **4**: 752-764.

Weiss, J.V., Rentz, J.A., Plaia, T., Neubauer, S.C., Merrill-Floyd, M., Lilburn, T. et al. (2007) Characterization of neutrophilic Fe (II)-oxidizing bacteria isolated from the rhizosphere of wetland plants and description of Ferritrophicum radicicola gen. nov. sp. nov., and Sideroxydans paludicola sp. nov. *Geomicrobiology Journal* **24**: 559-570.

Widdel, F., Schnell, S., Heising, S., Ehrenreich, A., Assmus, B., and Schink, B. (1993) Ferrous iron oxidation by anoxygenic phototrophic bacteria. *Nature* **362**: 834-836.

Zopfi, J., Ferdelman, T., and Fossing, H. (2004) Distribution and fate of sulfur intermediates—sulfite, tetrathionate, thiosulfate, and elemental sulfur—in marine sediments. *Geological Society of America Special Papers* **379**: 97-116.

2. MANUSCRIPTS

Polysulfides as intermediates in the oxidation of sulfide to sulfate by *Beggiatoa* spp.

Jasmine S. Berg[1], Anne Schwedt[2], Anne-Christin Kreutzmann[2], Marcel M.M. Kuypers[1], Jana Milucka[1]

[1]Department of Biogeochemistry, Max Planck Institute for Marine Microbiology, Bremen, Germany
[2]Department of Microbiology, Max Planck Institute for Marine Microbiology, Bremen, Germany

doi: 10.1128/AEM.02852-13

Published in: *Applied and Environmental Microbiology*

Author contributions: JSB developed methodology, performed Raman analyses, and analyzed data. JSB, AS, and ACK performed microbial cultivation experiments. MMMK and JM designed the research. JSB and JM conceived, wrote, and edited the manuscript.

ABSTRACT

Zero-valent sulfur is a key intermediate in the microbial oxidation of sulfide to sulfate. Many sulfide-oxidizing bacteria produce and store large amounts of sulfur intra- or extra-cellularly. It is still not understood how the stored sulfur is metabolized, as the most stable form of S^0 under standard biological conditions – orthorhombic α-sulfur – is most likely inaccessible to bacterial enzymes. Here we analyzed the speciation of sulfur in single cells of living sulfide-oxidizing bacteria via Raman spectroscopy. Our results showed that under various ecological and physiological conditions, all three investigated *Beggiatoa* strains stored sulfur as a combination of S_8 rings and inorganic polysulfides (S_n^{2-}). Linear sulfur chains were detected during both the oxidation and reduction of stored sulfur suggesting that S_n^{2-} species represent a universal pool of bio-available sulfur. Formation of polysulfides due to the cleavage of sulfur rings could occur biologically by thiol-containing enzymes or chemically by the strong nucleophile HS^- as *Beggiatoa* migrate vertically between oxic and sulfidic zones in the environment. Most *Beggiatoa* thus far studied can oxidize sulfur further to sulfate. Our results suggest that the ratio of produced sulfur and sulfate varies depending on the sulfide flux. Almost all of the sulfide was oxidized directly to sulfate under low sulfide flux conditions, whereas only 50% was oxidized to sulfate under high sulfide flux conditions leading to S^0 deposition. With Raman spectroscopy we could show that sulfate accumulated in *Beggiatoa* filaments, reaching intracellular concentrations between 0.72-1.73 M.

INTRODUCTION

Sulfur storage in bacteria was first documented in the 19th century when Winogradsky (1887) proposed the concept of chemolithotrophy from observations of sulfur globules in *Beggiatoa* filaments. Since then, taxonomically diverse microorganisms have been reported to store zero-valent sulfur either intracellularly (e.g. *Beggiatoaceae, Chromatiaceae*) or extracellularly (e.g. *Ectothiorhodospiraceae*, *Chlorobiaceae*, genus *Thiobacillus*) as an intermediate in the oxidation of reduced sulfur compounds (Dahl and Prange, 2006). Internal sulfur, which is contained within invaginations of the periplasm, is often surrounded by a protein envelope thought to be purely structural in function (Nicolson and Schmidt, 1971; Brune, 1995). External sulfur globules are not enclosed in a membrane; rather, they feature a hydrophilic surface of e.g. polythionates (Steudel et al., 1987; He et al., 2010). It has been noted that biological sulfur is characterized by a lower density and different crystalline structure than orthorhombic sulfur (Trüper, 1967; Mas and Van Gemerden, 1987). However, our understanding of the chemical nature of stored sulfur is still limited by conventional methods of extraction and analysis because they can induce artificial changes in the chemistry of biogenic sulfur compounds. In transmission electron micrographs, for example, the presence of sulfur in cells must be inferred from empty vesicles resulting from the dissolution of sulfur in ethanol during the dehydration step in resin embedding (e.g. Vetter, 1985). Only recently has the novel application of spectroscopic methods on biological samples indicated that the chemical speciation of stored sulfur may differ across groups of ecologically and physiologically distinct bacteria (e.g. Pasteris et al., 2001; Prange et al., 2002; He et al., 2010). This has implications for the metabolism of stored sulfur, as enzyme-S^0 interactions may be highly specific for the sulfur species utilized.

Sulfur atoms readily catenate to form linear or cyclic molecules and can form bonds with both organic and inorganic end groups. The resulting sulfur compounds are often extremely pH and redox-sensitive, and thus difficult to measure. The most thermodynamically stable form of elemental sulfur under standard biological conditions is orthorhombic α-sulfur, which consists of puckered S_8 rings (Roy and Trudinger, 1970), but more than 30 allotropes have been described (Meyer, 1964). Thus far, a variety of species other than cyclooctasulfur have been identified in the sulfur-storing bacteria including inorganic polysulfides (S_n^{2-}), polythionates ($^-O_3S–S_n–SO_3^-$), and long-chain organosulfanes (R–S_n–R); (Prange et al., 1999; Prange et al., 2002; He et al., 2010). The solubility these S^0 species in water is very different, ranging from the nearly insoluble S_8 rings to extremely soluble polysulfides. Sulfur-oxidizing and sulfur-reducing bacteria growing on solid sulfur preferentially take up the charged and soluble fraction, leaving behind the insoluble rings (Blumentals et al., 1990; Engel et al., 2007; Franz et al., 2009). In *Beggiatoa* spp., oxidation of elemental sulfur to sulfate is mediated by the cytoplasmic enzyme reverse dissimilatory sulfite reductase (rDSR; Mußmann et al., 2007). It is not yet understood how extracellularly and periplasmically stored S_8 rings are accessed by the Dsr system, as this implies trans-membrane transport. It has been hypothesized that cyclooctasulfur is either reduced to H_2S or taken up via an unknown persulfide (R–S–SH) carrier molecule across the cytoplasmic membrane (Pott and Dahl, 1998). Furthermore, enzyme active sites probably do not accommodate large molecules of cyclooctasulfur, and recent studies indicate that at least the archaeal sulfur oxygenase reductase from *Acidianus ambivalens* contains an elongated active-site pocket which can accommodate only linear polysulfides of up to 8 atoms in length (Kletzin,

2008). The enzymes involved in sulfur utilization in bacteria are still poorly characterized and therefore mechanisms of sulfur activation and transport remain speculative.

Published studies on the chemistry of stored sulfur frequently report contradictory findings: the same organism appears to contain different sulfur species depending on the culture conditions, sample preparation, and analytical techniques used. Moreover, many of these investigations were performed on dead bacteria at the risk of altering the sulfur chemistry. We tried to resolve some of the conflicting results while investigating the link between sulfur speciation and enzymatic pathways of sulfur utilization by comparing three strains of *Beggiatoa* under various growth conditions. In this study, sulfur compounds in single cells of living bacteria were characterized and their distribution was mapped using confocal Raman microscopy, a technique which relies on the inelastic scattering of light to provide a unique molecular-structural fingerprint of a compound, allowing for its identification. The non-invasive, non-destructive nature of Raman spectroscopy makes it ideal for biological applications, and especially for measuring pH- and redox-sensitive sulfur species.

MATERIALS & METHODS

Culturing *Beggiatoa* sp. 35Flor was cultivated in agar-stabilized sulfide gradient medium prepared in glass test tubes (1.4 × 14.5 cm) as described by Schwedt *et al.* ((Schwedt et al., 2012)). Each tube contained a ~2 cm bottom layer of solid agar (1.5% w/v agar) and a ~5 cm top layer of semisolid agar (0.25% w/v agar) which allowed *Beggiatoa* to glide through the medium. Agar layers were prepared by mixing separately autoclaved sulfate-free artificial seawater (24.34 g NaCl, 8.34 g $MgCl_2 \cdot 6H_2O$, 0.66 g $CaCl_2 \cdot 2H_2O$, and 1.02 g KCl per 1 liter Milli-Q water) and

triple-washed agar solutions. The bottom agar was amended with sterile 1M sulfide solution to final concentrations of 4, 12, or 16 mM, subsequently referred to as low, medium, and high sulfide flux conditions, respectively. The top agar received additional trace elements, vitamin solution, mineral solution (555 mg K_2HPO_4, 28.72 mg Na_2MoO_4, 750 mg $Na_2S_2O_5$, and 29 mg $FeCl_3 \cdot 6H_2O$ per liter), and HCO_3^- to a final concentration of 2 mM, as specified by Schwedt *et al* (2012). Culture tubes were loosely capped, allowing gas exchange with the atmosphere. Oxygen gradients were allowed to develop overnight before inoculation with 100 µl filament suspension approximately 1 cm below the agar surface. *Beggiatoa alba* strains B15LD and B18LD were grown in freshwater-based agar-stabilized gradient medium (Strohl and Larkin, 1978) with a bottom agar sulfide concentration of 8 mM.

For Raman spectroscopy, 10-50 µl of each live bacterial culture was pipetted onto a 20 × 20 mm glass coverslip previously coated with 0.1% Poly-L-lysine solution (Sigma-Aldrich). Samples were protected with a second coverslip and then sealed with electrical tape to minimize oxygen diffusion and prevent drying. At least 15 different filaments from each time point and culture condition were analyzed, but only representative point spectra are presented in the results.

Reference compounds The following reagent grade (purity > 99%) compounds were used as references: elemental sulfur (Roth GmbH), sodium sulfate (Sigma-Aldrich), potassium sulfate (Merck), magnesium sulfate (Merck) and calcium sulfate (Applichem). A polysulfide solution was prepared from 5.06 g $Na_2S \cdot 9H_2O$ and 5.8 g elemental sulfur per 100 ml H_2O, with a final pH of 9.5 and sulfide concentration of 210 mM. Spectra for aqueous polysulfides were recorded under anoxic to oxic conditions by transferring a 100 µl drop to a glass coverslip and immediately measuring in live mode, with a point spectrum taken every 1.0 seconds. A subsample of the

polysulfide solution was dried under a 90:10 N_2:CO_2 atmosphere for comparison. Crystalline standards, such as sodium sulfate, were measured directly on glass coverslips.

Raman spectroscopy All measurements were carried out with an NTEGRA Spectra confocal spectrometer (NT-MDT, Eindhoven, Netherlands) coupled to an inverted Olympus IX71 microscope. The excitation light from a 532 nm solid-state laser was focused on the sample through an Olympus 100X/NA1.3 oil-immersion objective. The pinhole aperture was maintained at 55 µm corresponding to a spatial resolution of 250-300 µm. Raman scattered light was dispersed with a 150 $l \cdot mm^{-1}$ grating and collected by an electron multiplying charge coupled device (EMCCD) camera (Andor Technology, Belfast, Northern Ireland) cooled to -70°C. To verify resonance Raman spectra, a 785 nm diode laser coupled to an IR-CCD camera (Andor Technology, Belfast, Northern Ireland) was used, and the pinhole aperture was set at 80 µm. Exposure times varied between 0.2 and 6 seconds and the Raman spectra were recorded between 0 and ~4,500 cm^{-1} with a spectral resolution of 0.2 cm^{-1}. The laser power at the sample was checked with a laser power meter and did not exceed 1 mW. The instrument was also equipped with a motorized piezostage for X-Y scanning. Full-spectrum maps were taken with a maximum 1.2 second dwelling time per point and 0.3 mW laser power.

Data processing The software Nova_Px 3.1.0.0 (NT-MDT, Eindhoven, Netherlands) was used for all spectral analyses. Spectra were normalized to an arbitrary unit of intensity on the y-axis, maintaining relative peak heights, for easier comparison. Noisy spectra were smoothed using a Gaussian function with a tau value of 3. In order to map specific compounds, relevant peak areas were first background-corrected and then images were overlaid and brightness/contrast adjusted in Adobe Photoshop CS2.

For the Raman quantification of sulfate, spectra of 8 different *Beggiatoa* sp. 35Flor filaments grown on sulfate-free medium were baseline-corrected using a modified average fit curve with a period of 20 (example is provided in Fig. S1A of the supplemental material). Although peak area is generally used for Raman quantification, peak height can also be used as an accurate measure of intensity (e.g., Barletta et al., 2009). In our study, standard-curves were generated from the height of the S=O peak at 997 cm^{-1} in spectra from a 0.2-2.0 M dilution series of Na_2SO_4 in Milli Q water, and resulted in a good fit with an $R^2 \geq 0.9309$ for the three different measurement conditions used (Fig. S1B). The detection limit for sulfate under the applied conditions on the instrument used was ~25 mM.

Chromatographic sulfate measurements Sulfate was analyzed on a 761 Compact ion chromatograph (Metrohm) with a Metrosep A SUPP 5 column. A carbonate buffer, prepared with 3.2 mmol l^{-1} Na_2CO_3 and 1 mmol l^{-1} Na_2CO_3, was used as eluent. The duration of a run was 14 min, with sulfate eluting at ~11.5 min. Sodium sulfate standards 1-400 µM and IAPSO standard seawater were used as references.

The intra-cellular sulfate content of *Beggiatoa* sp. 35Flor was determined by picking individual filaments with a glass needle and transferring them to 3 ml of 10 mM HCl. Samples contained 25, 50, or 100 filaments, in triplicates, and these were freeze-thawed twice to ensure cell lysis and the resulting solution was passed through a 0.45 µm filter into IC vials before analysis. Because some liquid adhering to filaments is inevitably transferred with each sample, single liquid droplets from the inoculated medium were also measured in 10 mM HCl. Sulfate concentrations in these control samples were so close to the detection limits of our instrument that single-droplet effects were considered negligible here.

Extra-cellular sulfate concentrations were determined by extracting porewater from the agar medium with 2-cm-long micro-rhizones (Rhizosphere Research Products, Wageningen, Netherlands) inserted vertically into the culture tubes. It is possible that differential pressures occurred along the rhizone, resulting in unequal sampling of the upper 2 cm of medium. Parallel cultures with different bottom agar sulfide concentrations (4 mM, 12 mM, or 16 mM) were inoculated at the same time and sampled over a period of 14 days. Uninoculated cultures containing 4 mM sulfide were monitored for the chemical formation of sulfate. At every time point, one tube from each culture condition was sampled and then discarded. All liquid samples were diluted in 10 mM HCl and filtered through a 0.2 µm filter before analysis.

For sulfate depth profiles, gradient media with a sulfide concentration in the bottom agar of 4 mM were prepared in open-bottom glass tubes (1.4 × 14.5 cm), plugged from below with a tapered rubber stopper. After approximately two weeks of incubation, the lower end of the tube was immersed in liquid nitrogen up to a depth of 2 cm and the rubber stopper was removed. Agar cores were then mounted on a micromanipulator which allowed for sectioning of the non-frozen top agar in 2 mm steps. Each slice of semisolid agar was gently passed through a 0.45 µm syringe filter and diluted in 3 ml of 10 mM HCl for analysis by ion chromatography. A total of three agar cores were analyzed, and fluxes were calculated from each sulfate profile using the model of Lettmann *et al.* (2012) assuming an instantaneous steady state (see Fig. S2). The diffusion coefficient D used for SO_4^{2-} at 20°C was 8.91×10^{-9} m^2s^{-1}. The Tikhonov parameter ($\alpha = 269.822$) was selected from the interval 10^2 and 10^3 using a ratio-criterion function with 400 tested optima and a smoothing parameter $\lambda = 10$.

Microsensor measurements Gradients of pH and H_2S were recorded in triplicates, parallels of those cultures used for sulfate profiling. The profiles were measured in 250 µm intervals from the agar surface to a depth of 1 cm. Microsensors for pH (pH-10) and H_2S (H_2S-10) purchased from Unisense A/S (Aarhus, Denmark) were calibrated and total sulfide concentrations were calculated as described by Schwedt *et al*. (2012). Sulfide fluxes were calculated using Fick's law of diffusion with a diffusion coefficient *D* of 1.52×10^{-9} m^2 s^{-1} for H_2S/HS^- at 20°C (Jørgensen et al., 1979). All microsensors were calibrated immediately before use and then after the final measurement to check for a possible drift.

RESULTS

Sulfur speciation during sulfur oxidation and reduction in marine *Beggiatoa* sp. All *Beggiatoa* were grown in sulfide gradient tubes simulating the environmental conditions in which *Beggiatoa* can migrate vertically between oxic and anoxic sediment zones. In gradient media with a low sulfide flux, filaments of the marine strain *Beggiatoa* sp. 35Flor were present in a dense mat circa 0.5 cm below the air-agar interface at 16 days after inoculation. Within this mat, the *Beggiatoa* completely oxidized upward-diffusing sulfide. A peak in the sulfate concentration profile indicated that sulfate formed as an end product (Fig. 1). The *Beggiatoa* mat was whitish in color due to intracellular deposition of sulfur globules (Figs. 1 and 2A), as demonstrated by Schwedt *et al*. using high-performance liquid chromatography of methanol

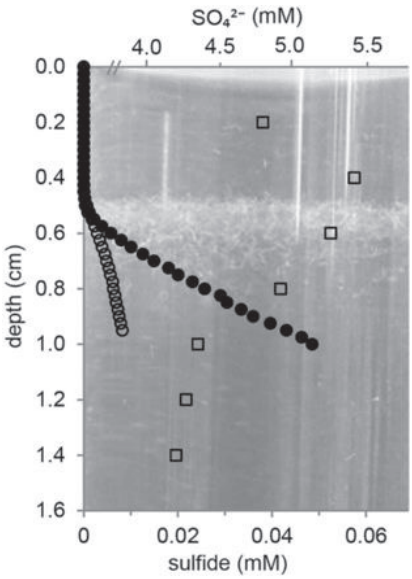

Figure 1: Profiles of H_2S (○), total sulfide (●), and SO_4^{2-} (□) in a *Beggiatoa* sp. 35Flor culture after 16 days of incubation with a low sulfide flux. The *Beggiatoa* mat was located at 0.5-0.7 cm depth.

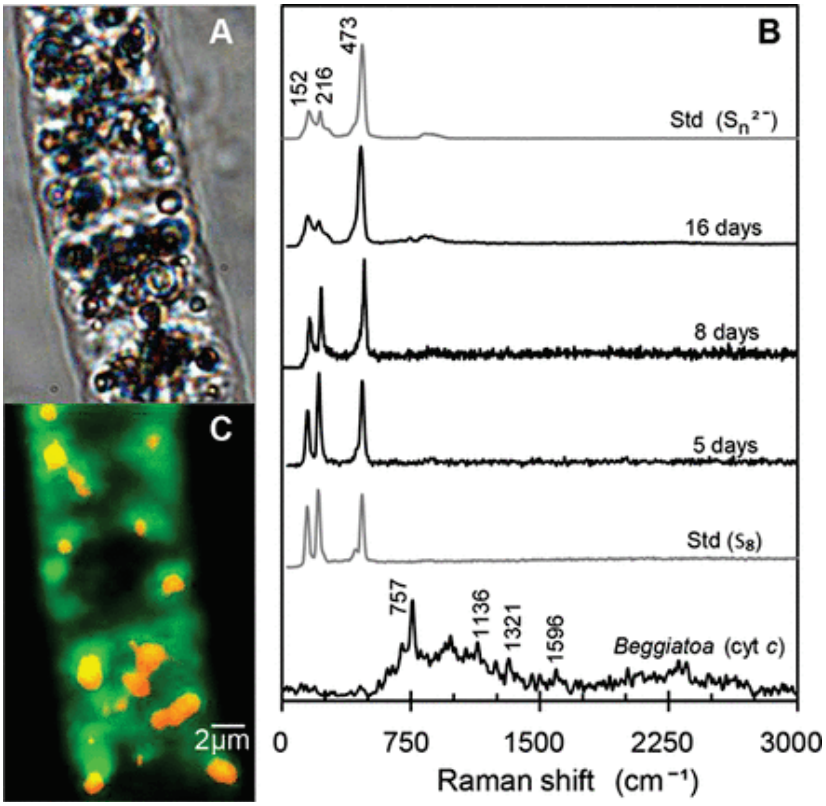

Figure 2: **(A)** Optical micrograph of a *Beggiatoa* sp. 35Flor filament grown with a low sulfide flux. **(B)** Point spectra of sulfur inclusions measured 5, 8, and 16 days after inoculation using constant 180 µW laser power and 1 sec exposure time, compared to sulfur standards (gray). A spectrum (top) of cytochrome *c* identified in the *Beggiatoa* membrane region is also shown **(C)** A Raman map of a filament showing the 473 cm^{-1} sulfur peak in yellow and autofluorescence of the cell in green.

extracts from filaments (Schwedt et al., 2012). Using Raman spectroscopy, we could confirm presence of zero-valent sulfur in these inclusions of living *Beggiatoa*. In Fig. 2B, Raman spectra of these sulfur inclusions are shown together with spectra of two sulfur standards for comparison. The spectrum of the cyclooctasulfur standard is characterized by two strong peaks at 152 and 216 cm^{-1} corresponding to the bending and stretching modes of the 8-fold ring and a third strong peak at 473 cm^{-1} corresponding to the vibration of the S–S bond (Harvey and Butler, 1986). It is important to note that not only the absolute positions of peaks but also their relative heights are significant in a Raman spectrum, and that the three peaks of S_8 are similar in height. The spectrum of a globule from 5-day old cultures matched that of S_8, but spectra from 8- and 16-day cultures exhibited a weakening of the 152 and 216 cm^{-1} peaks relative to the 473 cm^{-1} S–S peak, a ratio which is typical of aqueous polysulfides as visible in the S_n^{2-} standard spectrum (see also, Janz et al., 1976; Khan et al., 2011). Thus, globules in filaments from a later growth

phase were composed of a mixture of polysulfides and cyclooctasulfur, with the ratio of S_n^{2-} to S_8 apparently increasing over time.

The distribution of sulfur within the cells was mapped using the characteristic S—S vibration peak at 473 cm^{-1} (Fig. 2C). A peak at 757 cm^{-1}, which is depicted in the uppermost spectrum in Fig. 2B, was tentatively attributed to cytochrome *c* and used in the spectral map as a proxy for the *Beggiatoa* cell membrane. The 757 cm^{-1} peak co-occurred with peaks at 979, 1136, 1321, and 1584 cm^{-1} which are the characteristic resonance Raman bands for cytochrome *c* at an excitation wavelength of 532 nm (Pätzold et al., 2008). The phenomenon of resonance Raman scattering occurs when the excitation frequency is close to an electronic transition of a molecule and thus is specific to the wavelength of the laser used. The fact that the peaks at 979, 1136, 1321, and 1584 cm^{-1} were not observed under excitation with a 785 nm diode laser (Fig. S3) provides further support for the assignment of these peaks to cytochrome *c*.

In cultures grown with a high sulfide flux, filaments at the sulfide-oxygen interface accumulated so much sulfur (Fig. 3A and B) that some eventually burst. Presumably to avoid this fate, a subpopulation of filaments migrated downwards and established a second bacterial mat in the anoxic, sulfidic zone. In this

Figure 3: **(A)** Optical micrograph of *Beggiatoa* sp. 35Flor from the upper mat of a culture grown with a high sulfide flux. **(B)** A corresponding Raman map showing the occurrence of the 473 cm^{-1} sulfur peak in yellow/red and autofluorescence of the cell in green.

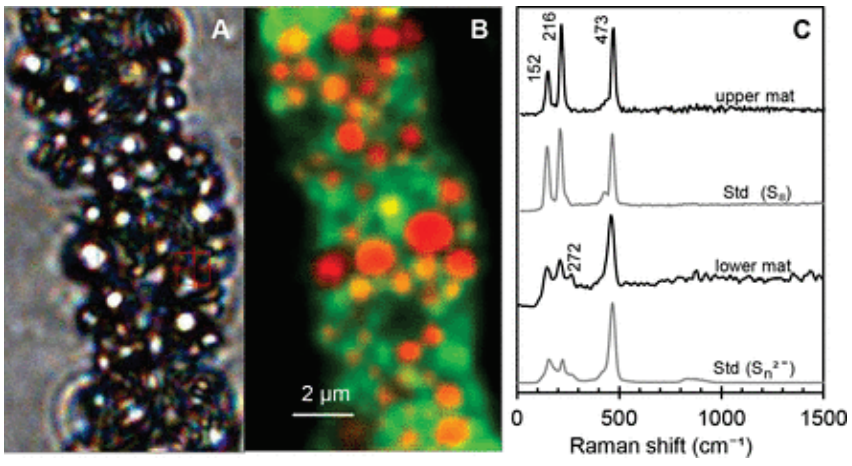

subpopulation a depletion of internal sulfur was observed coinciding with the production of sulfide (Schwedt et al., 2012). It has been hypothesized that the anoxic subpopulation of *Beggiatoa* sp. 35Flor reduces intracellular sulfur with stored polyhydroxyalkanoates (PHAs), which were identified using the lipid stain Nile Red (Schwedt et al., 2012). Although PHA is a strong Raman scatterer, we were not able to detect this particular carbon storage compound in *Beggiatoa* sp. 35Flor filaments under any of investigated growth conditions. The remaining sulfur globules in filaments of this lower *Beggiatoa* mat were composed of both S_8 rings and linear S_n^{2-} species (Fig. 3C) as indicated by the dominant S–S peak at 473 cm^{-1}. Additionally, two weak S_8 ring vibration peaks and a 272 cm^{-1} peak occurred in the S–S–S bending region. The 272 cm^{-1} peak is characteristic of long-chain ($n \geq 8$) polymeric sulfur (Eckert and Steudel, 2003).

Sulfate, a strong Raman scatterer with a signature peak belonging to the S=O stretch at 997 cm^{-1} (Fig. 4A), was also identified in *Beggiatoa* sp. 35Flor filaments but not in the surrounding medium. Porewater sulfate concentrations as measured by ion chromatography were below the ~25 mM detection limit of the Raman microscope. In *Beggiatoa* filaments sulfate appeared to be concentrated in particular regions of the cell, in some cases in association with the sulfur globules (Fig. 4B). The intracellular sulfate

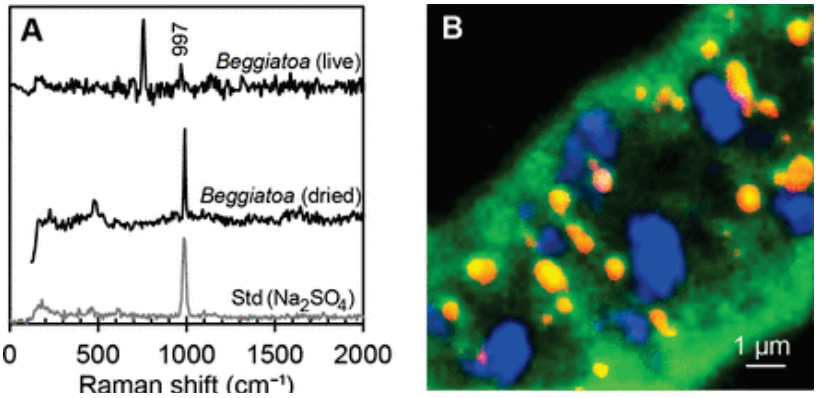

Figure 4 **: (A)** From top to bottom: (i) a background-corrected spectrum of live *Beggiatoa* sp. 35Flor grown on sulfate-free medium exhibiting a sulfate peak at 997 cm^{-1}, (ii) sulfate detected in a dried filament in comparison to a (iii) Na_2SO_4 standard. **(B)** A Raman map of a dried *Beggiatoa* sp. 35Flor filament with the 473 cm^{-1} S–S peak shown in yellow/red, the 997 cm^{-1} S=O peak of sulfate in blue, and autofluorescence of the cell in green.

was further quantified by Raman spectroscopy using the height of the S=O peak as an indicator of sulfate concentration (Fig. S1). Assuming that sulfate alone contributed to the 997 cm^{-1} peak, the estimated concentrations of intracellular sulfate were between 0.72-1.73 M with an average of 1.14 M. Ion chromatography of individual, hand-picked filaments confirmed the presence of molar concentrations of sulfate in this marine *Beggiatoa* strain. We then monitored the production of sulfate from biological sulfide oxidation in the porewater of cultures grown in medium prepared with sulfate-free seawater. The porewater sulfate concentrations increased linearly during the first two weeks of incubation in all cultures (Fig. 5). The sulfate production increased proportionally to the sulfide flux, resulting in concentrations of 4.9, 7.3, and 9.9 mM in the 2-mm thick layer the around the *Beggiatoa* mat in 14-days-old cultures with initial bottom agar sulfide concentrations of 4, 12, and 16 mM, respectively. No abiotic sulfate production was detected in the uninoculated controls (Fig. 5).

Figure 5: Porewater SO_4^{2-} concentrations in the upper 2 cm of agar medium from cultures grown with different sulfide concentrations in the bottom agar: uninoculated control (■), 4 mM (□), 12 mM (▲), and 16 mM (○).

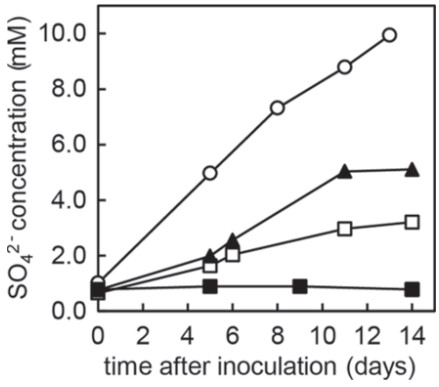

In order to relate the observed sulfate production to sulfide consumption, we estimated sulfide consumption rates by integrating the sulfide fluxes in *Beggiatoa* sp. 35Flor cultures measured by Schwedt *et al*. (2012) over the height of the *Beggiatoa* mat. The resulting sulfide oxidation rates (± the standard deviation) for cultures with 16 mM sulfide were 13.65 ± 2.5 and 8.55 ± 1.8 $mol \cdot m^{-3} \cdot day^{-1}$, after 7 and 13 days, respectively. These rates were 30-40% higher than the corresponding sulfate production rates of 7.9 and 5.8 $mol \cdot m^{-3} \cdot day^{-1}$. The sulfide flux in cultures with 4 mM sulfide did not fluctuate

significantly over the 13-day period, which can be explained by a continuous downward migration of the *Beggiatoa* mat, adjusting the oxygen-sulfide interface to the decreasing flux. The average sulfide oxidation rate was 2.88 ± 0.6 $mol \cdot m^{-3} \cdot day^{-1}$ and the sulfate production rate was 2.14 $mol \cdot m^{-3} \cdot day^{-1}$ showing that at a low sulfide flux, sulfide may be directly oxidized to sulfate.

Although the sulfate production rate remained relatively constant within the first two weeks after inoculation, sulfide consumption decreased, implying that the ratio of H_2S and S^0 oxidation rates varied over time. To better compare the ratio of sulfide oxidation products, sulfate and sulfide fluxes were modeled from the respective chemical profiles (Fig. 1) measured in low sulfide flux cultures after 16 days of incubation. The sulfate flux was 488 ± $mmol \cdot m^{-2} \cdot day^{-1}$, more than two orders of magnitude higher than the sulfide flux of 1.60 ± 0.51 $mmol \cdot m^{-2} \cdot day^{-1}$. The calculated average sulfate production rate was 151 $mol \cdot m^{-3} \cdot day^{-1}$ and the sulfide consumption rate was 0.80 $mol \cdot m^{-3} \cdot day^{-1}$. Visual inspection of the filaments at this time point confirmed that most of refractive sulfur globules had disappeared.

Sulfur speciation in freshwater *Beggiatoa* not oxidizing sulfur to sulfate. *Beggiatoa alba* B18LD is a heterotrophic, freshwater strain capable of oxidizing sulfide to elemental sulfur, but not to sulfate (Schmidt et al., 1987). Instead the strain can reduce internally stored sulfur to sulfide, presumably by degrading carbon-rich compounds such as PHAs during periods of anoxia (Schmidt et al., 1987). In contrast to the autotrophic *Beggiatoa* sp. 35Flor, polyhydroxybutyrate (PHB) inclusions (Fig. 6A) were easily identified in *B. alba* B18LD based on their characteristic Raman bands at 906, 1357, 1431, 1733 and ~2940 cm^{-1} (De Gelder et al., 2008). After 4 days of growth in gradient cultures with a medium sulfide flux, highly refractive intracellular inclusions

Figure 6: (A) From top to bottom: (i) representative point spectra of sulfur inclusions from *B. alba* B18LD, (ii) extracellular sulfur from *B. alba* B15LD, (iii) a polysulfide standard, (iv) cytochrome *c,* and (v) PHB. **(B)** Optical micrographs of strain B18LD and **(C)** strain B15LD grown with 8 mM sulfide in the bottom agar. **(D)** A Raman map of a B15LD filament with the 2900 cm^{-1} C–H peak in pink and the 757 cm^{-1} cytochrome *c* resonance peak in green and **(E)** the corresponding optical image. The red square outlines the Raman map.

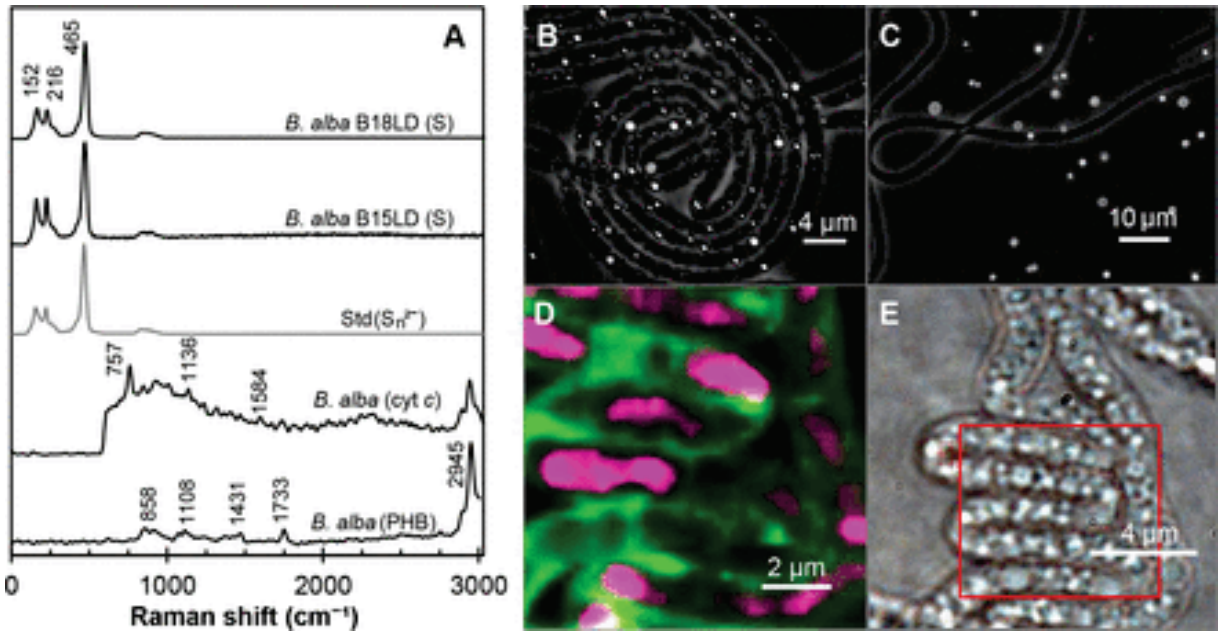

were visible under the optical microscope (Fig. 6B). These were identified as sulfur globules composed of a mixture of S_8 rings and polysulfides by their characteristic Raman spectra (Fig. 6A). The wavenumbers of the S–S vibration varied in different point spectra from 466 to 486 cm^{-1} (data not shown). Because the vibration frequency of the S–S bond depends on the number of sulfur atoms in a chain (Khan et al., 2011), the shift in peak position may reflect S_n^{2-} species of different chain lengths (n) coexisting in a polysulfide "pool" within the sulfur globules. The characteristic sharp S=O peak of sulfate at 997 cm^{-1} was not detected in this freshwater *Beggiatoa*.

Beggiatoa alba BL15D appears to be a special case in the family *Beggiatoaceae,* members of which have thus far all been reported to deposit sulfur intracellularly (Strohl et al., 1982).

Surprisingly no sulfur could be detected inside of *B. alba* B15LD filaments, but instead abundant, refractive spherules, composed of a mixture of S_8 rings and polysulfides (Fig. 6A), were found in the medium surrounding the cells (Fig. 6C). Previously, this strain was observed to deposit intracellular sulfur (Strohl et al., 1981) and therefore it is possible that a mutation occurred in one of the electron accepting enzymes. In uninoculated controls the chemically-formed sulfur precipitated as crystals rather than globules suggesting that the extracellular sulfur globules associated with the *Beggiatoa alba* filaments might be biologically produced. Indeed, these sulfur globules behaved differently from chemically-produced crystalline sulfur; for example, exposure to strong laser radiation caused burning of the sulfur globules, suggesting that globules were more amorphous in structure. Full-spectrum Raman mapping of a B15LD filament after four days growth in sulfide-gradient medium revealed PHB stored as inclusions within the cells and *c*-type cytochromes associated with the cell membrane (Fig. 6D and E). After eleven days, PHB could no longer be detected in *Beggiatoa alba* B15LD filaments.

DISCUSSION

All of the species of *Beggiatoa* that we studied deposited sulfur globules as a mixture of S_8 rings and linear polysulfides, with the relative abundances of the different sulfur species depending on the growth conditions. Although only cyclooctasulfur was detected in *Beggiatoa* sp. 35Flor cultures at the earliest growth stage, it is possible that minor amounts of polysulfides were also present but could not be distinguished due to the overlap with the strong Raman signal of predominant S_8 rings. This observation is consistent with X-ray absorption near edge structure (XANES) spectroscopy of *Allochromatium vinosum* which demonstrated a correlation between intracellular concentrations of polysulfides (among other sulfur species) and bacterial growth

phase (Franz et al., 2009). In cultures of *Beggiatoa* sp. 35Flor, an increase of the polysulfide fraction under both sulfur-oxidizing and reducing conditions suggests that S_n^{2-} species represent a universal pool of activated sulfur utilized in both the oxidative and reductive parts of the sulfur cycle. Polysulfides can be derived from circular sulfur species by enzymatic cleavage of S–S bonds with membrane-bound thiol groups or glutathione, as postulated for e.g. *Thiobacillus thiooxidans* which oxidizes solid elemental sulfur (Suzuki, 1965). Alternatively, sulfur rings can be opened chemically by strong nucleophiles such as HS^- according to the following reaction: $n/8\ S_8 + HS^- \leftrightarrow S_{n+1}^{2-} + H^+$ (Schauder and Müller, 1993). Polysulfide anions are also strong nucleophiles and therefore their formation could have an autocatalytic effect on S–S bond cleavage. It has been shown that the addition of sodium sulfide to cultures of sulfur-reducing bacteria enhances the solubilization and reduction of crystalline sulfur (Zöphel et al., 1988; Blumentals et al., 1990). Thus, the cleavage of sulfur rings by HS^- or S_n^{2-} could provide a fortuitous pool of linear sulfur species, which, in contrast to large sulfur ring structures, are accessible to enzymes involved in sulfur oxidation and sulfur reduction.

In the case of the Beggiatoa species that we investigated, it could not be determined whether the activation of cyclooctasulfur to polysulfide was biologically or chemically regulated. It is, nonetheless, tempting to speculate that bacteria may harness the chemical reaction instead of expending energy to cleave sulfur rings. In the presence of free sulfide, bacteria might not be able to prevent the decomposition of elemental sulfur to polysulfides. This could explain the presence of polysulfides in the *Beggiatoa alba* strains that cannot further oxidize zero-valent sulfur to sulfate. In the environment *Beggiatoa* can migrate vertically between oxic and anoxic sediment zones, thus experiencing dramatic fluctuations in the sulfide supply. Periodic sulfide

starvation would require the sulfur-oxidizing *Beggiatoa* to enzymatically activate S_8 rings in order to utilize stored sulfur. Thus, a combination of environmental and physiological factors may influence the speciation of stored sulfur compounds in these sulfide-oxidizing bacteria.

It is important to note that the speciation of sulfur as a combination of S_8 and S_n^{2-} described here is discussed only for inclusions in neutrophilic, microaerophilic bacteria. Sufficient concentrations of polysulfides (~10% of total dissolved HS^-) exist in solution to support bacterial growth at circumneutral to alkaline pH, but polysulfides undergo hydrolysis in acid (Schauder and Müller, 1993). The acidophile *Acidithiobacillus ferrooxidans* produces extracellular globules thought to be composed of a cyclooctasulfur core and surrounded by a hydrophilic layer of polythionates, which are only stable at extremely low pH (Steudel, 1989; He et al., 2010). Although the ultrastructure of sulfur globules in *Beggiatoa* spp. could not yet be resolved, it is possible that polysulfides contribute to the hydrophilic behavior of the biogenic sulfur, analogous to the function of polythionates in *Acidithiobacillus* spp. sulfur globules. A proteinaceaous membrane which encloses intracellular sulfur of *Beggiatoa* spp. (Larkin and Strohl, 1983) may protect other cellular components from the highly reactive S_n^{2-} ions. With Raman spectroscopy, we were unable to resolve the exact localization of the sulfur globules within the cell. However, we could observe associations of the sulfur inclusions with cell membrane, identified by the presence of *c*-type cytochromes. These observations further confirm previous reports of unusually high cytochrome *c* content in many *Beggiatoa* (Larkin and Strohl, 1983; Schmidt and DiSpirito, 1990) that in some cases causes pink or orange coloration of the bacteria (Prince et al., 1988; MacGregor et al., 2013).

Our data suggests that elemental sulfur is temporarily stored as an electron reserve, and the activated polysulfide fraction is further oxidized by many *Beggiatoa* to sulfate. Our study of sulfate production by *Beggiatoa* sp. Flor provides further insight into the complete biological pathway of sulfide oxidation. Unlike other sulfur bacteria such as *Thiobacillus denitrificans*, which only oxidize stored sulfur after other reduced sulfur compounds like thiosulfate have been depleted (Schedel and Trüper, 1980), *Beggiatoa* spp. oxidize sulfide and sulfur simultaneously. Our data suggest that sulfide is completely oxidized to sulfate by *Beggiatoa*, when these are grown with a low sulfide flux. However, it appears that under high sulfide fluxes the rate of sulfur oxidation cannot keep up with sulfide oxidation, resulting in up to half of the oxidized sulfide being deposited as sulfur, and in some cases causing cells to rupture (Schwedt et al., 2012). To date it has been shown that *Beggiatoa* spp. store phosphate, nitrate, carbon-compounds (such as PHA), and elemental sulfur intracellularly. Our results show that *Beggiatoa* filaments can also contain molar concentrations of sulfate. Similarly, sulfate has been found inside the related Gammaproteobacterium *Thioploca* in concentrations up to 100-1,000 times higher than that of its freshwater environment (Kojima et al., 2007). Storing sulfate offers no apparent advantage to marine bacteria and it is therefore likely that sulfate is not stored *per se* but accumulates inside the cell as a product of the sulfate-evolving enzyme complex APS reductase/ATP sulfurylase or SoeABC-type sulfite-oxidizing enzyme, depending on the organism (Kappler and Dahl, 2001). In fact, sulfate appears to be localized in regions around degraded sulfur globules (Fig. 4B) where it is produced. Not much is known about the mechanism of sulfate export in *Beggiatoa.* A gene for the H^+-driven sulfate permease *sulP* was identified in the genome of *Beggiatoa* sp. 35Flor (M. Mussmann *et al.* unpublished data). The activity of this

symporter may be limited by the energy required for ion export, or by the low surface-to-volume ratio of these large sulfur bacteria which restricts substrate-product exchange with the environment.

With our *in vivo* Raman analyses presented here we attempted to resolve some of the discrepancies surrounding the discussions of the chemical speciation of bacterial sulfur globules. In the literature there are conflicting reports of sulfur rings (Pasteris et al., 2001; George et al., 2008), polysulfides (Prange et al., 2002), or polythionates (Steudel et al., 1987; He et al., 2010) in these inclusions. Based on our results we hypothesize that even within the same species of bacteria, the speciation of stored sulfur varies under different ecophysiological conditions.

ACKGNOWLEDGMENTS

We thank Martina Meyer and Kirsten Imhoff for technical support and Sandra Havemeyer for kindly providing *Beggiatoa alba* strains B15LD and B18LD. We are grateful to Heide Schulz-Vogt for helpful discussions and for providing cultures of *Beggiatoa* sp. 35Flor. Funding was provided by the International Max Planck Research School of Marine Microbiology, the Max Planck Society, and the MARUM Center for Marine Environmental Sciences.

REFERENCES

Barletta, R.E., Gros, B.N., and Herring, M.P. (2009) Analysis of marine biogenic sulfur compounds using Raman spectroscopy: dimethyl sulfide and methane sulfonic acid. *Journal of Raman Spectroscopy* **40**: 972-981.

Blumentals, I., Itoh, M., Olson, G., and Kelly, R. (1990) Role of polysulfides in reduction of elemental sulfur by the hyperthermophilic archaebacterium Pyrococcus furiosus. *Applied and Environmental Microbiology* **56**: 1255-1262.

Brune, D.C. (1995) Sulfur compounds as photosynthetic electron donors. In *Anoxygenic Photosynthetic Bacteria*: Springer, pp. 847-870.

Dahl, C., and Prange, A. (2006) Bacterial sulfur globules: occurrence, structure and metabolism. In *Inclusions in Prokaryotes*: Springer, pp. 21-51.

De Gelder, J., Willemse-Erix, D., Scholtes, M.J., Sanchez, J.I., Maquelin, K., Vandenabeele, P. et al. (2008) Monitoring poly (3-hydroxybutyrate) production in Cupriavidus necator DSM 428 (H16) with Raman spectroscopy. *Analytical Chemistry* **80**: 2155-2160.

Eckert, B., and Steudel, R. (2003) Molecular spectra of sulfur molecules and solid sulfur allotropes. In *Elemental Sulfur und Sulfur-Rich Compounds II*: Springer, pp. 31-98.

Engel, A.S., Lichtenberg, H., Prange, A., and Hormes, J. (2007) Speciation of sulfur from filamentous microbial mats from sulfidic cave springs using X-ray absorption near-edge spectroscopy. *FEMS Microbiology Letters* **269**: 54-62.

Franz, B., Gehrke, T., Lichtenberg, H., Hormes, J., Dahl, C., and Prange, A. (2009) Unexpected extracellular and intracellular sulfur species during growth of Allochromatium vinosum with reduced sulfur compounds. *Microbiology* **155**: 2766-2774.

George, G.N., Gnida, M., Bazylinski, D.A., Prince, R.C., and Pickering, I.J. (2008) X-ray absorption spectroscopy as a probe of microbial sulfur biochemistry: the nature of bacterial sulfur globules revisited. *Journal of Bacteriology* **190**: 6376-6383.

Harvey, P.D., and Butler, I.S. (1986) Raman spectra of orthorhombic sulfur at 40 K. *Journal of Raman Spectroscopy* **17**: 329-334.

He, H., Xia, J.-L., Jiang, H.-C., Yan, Y., Liang, C.-L., Ma, C.-Y. et al. (2010) Sulfur species investigation in extra-and intracellular sulfur globules of Acidithiobacillus ferrooxidans and Acidithiobacillus caldus. *Geomicrobiology Journal* **27**: 707-713.

Janz, G., Downey Jr, J., Roduner, E., Wasilczyk, G., Coutts, J., and Eluard, A. (1976) Raman studies of sulfur-containing anions in inorganic polysulfides. Sodium polysulfides. *Inorganic Chemistry* **15**: 1759-1763.

Jørgensen, B.B., Revsbech, N.P., Blackburn, T.H., and Cohen, Y. (1979) Diurnal cycle of oxygen and sulfide microgradients and microbial photosynthesis in a cyanobacterial mat sediment. *Applied and Environmental Microbiology* **38**: 46-58.

Kappler, U., and Dahl, C. (2001) Enzymology and molecular biology of prokaryotic sulfite oxidation. *FEMS Microbiology Letters* **203**: 1-9.

Khan, S.A., Hughes, R.W., and Reynolds, P.A. (2011) Raman spectroscopic determination of oxoanions in aqueous polysulfide electrolyte solutions. *Vibrational Spectroscopy* **56**: 241-244.

Kletzin, A. (2008) Oxidation of sulfur and inorganic sulfur compounds in Acidianus ambivalens. In *Microbial Sulfur Metabolism*: Springer, pp. 184-201.

Kojima, H., Nakajima, T., and Fukui, M. (2007) Carbon source utilization and accumulation of respiration-related substances by freshwater Thioploca species. *FEMS Microbiology Ecology* **59**: 23-31.

Larkin, J.M., and Strohl, W.R. (1983) Beggiatoa, thiothrix, and thioploca. *Annual Reviews in Microbiology* **37**: 341-367.

Lettmann, K.A., Riedinger, N., Ramlau, R., Knab, N., Böttcher, M.E., Khalili, A. et al. (2012) Estimation of biogeochemical rates from concentration profiles: A novel inverse method. *Estuarine, Coastal and Shelf Science* **100**: 26-37.

MacGregor, B.J., Biddle, J.F., Siebert, J.R., Staunton, E., Hegg, E.L., Matthysse, A.G., and Teske, A. (2013) Why orange Guaymas Basin Beggiatoa spp. are orange: single-filament-genome-enabled identification of an abundant octaheme cytochrome with hydroxylamine oxidase, hydrazine oxidase, and nitrite reductase activities. *Applied and Environmental Microbiology* **79**: 1183-1190.

Mas, J., and Van Gemerden, H. (1987) Influence of sulfur accumulation and composition of sulfur globule on cell volume and buoyant density of Chromatium vinosum. *Archives of Microbiology* **146**: 362-369.

Meyer, B. (1964) Solid allotropes of sulfur. *Chemical Reviews* **64**: 429-451.

Mußmann, M., Hu, F.Z., Richter, M., de Beer, D., Preisler, A., Jørgensen, B.B. et al. (2007) Insights into the genome of large sulfur bacteria revealed by analysis of single filaments. *PLoS Biology* **5**: e230.

Nicolson, G.L., and Schmidt, G.L. (1971) Structure of the Chromatium sulfur particle and its protein membrane. *Journal of Bacteriology* **105**: 1142-1148.

Pasteris, J.D., Freeman, J.J., Goffredi, S.K., and Buck, K.R. (2001) Raman spectroscopic and laser scanning confocal microscopic analysis of sulfur in living sulfur-precipitating marine bacteria. *Chemical Geology* **180**: 3-18.

Pätzold, R., Keuntje, M., Theophile, K., Müller, J., Mielcarek, E., Ngezahayo, A., and Anders-von Ahlften, A. (2008) In situ mapping of nitrifiers and anammox bacteria in microbial aggregates by means of confocal resonance Raman microscopy. *Journal of Microbiological Methods* **72**: 241-248.

Pott, A.S., and Dahl, C. (1998) Sirohaem sulfite reductase and other proteins encoded by genes at the dsr locus of Chromatium vinosum are involved in the oxidation of intracellular sulfur. *Microbiology* **144**: 1881-1894.

Prange, A., Chauvistré, R., Modrow, H., Hormes, J., Trüper, H.G., and Dahl, C. (2002) Quantitative speciation of sulfur in bacterial sulfur globules: X-ray absorption spectroscopy reveals at least three different species of sulfur. *Microbiology* **148**: 267-276.

Prange, A., Arzberger, I., Engemann, C., Modrow, H., Schumann, O., Trüper, H.G. et al. (1999) In situ analysis of sulfur in the sulfur globules of phototrophic sulfur bacteria by X-ray absorption near edge spectroscopy. *Biochimica et Biophysica Acta (BBA)-General Subjects* **1428**: 446-454.

Prince, R.C., Stokley, K.E., Haith, C.E., and Jannasch, H.W. (1988) The cytochromes of a marine Beggiatoa. *Archives of Microbiology* **150**: 193-196.

Roy, A.B., and Trudinger, P.A. (1970) *The biochemistry of Inorganic Compounds of Sulphur*: Cambridge University Press.

Schauder, R., and Müller, E. (1993) Polysulfide as a possible substrate for sulfur-reducing bacteria. *Archives of Microbiology* **160**: 377-382.

Schedel, M., and Trüper, H.G. (1980) Anaerobic oxidation of thiosulfate and elemental sulfur in Thiobacillus denitrificans. *Archives of Microbiology* **124**: 205-210.

Schmidt, T., Arieli, B., Cohen, Y., Padan, E., and Strohl, W. (1987) Sulfur metabolism in Beggiatoa alba. *Journal of Bacteriology* **169**: 5466-5472.

Schmidt, T.M., and DiSpirito, A.A. (1990) Spectral characterization of c-type cytochromes purified from Beggiatoa alba. *Archives of Microbiology* **154**: 453-458.

Schwedt, A., Kreutzmann, A.-C., Polerecky, L., and Schulz-Vogt, H.N. (2012) Sulfur respiration in a marine chemolithoautotrophic Beggiatoa strain. *Frontiers in Microbiology* **2**: 276.

Steudel, R. (1989) On the nature of the "elemental sulfur"(S^0) produced by sulfur-oxidizing bacteria—a model for S^0 globules. *Autotrophic Bacteria*: 289-303.

Steudel, R., Holdt, G., Göbel, T., and Hazeu, W. (1987) Chromatographic separation of higher polythionates Sn^O 62⊖(n= 3… 22) and their detection in cultures of Thiobacillus ferroxidans; Molecular Composition of Bacterial Sulfur Secretions. *Angewandte Chemie International Edition in English* **26**: 151-153.

Strohl, W.R., and Larkin, J.M. (1978) Enumeration, isolation, and characterization of Beggiatoa from freshwater sediments. *Applied and Environmental Microbiology* **36**: 755-770.

Strohl, W.R., Geffers, I., and Larkin, J.M. (1981) Structure of the sulfur inclusion envelopes from four Beggiatoas. *Current Microbiology* **6**: 75-79.

Strohl, W.R., Howard, K.S., and Larkin, J.M. (1982) Ultrastructure of Beggiatoa alba strain B15LD. *Microbiology* **128**: 73-84.

Suzuki, I. (1965) Oxidation of elemental sulfur by an enzyme system of Thiobacillus thiooxidans. *Biochimica et Biophysica Acta (BBA)-General Subjects* **104**: 359-371.

Trüper, H.G. (1967) Orthorhombic sulphur formed by photosynthetic sulphur bacteria. *Nature* **215**: 435-436.

Vetter, R. (1985) Elemental sulfur in the gills of three species of clams containing chemoautotrophic symbiotic bacteria: a possible inorganic energy storage compound. *Marine Biology* **88**: 33-42.

Winogradsky, S. 1887. Über Schwefelbakterien. *Botanische Zeitung* **45**:489-610.

Zöphel, A., Kennedy, M., Beinert, H., and Kroneck, P. (1988) Investigations on microbial sulfur respiration. *Archives of Microbiology* **150**: 72-77.

SUPPLEMENTARY MATERIALS

Example of spectrum processing and a sulfate standard curve constructed from background-adjusted peak intensity for the S=O stretch of sulfate at 997 cm^{-1} (Fig. S1) and spectra of *Beggiatoa* sp. 35Flor showing the resonance peaks of cytochrome *c* at 757 and 1136 cm^{-1} visible under 532 nm but not 785 nm laser excitation (Fig. S2).

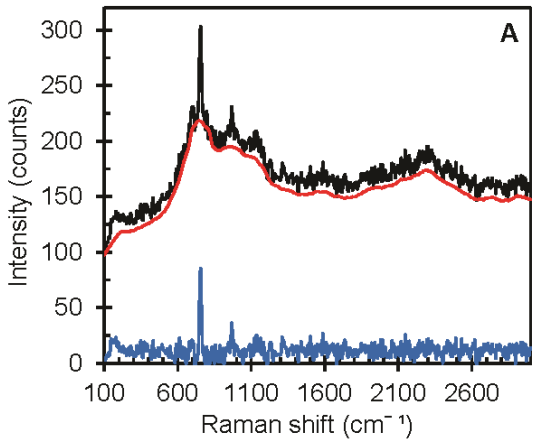

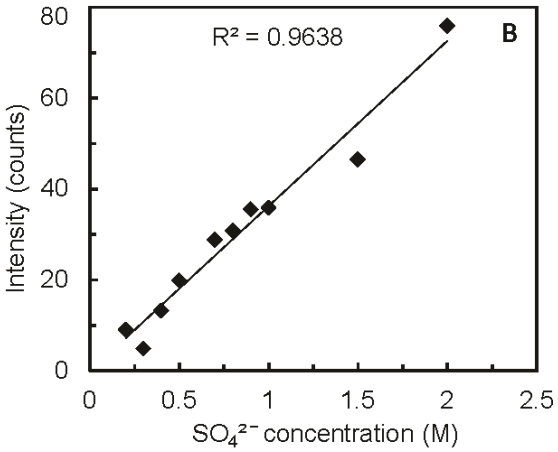

Intensive cryptic microbial iron cycling in the low iron water column of Lake Cadagno

Jasmine S. Berg[1], Dolma Michellod[1], Petra Pjevac[1,2], Clara Martinez-Perez[1], Caroline R.T. Buckner[1], Philipp F. Hach[1], Carsten J. Schubert[3], Jana Milucka[1], Marcel M.M. Kuypers[1]

[1]Department of Biogeochemistry, Max Planck Institute for Marine Microbiology, 28359 Bremen, Germany
[2]Division of Microbial Ecology, Department of Microbiology and Ecosystem Science, University of Vienna, Vienna, Austria
[3]Eawag, Swiss Federal Institute of Aquatic Science and Technology, Kastanienbaum, Switzerland

doi:-

submitted: *Environmental Microbiology*

Author contributions: JSB designed research. DM and JSB performed experiments. PP performed genomics analyses. CMP, CRTB, and CJB contributed data. JSB and PFH analysed data. JSB, JM, and MMK conceived, wrote, and edited this manuscript.

SUMMARY

Iron redox reactions play an important role in carbon remineralization, supporting large microbial communities in terrestrial and aquatic sediments where iron is abundant. Stratified water columns with comparably low iron concentrations are globally widespread, but microbial iron cycling in these systems has largely been ignored. We found evidence for unexpectedly high turnover rates of iron in the low (1-2 µmol·l-1) iron in the Lake Cadagno water column. Light-dependent, biological iron oxidation rates of 1.4-13.8 µmol·l-1·d-1 were observed, which is even higher than rates in ferruginous lakes with well-studied microbial iron cycles. This microbially-mediated iron oxidation by photoferrotrophs may account for up to 10% of total primary production in the chemocline. However, we could not detect the formation of any iron oxides which were presumably reduced immediately by heterotrophic iron-reducing bacteria. We could identify the iron-oxidizers and iron-reducers responsible for this intense iron cycling in 16S rRNA gene amplicon libraries and by the cultivation of some of these bacteria. Based on our combined results, we propose a model in which iron is oxidized by photoferrotrophs and microaerophiles, and iron oxides are immediately reduced by heterotrophic iron reducers, resulting in a cryptic iron cycle. We hypothesize that microbial iron cycling in water column redoxclines with low iron content, especially those within the photic zone, may be much more widespread than previously believed.

INTRODUCTION:

Although iron (Fe) is the fourth most abundant element in the earth's crust, the majority of it is bound in mineral form and therefore not readily accessible to living organisms. Iron is an extremely redox-sensitive element, oxidizing rapidly (at neutral pH) in the presence of oxygen to form poorly soluble iron-oxides or reacting with sulfide to form FeS and FeS_2 precipitates. Solid-phase iron therefore accumulates in sediments where large pools of reactive iron can be actively maintained through biotic and abiotic benthic iron cycling at redox transitions zones. Dissolved iron in porewaters can reach hundreds of micromolar, and reactive solid phase iron may be several 100-fold higher (e.g. Thamdrup et al., 1994). Concentrations of dissolved iron in water columns are generally much lower, from a few micromolar in lacustrine systems depending on inflow source (e.g. Davison et al., 1982; Nagai et al., 2007) to subnanomolar in the open ocean gyres (e.g. Johnson et al. 2003). Exceptions are stratified, ferruginous lakes such as Lake Matano, Indonesia and Lake La Cruz, Spain which contain hundreds of micromolar dissolved Fe(II) in the anoxic bottom waters (Crowe et al., 2008; Walter et al., 2014). Although these environments are rare today, they represent model systems for early Earth's ferruginous Archaean Ocean (Konhauser et al., 2002) and have therefore been subject of intense investigations.

The prokaryotes known to catalyze iron transformations are extremely diverse in phylogeny and metabolism. So far, microbial iron oxidation has been demonstrated with O_2, NO_2^-, NO_3^-, and N_2O in cultures and in the environment (e.g. (Emerson and Moyer, 1997; Straub et al., 1996; Benz et al., 1998). The lithotrophic iron oxidizers belong mainly to the phylum *Proteobacteria*, such as *Leptothrix* spp. (Fleming et al., 2013) or *Siderooxydans* spp. (Weiss et al., 2007). In

addition, some anoxygenic phototrophic bacteria such as *Chlorobium ferrooxidans* (Heising et al., 1999) and *Rhodomicrobium vannielli* (Heising and Schink, 1998) can oxidize iron using light as an energy source (Widdel et al., 1993). Organisms with photoferrotrophic potential are common in aquatic environments but their ecological role and quantitative contribution to iron cycling remain unknown. The microorganisms capable of iron reduction are also diverse (e.g. *Geobacter* spp*., Shewanella* spp*.,* and *Geothrix* spp*.*) and can utilize H_2 or simple organic carbon compounds as substrates (Lovley et al., 1993; Kostka et al., 1996; Coates et al., 1999). Up to 50% of carbon remineralization in marine sediments can be driven by microbial iron reduction (Thamdrup, 2000), and this number is expected to be even higher in low-sulfate, freshwater systems. All the microbes involved in iron redox transformations compete with the spontaneous oxidation of iron by O_2, NO_2^- and MnO_x and reduction by organic acids and sulfide (Thamdrup et al., 1994). Determining whether biotic or abiotic reactions control iron redox chemistry in different environments is still a major challenge.

The weak difference between the redox potentials of the Fe(II)/Fe(III) redox couple and O_2/H_2O and NO_3^-/N_2 means that Fe(II) oxidation is at the thermodynamic limit, generating very little energy. Furthermore, the redox transformation of iron is a one electron transfer process, which means large quantities of iron must be oxidized or reduced for microbes to gain sufficient energy for growth. It is therefore expected that microbial iron cycling predominantly occurs in environments with large pools of available iron. The importance of microbial iron cycling in stratified anoxic lakes with low iron content, which are globally widespread, is largely unknown. Provided that turnover rates are sufficiently rapid, however, coupled iron oxidation and reduction could recycle even a small iron pool enough times to significantly contribute to the

energy flux and element cycling in a system. This type of closed microbial iron cycle has previously been demonstrated in the laboratory where heterotrophic iron reduction is directly coupled to iron oxidation with nitrate (Straub et al., 2004; Coby et al., 2011) and/or light (Melton et al., 2012). It has also recently been shown that microscale microbial iron cycling occurs in coastal marine sediments (Laufer et al., 2015). It is currently unknown whether such cryptic iron cycling can occur at oxic-anoxic interfaces in stratified lakes where iron concentrations are low and oxidized Fe(III) may immediately be reduced to Fe(II) and vice versa.

We investigated potential for microbial iron cycling in the permanently stratified Lake Cadagno where steep gradients of physicochemical parameters, nutrients, and trace metals point to high fluxes and thus high microbial activity. This lake has been cited as an Archaean ocean analogue (Canfield et al., 2010) for the study of sulfur cycling processes due to its low (1-2 $mmol \cdot l^{-1}$) sulfate concentrations relative to the modern oceans. However, sulfate is still sufficient to fuel sulfate reduction in the sediments and monolimnion. The ~2 m thick chemocline of Lake Cadagno remains both sulfide- and oxygen-free due to the activity of large populations of anoxygenic phototrophs (Tonolla et al., 1999; Storelli et al., 2013). In the absence of measureable nitrate and nitrite (Halm et al., 2009; Milucka et al., 2015) iron and manganese are the next likely alternative electron acceptors/donors for bacteria in the chemocline. We investigated the microbial potential for iron cycling in Lake Cadagno because it is representative of many present-day lakes which develop seasonal stratification with sulfidic bottom waters (see ref Holmer and Storkholm, (2001) for review). Manganese is discussed here alongside iron because of its tight link to the iron cycle. By combining results from chemical flux

measurements, molecular analyses, and cultivation experiments, we created a model of the iron cycle in aquatic, low iron environments.

RESULTS & DISCUSSION

In situ fluxes and rates

We measured *in situ* chemical profiles in Lake Cadagno both in Aug 2013 and Aug 2014 over the span of several days and under different light conditions to monitor potential changes in iron chemistry and related physico-chemical parameters over time. The representative example night and day profiles from August 2014 (Fig 1) reveal strong stratification of the lake with opposing gradients of oxygen and sulfide separated by a distance of ~2 m. The chemocline, defined as this 2 m region between the oxycline and the sulfidic monolimnion, coincided with a turbidity maximum where the total microbial cell numbers were on the order of 10^6-10^7 cells ·ml^{-1}. Conservative parameters such as conductivity (Ω) were constant throughout the layer indicating that it is well mixed. This relatively homogenous physico-

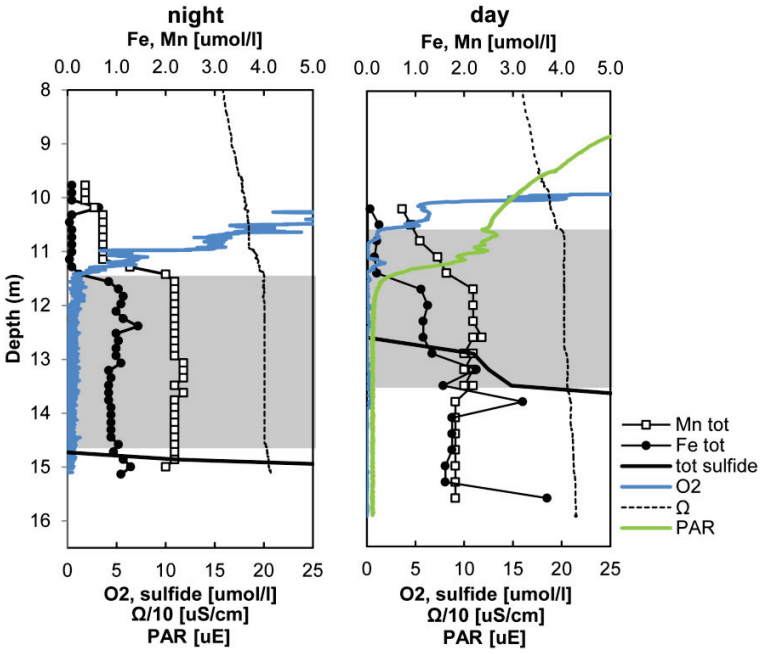

Figure 1: Chemical profiles measured after a full dark period, just before sunrise (left) and during the day (right). Sulfide is a sum of total species H_2S + HS^- + S^{2-}. Only total Mn and Fe profiles are shown, because these were identical to Mn(II) and Fe(II). Values of conductivity shown are to a factor of 10^{-1}. The region of constant conductivity, circa 11-14.5 m depth, corresponds to the well-mixed chemocline and turbidity maximum (shaded gray region).

chemical structure has been attributed to bacterially-driven mixing (Wüest, 1994). The evident vertical up and down movement of this layer over time may be a response to light conditions in addition to surface wind-driven internal waves (Egli et al., 1998).

Both manganese and iron were present almost exclusively in the dissolved, reduced form in all profiles. Iron below 13 m depth (day profile; Fig 1) was likely in the form of FeS due to the presence of sulfide. The total iron concentrations (1-2 $\mu mol \cdot l^{-1}$) in Lake Cadagno were only a fraction of those measured in ferruginous lakes (up to 200 $\mu mol \cdot l^{-1}$) where active microbial iron cycling is expected (Crowe et al., 2008) or has been demonstrated (Walter et al., 2014). The night profile (Fig 1), taken after a full 10 hours of darkness, was characterized by a redox zonation with electron acceptors (O_2, Mn, Fe, and SO_4^{2-}) apparently consumed in succession according to decreasing energy yield. In the night profile, both manganese and iron gradients correlated with conductivity suggesting that the distribution of these metals is determined by turbulent mixing within the chemocline. Dissolved manganese and iron disappeared at the oxycline as they were oxidized with O_2. However, in the profile taken at midday, gradients of manganese and iron indicated their consumption well below the oxycline (Fig 1). In this case, the independent behavior of manganese and iron from conductivity, which showed no gradient, indicates that these metals must be consumed faster than the rate of mixing in the layer. The calculated iron fluxes in Lake Cadagno (Table 1) were extremely

Table 1: Calculated ferrous iron fluxes and oxidation rates and fluxes in Lake Cadagno chemocline for each sampling period. The maximum and minimum turbulence coefficients experimentally determined in Uhde (1992) and Wüest (1994).*Lake La Cruz values from Walter et al. (2014). **Lake Matano values from Crowe et al (2008).

	D cm^2 s^{-1}	Fe(II) flux μmol cm^{-2} s^{-1}	Fe(II)-oxidation μmol l^{-1} d^{-1}
Lake Cadagno day	0.016-0.15	0.042-0.392	1.386-13.756
Lake Cadagno night	0.016-0.15	0.027-0.250	0.648-6.070
*Lake La Cruz	0.0005-0.004	0.031-0.244	0.174-1.396
**Lake Matano	0.0069-0.057	0.034-0.270	0.034-0.270

high, ranging from 0.027-0.392 µmol·cm^{-2}·d^{-1}, using the most and least conservative turbulence coefficients (*D*) reported for Lake Cadagno, respectively (Wüest, 1994). Interestingly, these calculated fluxes were comparable to the reported iron fluxes in the ferruginous Lake La Cruz and Lake Matano, which have 100-fold higher iron concentrations (Crowe et al., 2008; Walter et al., 2014; see also Table 1). This is likely due to the steep gradients with a consumption zone over cm rather than m, and relatively high turbulence (large *D* values). This high flux implies high turnover rates and a potential for intensive biotic and abiotic cycling of iron.

Steep gradients of dissolved metals suggest that manganese and iron are consumed below the oxycline via oxidation processes generating particulate metal that tend to sink in the water column. The oxidation of iron and manganese can be driven biotically or abiotically with oxygen. It is also possible that manganese serves as an oxygen carrier, forming MnO_x particles at the oxycline that rapidly oxidize iron and thus regenerating Mn(II). We tested this abiotic potential for iron oxidation by MnO_x by incubating lake water with added hydrous MnO_2 under alternating light and dark conditions (Fig S1). The addition of MnO_2 at 5-fold higher concentrations than lake water iron caused a complete oxidation of iron within the 15 min time period between MnO_2 addition and taking the first sample (t_0). Indeed, it is known that the reaction of MnO_2 with Fe(II) is almost instantaneous at > 1 µM concentrations and circumneutral lake water pH (Lovley and Phillips, 1988b; Myers and Nealson, 1988). Thus, manganese could be partially responsible for iron oxidation in the Lake Cadagno chemocline.

Light is an important factor regulating iron speciation by stimulating *in situ* oxygen production, driving anoxygenic phototrophic iron oxidation, or by direct photooxidation of iron (Braterman et al., 1983). In the day profile, the zone of iron consumption between 11 and 11.5 m coincided

with the sharp decrease in light intensity from 3.2 to 0.5 µE m^{-2} s^{-1} of photosynthetically active radiation (PAR). Given that the photolysis of Fe^{2+} has only been shown to occur with UV light at pH > 6.5 (Braterman et al., 1983), this process is unlikely to contribute significantly to iron turnover in Lake Cadagno). The lower threshold for oxygenic photosynthesis in freshwater is estimated to be 0.09 µE m^{-2} s^{-1} (Gibson, 1985; Raven et al., 2000) and therefore *in situ* oxygen production could fuel microaerophilic iron oxidation. Indeed, oxygenic photosynthesis in the upper part of the anoxic zone has previously been shown to play a major role in methane removal (Milucka et al., 2015). Because oxygen concentrations remained below detection limits, we could not assess the contribution of microaerophilic iron oxidizing bacteria based only on the chemical profiles. It has been shown that photoferrotrophs can thrive by oxidizing iron at comparably low light intensities (Llirós et al., 2015). It is likely that at these organisms play an important role in the chemocline considering the abundance of anoxygenic phototrophs in this zone. Photoferrotrophy is consistent with our observations that iron was consumed about 1 m below the oxycline during daylight hours, while iron and oxygen gradients intersected during the night (Fig 1). In sum, mainly light-driven processes are likely responsible for the oxidation of iron during the day, whereas oxidation of iron appears to be primarily driven by downwards-diffusing oxygen and/or Mn oxides in the dark.

Integrating the iron flux over the steep gradient region just below the oxycline, we obtained iron oxidation rates of 1.393-13.064 µmol $Fe \cdot l^{-1} \cdot d^{-1}$ during the day and 0.648-6.070 µmol $Fe \cdot l^{-1} \cdot d^{-1}$ at night. These light oxidation rates are very similar to rates of phototrophic iron oxidation estimated from Lake La Cruz (Table 1). The iron-oxidizing anoxygenic phototrophs use the following reaction to drive CO_2 fixation (Ehrenreich and Widdel, 1994):

(1) $HCO_3^- + 4Fe^{2+} + 10H_2O \rightarrow CH_2O + 4Fe(OH)_3 + 7H^+$

Assuming that photoferrotrophs account for all of the daylight iron oxidation in the chemocline, we calculated the amount of CO_2 fixed using the stoichiometry in equation (1). The estimated contribution of phototrophic iron oxidation to the total daytime carbon fixation processes in the chemocline of Lake Cadagno is 0.348-3.267 µmol $C \cdot l^{-1} \cdot d^{-1}$. With respect to average light carbon fixation rates of 23.7 µmol $C \cdot l^{-1} \cdot d^{-1}$ measured in 2014, photoferrotrophic activity could account for up to 10 % of the total primary production. Considering that phototrophic sulfide oxidation is responsible for up to 85% (Musat et al., 2008) of total carbon fixation in the chemocline, iron cycling could make up a large fraction of the remaining carbon fixation processes.

The failure to detect any oxidized manganese or iron species suggests that oxidation and reduction processes must be tightly coupled. In other words, no net oxidation could be observed because oxides were reduced as rapidly as they were formed. Oxidized manganese and iron can be reduced by bacteria utilizing simple organic carbon compounds or H_2 (Lovley and Phillips, 1988a). High primary productivity at and above the chemocline (Del Don et al., 2001) likely supplies ample organic compounds for bacterial iron reduction. Alternatively, sulfide can chemically reduce iron and manganese resulting in the formation of FeS and S^0 and various other products (Canfield, 1989; Thamdrup et al., 1994). According to Canfield et al., 2010), the highest rates of sulfate reduction in the water column occurred within the mixed bacterial layer, although no free H_2S was detected there. Because it is possible that any sulfide produced is immediately consumed, we used the same sensitive radiotracer method as (Canfield et al., 2010) to measure sulfate reduction rates at various depths. In contrast to (Canfield et al., 2010), we did not detect any sulfate reduction in the chemocline above the

sulfidic zone (data not shown). However, sulfide could also be formed from sulfur reduction or disproportionation. Low concentrations (0.6 μmol·l^{-1}) of reduced sulfur could occasionally be measured within the chemocline in the dark (Fig S2). Sulfide reacts rapidly with Fe (III) or Fe(II) to form FeS (Pyzik and Sommer, 1981), which is detected as total sulfide by the Cline (1969) method. It is therefore possible that when photosynthetic sulfide oxidation ceases in the dark, heterotrophic bacteria compete with abiotic Fe(III) reduction by sulfide.

Overall, our results confirm that zones of iron reduction and sulfate reduction in Lake Cadagno are spatially separated. This is in contrast to recent findings by (Hansel et al., 2015) that even in sulfate-poor environments, sulfur cycling largely drives iron cycling in a manner inverse to thermodynamic predictions. Hansel *et al.* did not observe microbial iron respiration until sulfate in the system was depleted by sulfate-reducing microorganisms. In Lake Cadagno, iron reduction is not fueled by sulfate reduction despite the ~1 mmol·l^{-1} available sulfate in the chemocline. It is therefore not possible to generalize that sulfur cycling is the dominant force in iron cycling, but the environmental factors governing the competition between iron-reducing and sulfate-reducing bacteria remain to be investigated.

Diversity of putative iron-oxidizing and -reducing bacteria

We investigated the diversity of putative iron-oxidizing and -reducing bacteria by 16S rRNA gene amplicon sequencing from the chemocline in 2013 and 2014. A total of 213,726 sequences were recovered from 2013, which clustered into 8,395 operational taxonomic units (OTUs) at 98% sequence identity, whereas the 159,032 sequences recovered from 2014 clustered into 7,221 OTUs. Taxonomic classification based on closest BLAST hit revealed that majority of 16S rRNA gene sequences, ~63 % from libraries from both 2013 and 2014, affiliated with the purple sulfur

bacteria from the genus *Chromatium* (Fig 2). Among the remaining 16S rRNA gene sequences, we identified putative Fe(II)-oxidizers and Fe(III)-reducers based on close sequence affiliation with known iron-oxidizing and -reducing organisms. Approximately 6-7% of all sequences affiliated with known Fe(III)-oxidizing bacteria, and 1% affiliated with known Fe(III)-reducers. It is likely that the full diversity of iron cycling bacteria was underestimated here because many

Figure 2: Bacterial 16S rRNA gene amplicon libraries from the chemocline of Lake Cadagno in 2013 and 2014. Sequences were classified based on best BLAST hit results, and putative iron metabolizing bacteria were identified based on phylogenetic affiliation with known iron oxidizers and reducers.

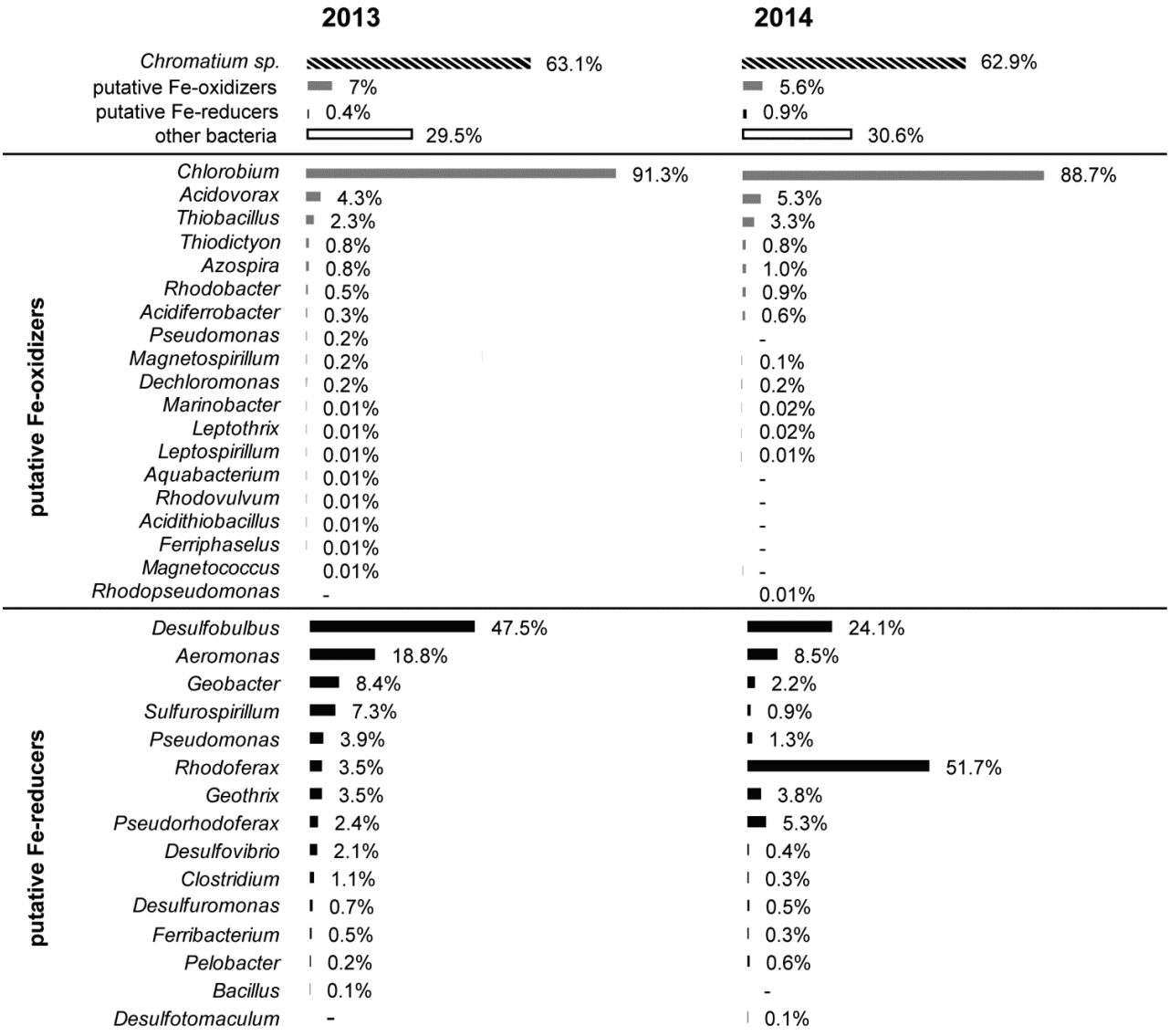

sequences affiliated with groups containing no cultured representatives and as such their metabolism is not yet known.

The fraction of bacteria capable of iron reduction was comprised of heterotrophs capable of reducing iron directly (e.g. *Geobacter, Geothrix*) or indirectly (e.g. *Pseudomonas, Clostridium*). The bacteria capable of iron oxidation were comprised of both phototrophic bacteria (e.g. *Chlorobium*, *Rhodobacter*) and microaerophilic as well as nitrate-reducing chemotrophic bacteria (e.g. *Leptothrix*, *Leptospirillum*). Sequences from microaerophilic Fe(II)-oxidizers accounted for less than 10% of the sequences of putative Fe(II)-oxidizing bacteria. A few of the bacteria identified are capable of biomineralizing iron without utilizing it for energy gain (e.g. *Magnetospirillum*). These magnetotactic bacteria contribute to the fate of iron by manufacturing magnetosomes composed of mixed valence iron, either as magnetite (Fe_3O_4) or greigite (Fe_3S_4).

Cryptic iron cycling in a co-culture of iron-oxidizing and -reducing bacteria

Although the 16S rRNA gene amplicons revealed a potential for microbial iron cycling in the water column of Lake Cadagno, it remained to be demonstrated that these bacteria were truly capable of actively oxidizing or reducing iron. We set up enrichment cultures using water collected in August 2013 to investigate which of the organisms might be involved in iron cycling in Lake Cadagno. Fe(II) and acetate were added in a 10:1 ratio to lake water in anoxic serum bottles which were incubated under light of wavelength >780 nm to prevent oxygenic photosynthesis. After 3 months, a pink-to-orange coloration developed, suggesting the formation of iron oxide and/or photopigments. 16S rRNA gene clone libraries of this enrichment culture revealed 4 relevant groups of bacteria: *Rhodomicrobium* sp., *Rhodoferax* sp., *Geothrix*

sp., and *Chlorobium* sp. (Table S1). Cells tended to form aggregates in which close relatives of the known photoferrotroph *Rhodomicrobium vannielii* could be easily identified under the microscope based on its conspicuous stalk-like morphology (Fig S3a). Active iron oxidation by *R. vannielii*-like cells was evidenced in culture by cell encrustation in Fe-P oxides (Fig S3b,c,d). It is unlikely that such encrustation occurs in the water column where *in situ* iron and phosphate concentrations are much lower, and encrustation and aggregation of bacteria would cause them to sink out of the photic zone. Another member of the enrichment culture was closely related to *Rhodoferax ferrireducens*, which can reduce iron with acetate (Finneran et al., 2003) and was among the most abundant sequence (51.7%) of iron-reducers recovered from *in situ* samples in 2014. *Geothrix fermentans* and other *Geothrix*/*Geobacter* species are also capable of reducing iron with acetate, formate, and other short-chain fatty acids (Coates et al., 1999; Lovley et al., 1993; Caccavo et al., 1994). The remaining sequences from the enrichment belonged to anaerobic *Firmicutes* which were presumably growing by mixed fatty acid fermentation. In 2014 we were able to enrich bacteria closely related to *Chlorobium ferrooxidans* and *Rhodopseudomonas pseudopalustris*, the most abundant photoferrotrophs identified in our *in situ* 16S rRNA gene amplicon libraries, by adding Fe(II) and acetate (Table S1). It was thus apparent that although in our enrichment we targeted iron-oxidizing bacteria with the addition of Fe(II), we had simultaneously enriched Fe(III)-reducers. We speculate that the iron reducing bacteria in our cultures thrived on oxidized iron produced by phototrophic iron oxidizers. Our data suggest that these consortia were originally present in the lake water and readily re-established in our *in vitro* incubations.

To monitor whether iron cycling processes were linked to microbial growth, we set up incubations with iron and ^{13}C-DIC or ^{13}C-acetate using the enrichment culture dominated by *R. vannielii*- and *R. ferrireducens*-like bacteria. Fe(II)-sulfate was added to the cultures which had accumulated Fe(III) over time, resulting in a 50:50% mixture of Fe(II):Fe(III) and ultimately targeting the activity of both the iron oxidizers and reducers. During the 48 h incubation period, the iron speciation fluctuated slightly under both light and dark conditions as compared to the killed control (Fig 3a). This could be due to the delicate balance between oxidation and reduction processes, or the heterogeneous distribution of bacterial aggregates in replicate tubes. Overall, in dark incubations, we observed that Fe(II) concentrations continued to increase after 2 to 3 weeks and only 10% of Fe(III) remained. On the contrary, no net phototrophic iron oxidation could be observed in the light, presumably because heterotrophs immediately consumed Fe(III) products thus generating a cryptic iron cycle.

As with our *in situ* measurements, it was not possible to demonstrate microbial iron oxidation activity in our incubations based on changes in iron speciation alone. However, by measuring ^{13}C-CO_2 uptake into biomass (Fig 3b) we could detect light-dependent CO_2 fixation which was likely performed by the only potential autotroph in our cultures, the *Rhodomicrobium vannielii*-related bacteria. The carbon fixation rate was not linear, possibly due to heterogeneous activity of bacteria within aggregates, as heavily iron-encrusted bacteria (Fig S3b) were likely not active. Because of the variability in carbon assimilation in our time series, we calculated both a minimum carbon fixation rate (linear regression through t_0, t_2, t_3, and t_4; r^2 = 0.952) and a maximum carbon fixation rate (linear regression through t_0, t_1, and t_6; r^2 = 0.714), giving rates of 1.2 µmol C $l^{-1}{\cdot}d^{-1}$ and 7.6 µmol C $l^{-1}{\cdot}d^{-1}$, respectively. Based on these rates and using the

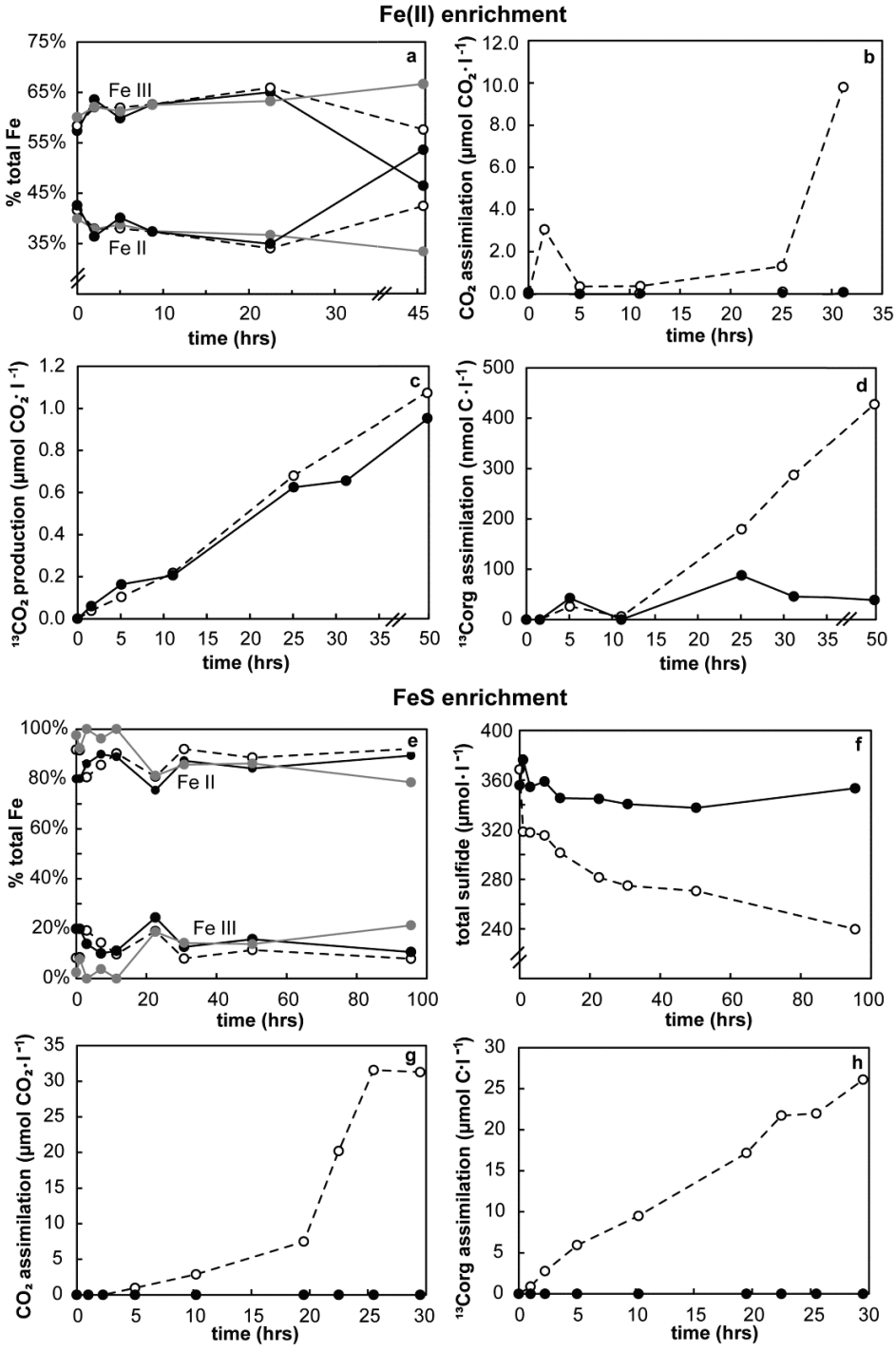

Figure 3: Top four panels from incubations performed with enrichment cultures grown on Fe(II) show iron speciation (a) and parallel carbon uptake measurements: CO_2 assimilation (b) in the presence of 13C-HCO_3^-, production of $13CO_2$ (c) and assimilation of 13C into biomass (d) in the presence of 13C-acetate and 13C-formate mixture. Lower four panels from incubations performed with enrichment cultures grown on FeS show iron speciation (e), sulfide (f), and parallel carbon uptake measurements: CO_2 assimilation (g) in the presence of 13C-HCO_3^-, and assimilation of 13C into biomass (h) in the presence of 13C-acetate. Symbols indicate light (○), dark (●) and the killed control + light (●) conditions.

stoichiometry from equation 1, we determined iron oxidation rates in the range of 4.9-30.6 µmol Fe $l^{-1} \cdot d^{-1}$. These rates are well within the range of volumetric iron oxidation rates experimentally determined for purple sulfur and non-sulfur bacteria (100-200 µmol Fe $l^{-1} \cdot d^{-1}$) at light intensities similar to our experiments (Hegler et al., 2008). Contrary to our expectations, the iron oxidation rates determined from our incubations were only slightly higher than the rates calculated from iron gradients in the lake (1.3-13.1 µmol Fe $l^{-1} \cdot d^{-1}$). We anticipated the *in vitro* rates to be much higher because iron cycling bacteria were highly enriched in our cultures and because we conducted experiments at higher than *in situ* light intensities. It has been shown that microbial iron oxidation rates are dependent on both light quality and light intensity (Straub et al., 1996), and the light level at the top of the chemocline is on average 1-2% of surface radiation (see PAR profile, Fig 1), or much lower than in our incubations. One explanation for these comparable iron oxidation rates is that the use of a light filter >750 nm halted oxygenic photosynthesis, which may in part contribute to iron oxidation *in situ*. In fact, this indicates that photosynthetic oxygen production is coupled to microaerophilic iron oxidation to a large extent, despite the low relative sequence abundance of microaerophilic Fe(II)-oxidizers compared to anaerobic Fe(II)-oxidizers in our 16S rRNA gene amplicon libraries.

Respiration of added ^{13}C-acetate and ^{13}C-formate, used as a proxy for heterotrophic activity, was measured as $^{13}CO_2$ production. As expected, $^{13}CO_2$ concentrations increased linearly in a light-independent manner (Fig 3c). The calculated CO_2 production rate was 5.8 µmol CO_2 $l^{-1} \cdot d^{-1}$. The respiration of acetate and formate with iron are stoichiometrically different. The oxidation of acetate to CO_2 coupled to iron reduction proceeds according to equation (2):

(2) $C_2H_3O_2^- + 8Fe^{3+} + 4\ H_2O \rightarrow 2HCO_3^- + 8Fe^{2+} + 9H^+$

Using the CO_2 production rate above, the iron reduction rate with acetate would be 23.2 µmol $Fe \cdot l^{-1} \cdot d^{-1}$. Alternatively, *Geothrix fermentans* and related organisms are known to utilize formate as an electron acceptor for iron reduction (Coates et al., 1999) with the following stoichiometry:

(3) $HCOO^- + 2\ Fe^{3+} + H_2O \rightarrow HCO_3^- + 2Fe^{2+} + 2H^+$

This converts to an iron reduction rate in our cultures of 11.6 µmol $Fe \cdot l^{-1} \cdot d^{-1}$. Therefore, we can approximate that the true iron reduction rate lies somewhere within the range of 11.6-23.2 µmol $Fe \cdot l^{-1} \cdot d^{-1}$, depending on the ratio of organic carbon compounds respired. These calculated *in vitro* iron reduction rates were very similar to the *in vitro* iron oxidation rates (4.9-30.6 µmol Fe $l^{-1} \cdot d^{-1}$) and this close balance between iron oxidation and reduction rates might explain why no net changes in iron speciation could be observed in our light incubations. This tight coupling of oxidation and reduction processes may also regulate iron speciation in the lake. There, the predominance of Fe(II) species indicates that Fe(III) is limiting because it is consumed before it can be detected, and thus iron reduction proceeds more rapidly than iron oxidation.

A fraction of the labeled organic compounds was also assimilated into biomass for growth. Evidently, uptake of ^{13}C-labeled fatty acids occurred both in the dark and the light (Fig 3d), but the much higher ^{13}C assimilation in the light can most likely be attributed to photoassimilation of ^{13}C-acetate by *Rhodomicrobium* sp. It has previously been shown that phototrophic growth of *R. vannielii* with Fe(II) as the electron donor was stimulated by the addition of acetate (Heising and Schink, 1998).

Microbial FeS oxidation

Due to the scavenging of iron by sulfides, significant iron cycling is not expected to occur in euxinic lakes where FeS particulates settle out of the water column. The periodic appearance

and disappearance of FeS in the Lake Cadagno chemocline suggests the potential for rapid microbial recycling of FeS rather than removal via sedimentation. Because bacteria in the lake are most likely recurrently exposed to FeS, we investigated the capacity for microbial FeS utilization by setting up enrichment cultures with FeS as the sole electron donor. Cultures were also provided with a light source >750 nm. After about 6 months of continuous incubation, cultures were dominated by purple sulfur bacteria morphologically similar to *Thiodictyon* sp. that appeared to contain gas vacuoles allowing them to float at the liquid surface and sequences of *Thiodyction* sp. were also recovered in our 16S rRNA clone library (Table S2). *Thiodyction sp*. have been shown capable of oxidizing FeS to Fe(III) in culture (Kappler and Newman, 2004). Our enrichment culture also contained sequences closely related to *Ectothiorhodospira* sp., *Rhodoferax* sp., *Rhodomicrobium* sp., and some *Flavobacteria*- and *Cytophaga*-related sequences with low similarity (80-90%) to any cultured representatives (Table S2). Active FeS oxidation could be observed from the change in coloration of the medium from black, immediately after FeS addition, to colorless within a few days. We set up incubations with stable isotopes to monitor autotrophic and heterotrophic ^{13}C uptake linked to FeS cycling processes. Throughout the experiment, the percentage of reduced iron remained stable in the light, dark, and killed control conditions (Fig 3e). However, phototrophic sulfide oxidation occurred, as evidenced by the steady decrease in sulfide (Fig 3f) and a concomitant uptake of CO_2 (Fig 3g) into biomass in the light, but not in the dark. Our cultures appeared to preferentially oxidized sulfide, presumably due to the higher energy gain of S^{2-} relative to iron oxidation. Still, the recovery of many *Rhodoferax* sp. sequences suggests that after the depletion of sulfide, iron may be oxidized and serves as a substrate for this heterotrophic iron

reducer. ^{13}C-organic carbon (Fig 3h) was assimilated into biomass in the light. We did not, however, observe any organic carbon assimilation in the dark, nor did we observe any $^{13}CO_2$ production (from ^{13}C-organic carbon respiration) in the light or the dark. This implies that heterotrophs were not active in the presence of FeS as they lacked an electron acceptor. Instead, the organic carbon uptake in the light most likely resulted from photoassimilation of acetate by *Thiodictyon* sp. or *Ectothiorhodospira* sp. (Imhoff and Trüper, 1981; Peduzzi et al., 2012). We recovered not only sequences of *Thiodictyon* from our *in situ* 16S rRNA gene libraries, but also sequences of other bacteria such as *Rhodobacter* and *Chromatium* previously shown to oxidize FeS (Ehrenreich and Widdel, 1994). Overall, our experiments imply that FeS_x is not the ultimate sink for iron (nor sulfide), as bacteria in the Lake Cadagno chemocline can rapidly recycle this compound.

CONCLUSIONS

Because the redox transformation of iron involves the transfer of a single electron, it has generally been assumed that high iron concentrations are a prerequisite for substantial microbial energy gain from iron metabolism. Microbial iron-cycling may therefore seem negligible in a system like Lake Cadagno with only several micromoles per liter of reactive iron, especially because concentrations of oxygen, methane, and sulfide are orders of magnitude higher. Here we show that it is not the absolute concentration of the iron that is important, but rather its rate of turnover. High fluxes of iron in the Lake Cadagno chemocline are evidence for high rates of microbial iron oxidation and reduction. Remarkably, these fluxes and rates are on the same order of magnitude as iron fluxes in ferruginous lakes where microbial iron cycling has previously been studied. It appears that microbial redox transformations of iron are important

in terms of energy generation and carbon turnover in Lake Cadagno, supporting diverse populations of iron metabolizing bacteria. Moreover, distinct populations of chemotrophic and phototrophic iron oxidizers coexist on this limiting substrate although it is not clear if these different microbes are in direct competition with one another or if they are adapted to specific light and chemical conditions. Light is an important driver in the Lake Cadagno iron cycle, intensifying microbial iron cycling either through direct stimulation of photoferrotrophy or indirectly fueling microaerophilic iron oxidation by stimulation of *in situ* oxygen production by photosynthetic algae.

Figure 4: Schematic representation of the proposed cryptic Fe cycle in the Lake Cadagno water column. Only reactions relevant to the lake are shown. Shaded purple region represents the chemocline.

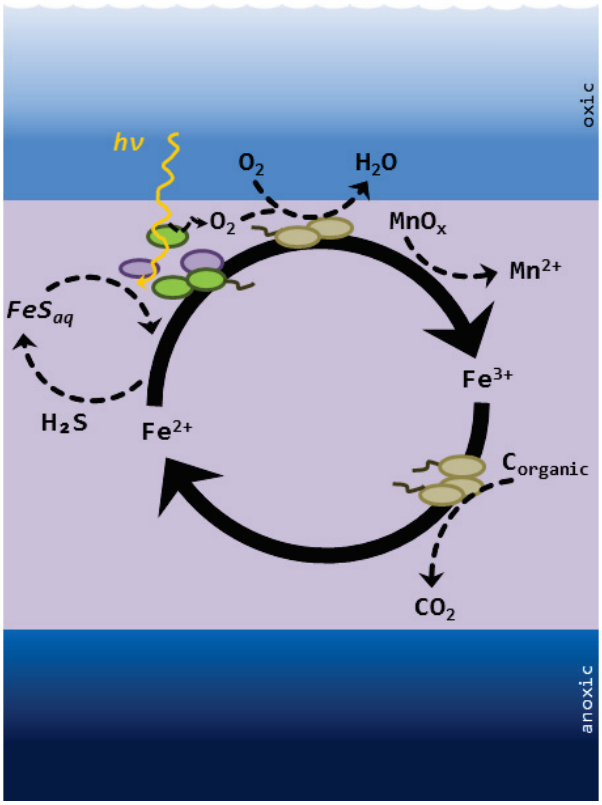

Our profiles indicate that Mn may also be intensively recycled at the chemocline of Lake Cadagno and strongly impacts the iron cycle. The flux of manganese (0.049-0.458 µmol $Mn \cdot cm^{-2} \cdot d^{-1}$) was even higher than the iron flux, revealing a large potential for microbial activity. Traditionally, manganese species have been measured as dissolved [Mn(II)] and particulate [Mn(IV)] fractions due to methods limitations in distinguishing these fractions directly. Recently, the more unstable Mn(III) species was shown to be an important intermediate in Mn redox cycles at oxic-anoxic interfaces (e.g. Trouwborst et al., 2006;

Madison et al., 2013). Using new methods to detect Mn(III) photometrically (Madison et al., 2011), it may be possible to elucidate a microbially-driven manganese cycle in Lake Cadagno as well.

Finally, our enrichment cultures served as a model for processes occurring in Lake Cadagno with co-existing populations of bacteria simultaneously oxidizing and reducing iron. This tight coupling between the oxidative and reductive reactions generates an invisible or "cryptic" iron cycle (Fig 4). Whereas iron oxidation in our *in vitro* incubations ceased in the dark, nighttime iron oxidation in the lake could be continuously driven by oxygen diffusing downwards from the oxycline or by sinking manganese oxides. These laboratory observations help to explain the *in situ* profiles of ferrous iron and emphasize that the failure to detect any reaction intermediates or net changes over time is not evidence of zero activity. Moreover, we must revise the common assumption that active iron cycling is negligible in stratified waters containing low iron concentrations. Given that such shallow, seasonally stratified, low-iron lakes are common, cryptic iron cycling may be a widespread process on modern Earth and not restricted to the ferruginous Archaean ocean.

EXPERIMENTAL PROCEDURES

Sampling

Lake Cadagno is a meromictic alpine lake located in the Piora valley, Switzerland. Samples were taken on field trips in August 2013, September 2013, and August 2014. For sampling and *in situ* measurements a profiling ion analyzer (see Kirf et al., 2014 for description) was lowered from a platform anchored at the deepest part of the lake (20.7 m). Conductivity, turbidity, depth (pressure), temperature and pH were measured with a multi-parameter probe (XRX 620, RBR).

Dissolved oxygen was recorded online with two micro-optodes with detection limits of 125 nM (normal) and 20 nM (trace) (types PSt1 and TOS7, PreSens). Samples for Winkler titration were taken from the lake surface to calibrate the oxygen sensors. Water samples for chemical analyses and cell counts were taken with a rosette syringe sampler equipped with twelve 60-ml syringes which were triggered online at the appropriate depths. The night profile from August 2014 was measured with a SBE 19 plus V2 CTD probe (Sea-Bird Electronics, WA, USA) with attached sensors for pressure, temperature and conductivity, and with additional sensors for turbidity (WET Labs Eco), oxygen (SBE 43), pH (18-I) and two fluorescence wavelengths (WET Labs ECO-AFL, FL, USA). Samples were obtained using a pump-cast system, pumping water through a tube attached to the CTD and filling 60-ml syringes on board after rinsing twice with the pumped water.

Filtered (0.22 µm pore size) samples for iron speciation were fixed immediately with ferrozine reagent. Filtered (0.45 µm pore size) and unfiltered samples for total manganese and iron were added to vials containing HNO_3 to a final concentration of 0.1M. Sulfide samples were fixed with Zn-acetate to a final concentration of 0.1 % (w/v). Water samples for incubation experiments and molecular analyses were pumped through clean tubing attached to the CTD and collected in 1 L Duran bottles. Bottles were stored at 4°C in the dark until further processing. Samples for catalyzed reporter deposition-fluorescence in situ hybridization (CARD-FISH) analysis were immediately fixed with 2% (v/v) formaldehyde. Samples for DNA analysis were filtered onto polycarbonate filters (0.22 µm pore size) on site and frozen at -20°C until further processing.

Analytical Techniques

Iron and sulfide were measured spectrophotometrically using the ferrozine method (Stookey, 1970) and the Cline (1969) methods, respectively. Total and dissolved iron and manganese were measured by inductively coupled plasma optical emission spectrometry (Optima 3300 R ICP-OES; PerkinElmer, Waltham, MA, USA). Sulfate was measured on a 761 Compact ion chromatograph (Metrohm, Filderstadt, Germany) equipped with a Metrosep A SUPP 5 column.

Sulfate reduction rates were measured in duplicates at four depths: 12, 13, 14 and 15 m. The radiotracer $^{35}SO_4^{2-}$ (5 MBq) was added to lake water incubated anoxically in 50-ml glass syringes. The ~20 µmol·l^{-1} background zero-valent sulfur served as a trap for any $H_2{}^{35}S$ that might be re-oxidized. At each sampling point, 10 ml of sample was dispensed into 5 ml of 20% (w/v) Zn-acetate. Reduced sulfur species (e.g. sulfur and sulfide as ZnS) were separated out via the chromium distillation method described in Kallmeyer et al., (2004) and the radioactivity per sample was determined via scintillation counting (Packard 2500 TR).

Flux Calculations

Turbulent fluxes (J) of iron and manganese within the mixed chemocline were calculated assuming steady state by applying Fick's first law: $J=-D\partial C/\partial x$. The maximum concentration change of total dissolved iron (∂C_{Fe}) was computed over 30 cm and 41.25 cm (∂x) in light and dark profiles (Fig 1), respectively, at the top of the chemocline where steep gradients exist. The change in total dissolved manganese (∂C_{Mn}) was calculated over 150 cm and 41 cm in light and dark profiles, respectively. Reported turbulent diffusion coefficients for the Lake Cadagno water column (that is, Eddy diffusivity D) are 1.6×10^{-6} m^2 s^{-1} at the chemocline boundaries and 1.5×10^{-5} m^2 s^{-1} within the chemocline (Wüest, 1994). We used these values as the minimum and maximum turbulence coefficients to calculate the upper and lower limits to iron fluxes.

***In situ* water incubations**

The 1-L Duran bottles with water collected from chemocline were bubbled with N_2 for 15 min to remove any contaminant O_2. Experiments to monitor the interaction of Fe and Mn were performed by supplementing water with hydrous MnO_2, prepared according to Golden et al. (1987). Water was distributed anoxically into 50-ml glass Winkler bottles and sealed with no headspace. Bottles in the incubation series were maintained at 4-6°C in a water bath and exposed to approximately 6 h darkness, 12 h light, and then 4 h darkness. At each sampling time point a bottle was sacrificed and sampled for iron, manganese, and sulfide as described above. CO_2 fixation rates were assessed separately by adding a ^{13}C-DIC solution to anoxic chemocline water to a final concentration of 200 µM (or 10% ^{13}C-DIC). The incubation series was performed in Winkler bottles at 4-6°C for 12 h in the light. Bottles were sampled destructively at each time point by concentrating ^{13}C-labeled biomass onto precombusted (6 h at 600 °C) GF/F filters (Whatman, St Louis, MO, USA). At the beginning of the experiment, a water sample was sterile-filtered into a glass HPLC vial to verify the ^{13}C-DIC labeling percentage.

Enrichment cultures

Water from the chemocline was distributed within an anoxic glove box (Mecaplex, Grenchen, Switzerland) into serum bottles containing N_2:CO_2 (90:10) headspace. To target Fe(II)-oxidizing bacteria, a sterile, anoxic solution of $FeSO_4$ was added to a final concentration of approximately 1 mmol·l^{-1}. To target FeS-oxidizing bacteria, a FeS solution was prepared by mixing equimolar concentrations of $FeSO_4$ and Na_2S and then added to Lake Water at concentrations of approximately 0.5 mmol·l^{-1}. Both cultures were periodically supplemented with 0.1 mmol·l^{-1} Na-acetate. Cultures were maintained at 10°C under a filter excluding light <750 nm to prevent the

growth of oxygenic phototrophs. After 2-3 months, Fe(II) cultures developed a faint reddish color, possibly due to purple bacterial pigments or the formation of ferric iron precipitates. The FeS cultures were colored black by the addition of FeS and turned clear after several days. Cultures were transferred to new artificial freshwater medium (see below) every 2-4 weeks for 1 year before experiments were performed.

Isotope labeling experiments

Freshwater medium was prepared according to the recipe of Pfennig (1991) for cultivation of purple and green non-sulfur bacteria using a concentration of 1-2 mmol·l^{-1} HCO_3^- to match *in situ* DIC concentrations. For incubations with Fe(II), approximately 0.5 mmol·l^{-1} $FeSO_4$ was added to medium mixed with enrichment culture to a ratio of 1:1. To monitor photoautotrophic iron oxidation, cultures received 2% ^{13}C-DIC and plus 100 µM acetate and 100 µM formate before being aliquoted anoxically as described above into Hungate tubes and sealed with rubber stoppers. Half of these tubes were incubated at room temperature in the light (~300 lux) and half of these were incubated in the dark. To monitor heterotrophic iron reduction, cultures received a mixture of 100 µM of 10% ^{13}C-labeled acetate ($^{13}CH_3{}^{13}CO_2$) and 100 µM of 10% ^{13}C-labelled sodium formate ($H^{13}COONa$) before being aliquoted anoxically into Hungate tubes and sealed with rubber stoppers. Half of these tubes were incubated in the light and half of these were incubated in the dark. After 0, 5, 11, 25, 31, and 50 hours a tube from each condition was sampled destructively for iron and carbon analyses. Iron species were measured immediately and diluted in 0.5 M HCl when necessary. Samples for ^{13}C incorporation into biomass were filtered as described above and parallel samples for $^{13}CO_2$ production measurements were sterile-filtered directly into glass HPLC vials and sealed with no headspace.

For incubations with FeS, approximately 0.5 mmol·l^{-1} FeS was added to medium mixed with enrichment culture to a 1:1 ratio. The resulting iron and sulfide concentrations measured were 450 µM and 350 µM, respectively, or a 100 µM excess of Fe(II). The incubation setup and sampling was identical to that described above, except that only 100 µM of 10% ^{13}C-labelled acetate was added. Additional samples were also taken for sulfide determinations by fixing in Zn-acetate to a final concentration of 1% (w/v).

Mass spectrometry isotope uptake analysis

Heterotrophic respiration of ^{13}C-acetate and ^{13}C-formate was measured as production of $^{13}CO_2$. For this, 1 ml of culture filtrate in HPLC vials was transferred into a 12 ml Exetainer (Labco Limited, High Wycombe, UK) and the headspace was exchanged with He. Samples were then acidified with the addition of ~100 µl concentrated H_3PO_4 so the outgassed $^{13}CO_2$ could be analyzed using a GasBench II coupled to a Delta Plus isotope ratio mass spectrometry (IRMS; Thermo Finnigan, Dreieich, Germany). The incorporation of ^{13}C from $^{13}CO_2$ or ^{13}C-labelled organic compounds into biomass was measured by combustion of the particulate organic carbon fraction on GF/F filters. Filters were first decalcified by incubation with 37% fuming HCl overnight, dried in an oven at 60°C, and packed into tin capsules for combustion analysis. The C-isotopic composition of particulate organic carbon in these experiments was determined by an automated elemental analyser (Thermo Flash EA, 1112 Series) coupled to a Delta Plus XP IRMS (Thermo Finnigan, Dreieich, Germany). Instrument accuracy and precision were estimated at 1.06589 ± 0.00079 ^{13}C atom% based on the mean and 3 standard deviations of caffeine standards measured in parallel with the samples.

SEM-EDS

Samples for SEM were fixed with 2% (v/v) formaldehyde for no more than 24 hours at 4°C and pelleted by centrifugation at 5000 RCF for 3 min. Cell pellets were washed with MilliQ water before dehydration in graded ethanol, followed by critical point drying (CPD). Because the harsh chemical treatment used in CPD tends to leach compounds from cells, samples for EDS analysis were simply fixed with formaldehyde, filtered onto gold-palladium sputtered filters, and washed with MilliQ. Dried aggregates or filter pieces were mounted on electrically conductive, adhesive stubs (Leit-Tab; Plano GmbH, Wetzlar, Germany). Imaging was performed with a FEI environmental field emission SEM Quanta 250 FEG (FEI, Eindhoven, Netherlands) at an electron energy of 2 keV using the Everhart-Thornley secondary electron detector (ETD). EDS measurements were performed at an electron energy of 10 keV with an EDS system Quantax 400 with an XFlash 6/30 double detector system (Bruker Nano GmbH, Berlin, Germany). The detectors have an energy resolution of < 123 eV at MnKα.

CARD-FISH

Samples were fixed with 2 % (v/v) formaldehyde for 24 hours at 4°C and filtered onto 0.2 µm polycarbonate filters (Millipore). CARD-FISH was performed on filter pieces following the protocol of Pernthaler et al. (2002). Filters were first embedded in 0.1 % (w/v) agarose to prevent cell detachment, then incubated for 10 min at room temperature in 0.01 M HCl to inactivate endogenous peroxidases. Cells were permeabilized by digestion with lysozyme (Sigma-Aldrich), 10 mg ml^{-1}, for 30 min at 37°C. The probe Cmok453 was used to target *Chromatium okenii* (Tonolla et al., 1999). Hybridization was performed at 46°C for 2.5 h using 2 µl of horseradish peroxidase(HRP)-labeled oligonucleotide probe mix per 600 µl of hybridization buffer containing 35% formamide. Filters were washed in 50 ml wash buffer at 48°C for 15 min

and 1xPBS for 10 min. The probe signal was amplified with the tyramide Oregon Green 488 (1 µl ml^{-1}) for 20 min at 37°C, and then washed in 1xPBS for 10 min, and then MilliQ. Filter pieces were counterstained with 4',6-diamidino-2-phenylindole (DAPI, 1 µg ml^{-1}) and embedded in a 4:1 mix of Citifluor/Vectashield and mounted onto glass slides. Cell numbers were enumerated with a grid ocular of an epifluorescence microscope (Nikon ECLIPSE Ci) by counting a minimum of 1000 total cells in randomly selected fields of view.

DNA extraction, sequencing, and analysis

DNA from the 2013 enrichment cultures was extracted by centrifuging 15 ml of culture and processing the cell pellet with the PowerSoil DNA Kit (MoBio Laboratories, Carlsbad, USA) according to the accompanying protocol with the following modification: the bead beading step was reduced to 30 sec followed by incubation on ice for 30 sec, and this was repeated a total of 4 times. The 16S rRNA genes were amplified using oligonucleotide primers GM3 (5´-AGAGTTTGATCMTGGC-3´) and GM4 (5'-TACCTTGTTACGACTT-3') (Muyzer et al., 1993) under standard PCR conditions (see *SI*). PCR products were purified by centrifugation through Multi Screen 96-well plates (Millipore, Billerica, MA, USA) filled with Sephadex G-50 Superfine powder (GE Healthcare Bio-science, Göteborg, Sweden). Cleaned PCR products were ligated to the vector pCR™4-TOPO® TA and cloned into the chemically competent *Escherichia coli* strain TOP10 using the TOPO-TA cloning kit (Thermo Fisher Scientific) following the manufacturer's protocol. Clones were screened by PCR for correct-sized inserts, re-purified on Sephadex plates, and sequenced with the BigDye Terminator cycle sequencing kit, version 3.1 (Applied Biosystems, Darmstadt, Germany), with vector primers M13R (5'-

TTCACACAGGAAACAGCTATGACC-3') and M13F (5'-ACGACGTTGTAAAACGACGGCCAG-3') using PCR conditions specified in the SI.

DNA from the 2014 enrichment culture and environmental DNA was extracted from polycarbonate filters with the MoBio PowerSoil DNA kit as described above. Primers 341F and 805R (Herlemann et al. 2011) were used to target the V3- V4 region of the 16S rRNA gene. The forward primers were modified to introduce a sample-specific barcode at the 5' end for multiplex sequencing. Ten parallel PCR reactions were run as specified in the SI. All replicate reactions were pooled and DNA was concentrated using the QIAquick PCR purification kit (Qiagen) according to the manufacturer's protocol, with a final elution step in 30 µl TE buffer. The DNA was then gel-purified using SYBR Green I Nucleic Acid Gel Stain (Invitrogen) and the QIAquick Gel Extraction Kit (Qiagen) according to the manufacturers' protocol. DNA concentration was determined fluorometrically at 260 nm, using the Qubit 2.0 Fluorometer and the Qubit dsDNA HS Assay KIT (Invitrogen). PCR products were pooled in equimolar concentrations and sent to the Max Planck-Genome Centre (Cologne, Germany) for sequencing. Bacterial 16S rRNA gene amplicons were sequenced by Illumina MiSeq (Illumina Inc., USA) paired end (2x 300 bp) sequencing following a TruSeq library preparation. Paired end reads were merged with the software package BBmap v4.2 (overlap >50 bases). Merged reads were quality trimmed (q30) and split by barcodes with MOTHUR (Schloss et al 2009) and uploaded to SilvaNGS (Quast et al. (2013)). Reads shorter than 200 bp, reads containing >2% homopolymers or ambiguities, and reads with an alignment identity <50% were excluded from analyses. The remaining reads were de-replicated and clustered at 98% sequence identity. Taxonomic

assignment was based on a local nucleotide BLAST (Camacho et al. 2009) search against the SILVA 16S rRNA SSU reference database, release 119.

Nucleotide sequence accession numbers

All nucleotide sequences from this study have been deposited in the NCBI nucleotide database under GenBank accession numbers *pending*. The 16S rRNA gene Illumina tag sequences can be retrieved from the ENA Sequence Read Archive under study accession number PRJEB13589/ ERP015149 (not public; accessible to reviewers upon request). Additional fasta files for review are submitted alongside this manuscript.

ACKNOWLEDGMENTS

We thank Kirsten Oswald, Nadine Engbersen, and Daniela Tienken for assistance in the field, and especially the Alpine Biology Center Foundation (Switzerland) for use of its research facilities. We are also grateful to Gaute Lavik for helpful discussions and to Julien Dekaezemacker for technical support. Funding was provided by the International Max Planck Research School of Marine Microbiology, the Max Planck Society, and the Deutsche Forschungsgemeinschaft (through the MARUM Center for Marine Environmental Sciences). The authors declare no conflict of interest.

REFERENCES

Benz, M., Brune, A., and Schink, B. (1998) Anaerobic and aerobic oxidation of ferrous iron at neutral pH by chemoheterotrophic nitrate-reducing bacteria. *Archives of Microbiology* **169**: 159-165.

Braterman, P.S., Cairns-Smith, A.G., and Sloper, R.W. (1983) Photo-oxidation of hydrated Fe2+;—significance for banded iron formations. *Nature.* **303**: *163-164*

Camacho, C., Coulouris, G., Avagyan, V., Ma, N., Papadopoulos, J., Bealer, K., and Madden, T.L. (2009) BLAST+: architecture and applications. *BMC bioinformatics* **10**: 421.

Canfield, D.E. (1989) Reactive iron in marine sediments. *Geochimica et Cosmochimica Acta* **53**: 619-632.

Canfield, D.E., Farquhar, J., and Zerkle, A.L. (2010) High isotope fractionations during sulfate reduction in a low-sulfate euxinic ocean analog. *Geology* **38**: 415-418.

Cline, J.D. (1969) spectrophotometric determination of hydrogen sulfide in natural waters. *Limnology and Oceanography* **14**: 454-458.

Coates, J.D., Ellis, D.J., Gaw, C.V., and Lovley, D.R. (1999) *Geothrix fermentans* gen. nov., sp. nov., a novel Fe (III)-reducing bacterium from a hydrocarbon-contaminated aquifer. *International Journal of Systematic and Evolutionary Microbiology* **49**: 1615-1622.

Coby, A.J., Picardal, F., Shelobolina, E., Xu, H., and Roden, E.E. (2011) Repeated anaerobic microbial redox cycling of iron. *Applied and Environmental Microbiology* **77**: 6036-6042.

Crowe, S.A., Jones, C., Katsev, S., Magen, C., O'Neill, A.H., Sturm, A. et al. (2008) Photoferrotrophs thrive in an Archean Ocean analogue. *Proceedings of the National Academy of Sciences* **105**: 15938-15943.

Davison, W., Woof, C., and Rigg, E. (1982) The dynamics of iron and manganese in a seasonally anoxic lake; direct measurement of fluxes using sediment traps. *Limnology and Oceanography* **27**: 987-1003.

Del Don, C., Hanselmann, K.W., Peduzzi, R., and Bachofen, R. (2001) The meromictic alpine Lake Cadagno: orographical and biogeochemical description. *Aquatic Sciences* **63**: 70-90.

Egli, K., Wiggli, M., Klug, J., Gerss, J., and Bachofen, R. (2004) Spatial and temporal dynamics of a plume of phototrophic microorganisms in a meromictic alpine lake using turbidity as a measure of cell density. *Aquatic Microbial Ecology* **35**: 105-113.

Ehrenreich, A., and Widdel, F. (1994) Anaerobic oxidation of ferrous iron by purple bacteria, a new type of phototrophic metabolism. *Applied and Environmental Microbiology* **60**: 4517-4526.

Emerson, D., and Moyer, C. (1997) Isolation and characterization of novel iron-oxidizing bacteria that grow at circumneutral pH. *Applied and Environmental Microbiology* **63**: 4784-4792.

Finneran, K.T., Johnsen, C.V., and Lovley, D.R. (2003) *Rhodoferax ferrireducens* sp. nov., a psychrotolerant, facultatively anaerobic bacterium that oxidizes acetate with the reduction of Fe (III). *International Journal of Systematic and Evolutionary Microbiology* **53**: 669-673.

Fleming, E.J., Davis, R.E., McAllister, S.M., Chan, C.S., Moyer, C.L., Tebo, B.M., and Emerson, D. (2013) Hidden in plain sight: discovery of sheath-forming, iron-oxidizing Zetaproteobacteria at Loihi Seamount, Hawaii, USA. *FEMS Microbiology Ecology* **85**: 116-127.

Gibson, C. (1985) Growth rate, maintenance energy and pigmentation of planktonic cyanophyta during one-hour light: dark cycles. *British Phycological Journal* **20**: 155-161.

Golden, D., Chen, C., and Dixon, J. (1987) Transformation of birnessite to buserite, todorokite, and manganite under mild hydrothermal treatment. *Clays and Clay Minerals* **35**: 271-280.

Halm, H., Musat, N., Lam, P., Langlois, R., Musat, F., Peduzzi, S. et al. (2009) Co-occurrence of denitrification and nitrogen fixation in a meromictic lake, Lake Cadagno (Switzerland). *Environmental Microbiology* **11**: 1945-1958.

Hansel, C.M., Lentini, C.J., Tang, Y., Johnston, D.T., Wankel, S.D., and Jardine, P.M. (2015) Dominance of sulfur-fueled iron oxide reduction in low-sulfate freshwater sediments. *The ISME Journal* **9**: 2400-2412.

Hegler, F., Posth, N.R., Jiang, J., and Kappler, A. (2008) Physiology of phototrophic iron (II)-oxidizing bacteria: implications for modern and ancient environments. *FEMS Microbiology Ecology* **66**: 250-260.

Heising, S., and Schink, B. (1998) Phototrophic oxidation of ferrous iron by a Rhodomicrobium vannielii strain. *Microbiology* **144**: 2263-2269.

Heising, S., Richter, L., Ludwig, W., and Schink, B. (1999) *Chlorobium ferrooxidans* sp. nov., a phototrophic green sulfur bacterium that oxidizes ferrous iron in coculture with a "*Geospirillum*" sp. strain. *Archives of Microbiology* **172**: 116-124.

Holmer, M., and Storkholm, P. (2001) Sulphate reduction and sulphur cycling in lake sediments: a review. *Freshwater Biology* **46**: 431-451.

Imhoff, J.F., and Trüper, H.G. (1981) *Ectothiorhodospira abdelmalekii* sp. nov., a new halophilic and alkaliphilic phototrophic bacterium. *Zentralblatt für Bakteriologie Mikrobiologie und Hygiene: I Abt Originale C: Allgemeine, Angewandte und Ökologische Mikrobiologie* **2**: 228-234.

Johnson, K.S., Elrod, V.A., Fitzwater, S.E., Plant, J.N., Chavez, F.P., Tanner, S.J. et al. (2003) Surface ocean-lower atmosphere interactions in the northeast Pacific Ocean gyre: Aerosols, iron, and the ecosystem response. *Global Biogeochemical Cycles* **17**.

Kallmeyer, J., Ferdelman, T.G., Weber, A., Fossing, H., and Jørgensen, B.B. (2004) A cold chromium distillation procedure for radiolabeled sulfide applied to sulfate reduction measurements. *Limnol Oceanogr Methods* **2**: 171-180.

Kappler, A., and Newman, D.K. (2004) Formation of Fe (III)-minerals by Fe (II)-oxidizing photoautotrophic bacteria. *Geochimica et Cosmochimica Acta* **68**: 1217-1226.

Kirf, M.K., Dinkel, C., Schubert, C.J., and Wehrli, B. (2014) Submicromolar oxygen profiles at the oxic–anoxic boundary of temperate lakes. *Aquatic Geochemistry* **20**: 39-57.

Konhauser, K.O., Hamade, T., Raiswell, R., Morris, R.C., Ferris, F.G., Southam, G., and Canfield, D.E. (2002) Could bacteria have formed the Precambrian banded iron formations? *Geology* **30**: 1079-1082.

Kostka, J.E., Stucki, L.J.W., Nealson, K.H., and Wu, J. (1996) Reduction of structural Fe (III) in smectite by a pure culture of the Fe-reducing bacterium Shewanella putrifaciens strain MR-1. In *Clays and Clay Minerals*.

Laufer, K., Nordhoff, M., Røy, H., Schmidt, C., Behrens, S., Jørgensen, B.B., and Kappler, A. (2015) Co-existence of microaerophilic, nitrate-reducing, and phototrophic Fe (II)-oxidizers and Fe (III)-reducers in coastal marine sediment. *Applied and Environmental Microbiology* **82(5)**:1433-1447.

Llirós, M., García–Armisen, T., Darchambeau, F., Morana, C., Triadó–Margarit, X., Inceoğlu, Ö. et al. (2015) Pelagic photoferrotrophy and iron cycling in a modern ferruginous basin. *Scientific reports* **5**.

Lovley, D.R., and Phillips, E.J. (1988a) Novel mode of microbial energy metabolism: organic carbon oxidation coupled to dissimilatory reduction of iron or manganese. *Applied and Environmental Microbiology* **54**: 1472-1480.

Lovley, D.R., and Phillips, E.J. (1988b) Manganese inhibition of microbial iron reduction in anaerobic sediments. *Geomicrobiology Journal* **6**: 145-155.

Lovley, D.R., Giovannoni, S.J., White, D.C., Champine, J.E., Phillips, E., Gorby, Y.A., and Goodwin, S. (1993) *Geobacter metallireducens* gen. nov. sp. nov., a microorganism capable of coupling the complete oxidation of organic compounds to the reduction of iron and other metals. *Archives of Microbiology* **159**: 336-344.

Madison, A.S., Tebo, B.M., and Luther, G.W. (2011) Simultaneous determination of soluble manganese (III), manganese (II) and total manganese in natural (pore) waters. *Talanta* **84**: 374-381.

Madison, A.S., Tebo, B.M., Mucci, A., Sundby, B., and Luther, G.W. (2013) Abundant porewater Mn (III) is a major component of the sedimentary redox system. *Science* **341**: 875-878.

Melton, E.D., Schmidt, C., and Kappler, A. (2012) Microbial iron (II) oxidation in littoral freshwater lake sediment: the potential for competition between phototrophic vs. nitrate-reducing iron (II)-oxidizers. *Frontiers in Microbiology* **3**.

Milucka, J., Kirf, M., Lu, L., Krupke, A., Lam, P., Littmann, S. et al. (2015) Methane oxidation coupled to oxygenic photosynthesis in anoxic waters. *The ISME journal*.

Musat, N., Halm, H., Winterholler, B., Hoppe, P., Peduzzi, S., Hillion, F. et al. (2008) A single-cell view on the ecophysiology of anaerobic phototrophic bacteria. *Proceedings of the National Academy of Sciences* **105**: 17861-17866.

Myers, C.R., and Nealson, K.H. (1988) Microbial reduction of manganese oxides: interactions with iron and sulfur. *Geochimica et Cosmochimica Acta* **52**: 2727-2732.

Nagai, T., Imai, A., Matsushige, K., Yokoi, K., and Fukushima, T. (2007) Dissolved iron and its speciation in a shallow eutrophic lake and its inflowing rivers. *Water Research* **41**: 775-784.

Peduzzi, S., Storelli, N., Welsh, A., Peduzzi, R., Hahn, D., Perret, X., and Tonolla, M. (2012) Candidatus "*Thiodictyon syntrophicum*", sp. nov., a new purple sulfur bacterium isolated from the chemocline of Lake Cadagno forming aggregates and specific associations with *Desulfocapsa* sp. *Systematic and Applied Microbiology* **35**: 139-144.

Pernthaler, A., Pernthaler, J., and Amann, R. (2002) Fluorescence in situ hybridization and catalyzed reporter deposition for the identification of marine bacteria. *Applied and Environmental Microbiology* **68**: 3094-3101.

Pfennig, N., Trueper H. (1991) *The family Chromatiaceae. In The Prokaryotes, 2nd edn*. Berlin: Springer.

Pyzik, A.J., and Sommer, S.E. (1981) Sedimentary iron monosulfides: kinetics and mechanism of formation. *Geochimica et Cosmochimica Acta* **45**: 687-698.

Quast, C., Pruesse, E., Yilmaz, P., Gerken, J., Schweer, T., Yarza, P. et al. (2013) The SILVA ribosomal RNA gene database project: improved data processing and web-based tools. *Nucleic Acids Research* **41**: D590-D596.

Raven, J., Kübler, J., and Beardall, J. (2000) Put out the light, and then put out the light. *Journal of the Marine Biological Association of the UK* **80**: 1-25.

Stookey, L.L. (1970) Ferrozine –a new spectrophotometric reagent for iron. *Analytical Chemistry* **42**: 779-781.

Storelli, N., Peduzzi, S., Saad, M.M., Frigaard, N.-U., Perret, X., and Tonolla, M. (2013) CO2 assimilation in the chemocline of Lake Cadagno is dominated by a few types of phototrophic purple sulfur bacteria. *FEMS microbiology ecology* **84**: 421-432.

Straub, K.L., Benz, M., Schink, B., and Widdel, F. (1996) Anaerobic, nitrate-dependent microbial oxidation of ferrous iron. *Applied and Environmental Microbiology* **62**: 1458-1460.

Straub, K.L., Schönhuber, W.A., Buchholz-Cleven, B.E., and Schink, B. (2004) Diversity of ferrous iron-oxidizing, nitrate-reducing bacteria and their involvement in oxygen-independent iron cycling. *Geomicrobiology Journal* **21**: 371-378.

Thamdrup, B. (2000) Bacterial manganese and iron reduction in aquatic sediments. In *Advances in Microbial Ecology*: Springer, pp. 41-84.

Thamdrup, B., Fossing, H., and Jørgensen, B.B. (1994) Manganese, iron and sulfur cycling in a coastal marine sediment, Aarhus Bay, Denmark. *Geochimica et Cosmochimica Acta* **58**: 5115-5129.

Tonolla, M., Demarta, A., Peduzzi, R., and Hahn, D. (1999) In situ analysis of phototrophic sulfur bacteria in the chemocline of meromictic Lake Cadagno (Switzerland). *Applied and environmental microbiology* **65**: 1325-1330.

Trouwborst, R.E., Clement, B.G., Tebo, B.M., Glazer, B.T., and Luther, G.W. (2006) Soluble Mn (III) in suboxic zones. *Science* **313**: 1955-1957.

Walter, X.A., Picazo, A., Miracle, M.R., Vicente, E., Camacho, A., Aragno, M., and Zopfi, J. (2014) Phototrophic Fe (II)-oxidation in the chemocline of a ferruginous meromictic lake. *Frontiers in Microbiology* **5**.

Weiss, J.V., Rentz, J.A., Plaia, T., Neubauer, S.C., Merrill-Floyd, M., Lilburn, T. et al. (2007) Characterization of Neutrophilic Fe (II)-Oxidizing Bacteria Isolated from the Rhizosphere of Wetland Plants and Description of *Ferritrophicum radicicola* gen. nov. sp. nov., and *Sideroxydans paludicola* sp. nov. *Geomicrobiology Journal* **24**: 559-570.

Widdel, F., Schnell, S., Heising, S., Ehrenreich, A., Assmus, B., and Schink, B. (1993) Ferrous iron oxidation by anoxygenic phototrophic bacteria. *Nature* **362**: 834-836.

Wüest, A. (1994) Interactions in lakes: Biology as source of dominant physical forces. *Limnologica Jena* **24**: 93-104.

SUPPLEMENTARY FIGURES & TABLES

Figure S1: Manganese and iron speciation in *in situ* incubations supplemented with hydrous MnO_2. Note that all Fe was oxidized between MnO_2 addition and the first sampling point.

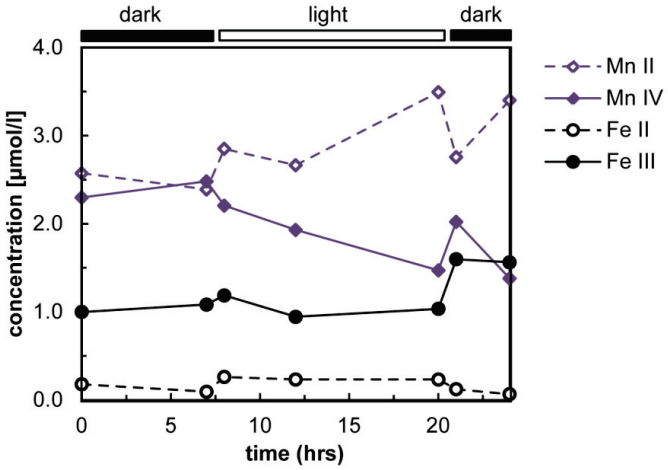

Figure S2: Lake Cadagno profile from 2013 taken 4 h after sunset. Where sulfide and Fe overlap, Fe is most likely speciated as FeS.

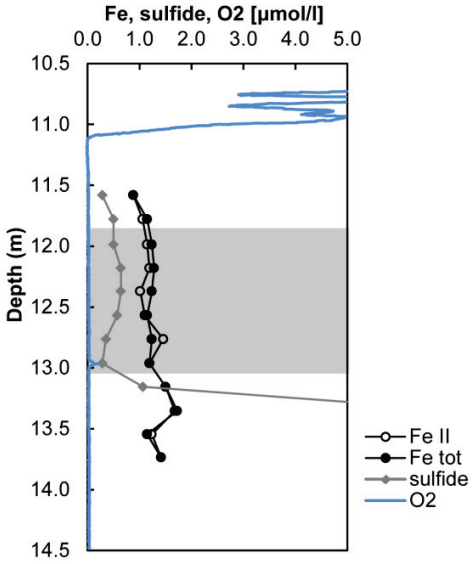

Figure S3: Scanning electron micrograph (SEM) of a bacterial aggregate in an Fe(II) enrichment culture. The photoferrotroph *Rhodomicrobium vanielii* can be distinguished based on its stalk-like morphology. Scale bar is 5 µm. SEM-EDX images of a bacterial aggregate in an aged culture. *Rhodomicrobium* and other rod-shaped bacteria are visibly encrusted in minerals identified as iron (blue), phosphorus (yellow), and oxygen (red). Scale bars are 2.5 µm.

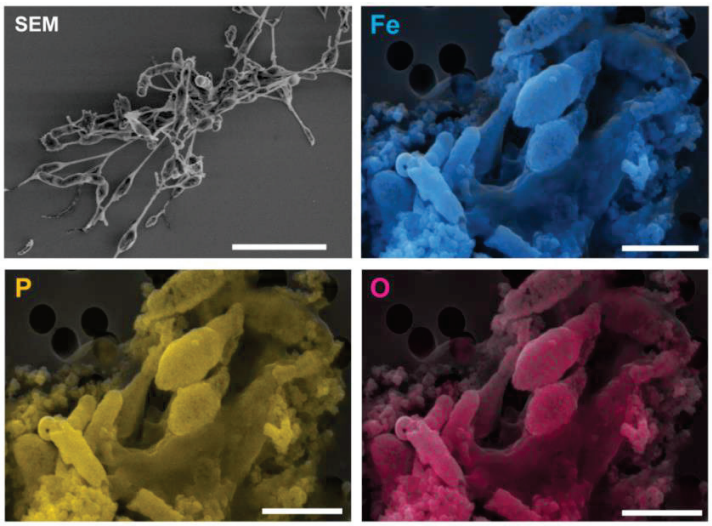

Table S1: Table of sequences identified in 2013 and 2014 Lake Cadagno enrichment cultures with added Fe(II) and acetate. Taxonomic identity of 16S rRNA gene sequences was assigned based on best BLAST hit identity. Sequences are listed in decreasing order of abundance as determined for the 2013 enrichment.

Closest relative	**Sequence abundance**	
	enrichment 2013 ($n_{sequences}$=37)	**enrichment 2014 ($n_{sequences}$=30,809)**
Rhodoferax sp.	62%	0.2%
other Bacteria	30%	26.0%
Rhodomicrobium sp.	3%	0.1%
Geothrix sp.	3%	-
Chlorobium sp.	3%	60.2%
Rhodopseudomonas sp.	-	12.8%
Sulfurospirillum sp.	-	0.7%

Table S2: Table of sequences identified in a 2013 Lake Cadagno enrichment culture with added FeS. Taxonomic identity of 16S rRNA gene sequences was assigned based on best BLAST hit identity. Sequences are listed in decreasing order of abundance as determined for the 2013 enrichment.

Closest relative	**Sequence abundance ($n_{sequences}$=33)**
Rhodoferax sp.	76%
other Bacteria	12%
Ectothiorhodospira sp.	6%
Thiodictyon sp.	3%
Rhodomicrobium sp.	3%

Aerobic sulfide oxidation by purple sulfur bacteria in anoxic waters

Jasmine S. Berg[1]*, Tobias Sommer[2], Petra Pjevac[1,3], Caroline R.T. Buckner[1], Philip F. Hach[1], Sten Littman[1], Francesco Danza[4], Carsten J. Schubert[2], Jana Milucka[1], Marcel M.M. Kuypers[1]

[1]Department of Biogeochemistry, Max Planck Institute for Marine Microbiology, 28359 Bremen, Germany
[2]Eawag, Swiss Federal Institute of Aquatic Science and Technology, Kastanienbaum, Switzerland
[3]Division of Microbial Ecology, Department of Microbiology and Ecosystem Science, University of Vienna, Vienna, Austria
[4]Cantonal Institute of Bacteriology, Microbial Ecology, University of Geneva, CH-6904 Lugano, Switzerland
*corresponding author: jberg@mpi-bremen.de (+49 4212028 ext. 646)

In preparation

doi:-

Author contributions: JSB, TS, FD, and CJS measured and analysed *in situ* data. JSB performed all the experiments. PP processed and analyzed metagenomic data. CRTB and PFH contributed mass spectrometry data. SL performed nanoSIMS analyses. JM and MMMK conceived of the project. JSB and MMMK conceived, wrote, and edited this manuscript.

ABSTRACT

Anoxygenic phototrophic bacteria oxidizing sulfide and fixing CO_2 with sunlight play an important role in the local carbon and sulfur cycles of sulfidic, shallow sediments and stratified water columns within the photic zone. Sulfide and CO_2 consumption are therefore expected to follow diel cycles in environments dominated by phototrophic sulfur bacteria. Surprisingly, we found that populations of purple sulfur bacteria in the anoxic chemocline of Lake Cadagno, Switzerland continue to oxidize sulfide and fix inorganic carbon in the dark. Using a combination of high-resolution chemical profiling and stable isotope incubations, we determined that the purple sulfur bacteria respire sulfide with O_2 and possibly an unknown storage compound in the dark as well as in the light. In fact, chemotrophic sulfide oxidation by these phototrophic bacteria may account for up to half of all primary production in the chemocline. Aerobic respiration in the anoxic zone is accomplished by bacteria bridging spatially separated gradients of oxygen and sulfide using a novel mechanism of storage and transport that is not yet fully understood. The ecophysiology of these anoxygenic phototrophic bacteria reveals that they are well adapted to their dynamic environment and have an important ecological function, even in the absence of light.

INTRODUCTION

Sulfide-oxidizing microorganisms play an important role in sulfide detoxification in stratified sulfidic environments such as oxygen minimum zones (OMZs), sulfidic sediments, and euxinic lakes and marine basins (Jørgensen et al., 1991; Kühl and Jørgensen, 1992; Overmann, 1997; Lavik et al., 2009). Microorganisms oxidizing sulfide with oxygen, nitrate, or sunlight can completely consume high fluxes of this toxic compound and so protect other, more sulfide-

sensitive bacteria. These different metabolic specialists (chemolithotrophs and phototrophs) compete for electron donors but can actually coexist in consortia and microbial mats due to their different limitations by electron acceptors (Stal et al., 1985; Jørgensen and Des Marais, 1986; Overmann, 2001).

Sulfide-oxidizing microorganisms generally exist in habitats characterized by steep gradients of sulfide and oxygen. In many cases these gradients overlap, though the scale of the oxygen-sulfide overlap varies greatly, from a couple of meters in the Chesapeake Bay (Findlay et al., 2015), 20 cm in Lake Cisó (Pedrós-Alió and Guerrero, 1993), to only a few µm in microbial mats (Van Gemerden and Mas, 1995). In physically stratified environments where sunlight penetrates the upper few millimeters of sediment and in shallow water columns with minimal mixing, activity of purple sulfur bacteria (PSB) and green sulfur bacteria (GSB) can significantly impact their local ecosystems by maintaining a spatial separation between gradients of oxygen and sulfide (e.g. Van Gemerden et al., 1989; De Wit et al., 1989; Wieland et al., 2005). Populations of GSB may even contribute to the development of a 20-30 m oxygen- and sulfide-free zone in the Black Sea (Jørgensen et al., 1991; Overmann et al., 1992) although direct evidence for this is still lacking. Diel cycles of sulfide consumption and oxygen production result in the vertical variation of chemical gradients, and often the zone inhabited by anoxygenic phototrophs becomes sulfidic in the dark (Jørgensen et al., 1979).

The dark survival strategies of anoxygenic phototrophic bacteria have been intensively studied in laboratory pure cultures. Many PSB have been found to switch to chemotrophic growth utilizing oxygen and reduced sulfur compounds under microoxic conditions (e.g. Kampf and Pfennig, 1980; de Witt and van Gemerden, 1990). Alternatively, the zero-valent sulfur (S^0) that is

accumulated as a storage product by these bacteria in the light can be reduced in the dark to produce cellular maintenance energy. Some members of the family *Chromatiaceae* concomitantly produce the carbon-storage compound glycogen in the light which can later be respired by stored sulfur, yielding polyhydroxyalkanoate (PHA) and sulfide (Van Gemerden, 1968).

In the environment, the ecophysiology of anoxygenic phototrophs is likely much more complex. In highly dynamic environments influenced by tidal cycling and fluctuating light intensities, PSB have been shown to switch between phototrophy and chemotrophy (Van Gemerden et al., 1989). Variable fluxes of oxygen and nitrate, among other environmental factors, may induce different physiological behaviors among anoxygenic phototrophs. We therefore investigated the light-dark dynamics of sulfur cycling in the permanently stratified Lake Cadagno where sulfide and oxygen gradients in the water column are separated by a 1-2 m thick layer of anoxygenic phototrophs. Evidence suggests that the local populations of PSB and GSB responsible for sulfide oxidation in the light also remain active in the dark. Using both *in situ* incubations and pure cultures it has previously been shown that the PSB and GSB are capable of dark carbon fixation (Musat et al., 2008; Halm et al., 2009; Storelli et al., 2013) but it is not yet known whether this dark activity is linked to dark sulfur cycling *in situ*. We therefore combined high-resolution biogeochemical profiling with single-cell activity measurements to gain insight into the light-dark changes in microbial metabolism of Lake Cadagno.

RESULTS

Biogeochemistry of Lake Cadagno

Lake Cadagno is characterized by an oxic epilimnion and a sulfidic monolimnion spatially separated from each other by a chemocline free of detectable oxygen and with little to no sulfide (Fig. 1a). Very low amounts of sulfide (< 5 µM) could be measured in the chemocline in the dark, but changes in the sulfide concentration gradient diffusing into the chemocline were independent of light-dark periods. Oxygen disappeared just above the chemocline between 11-12 m depth. The oxygen concentrations between 11-12 m depth showed some diurnal variability (Fig. 1a). Oxygen concentrations increased during day time indicating net photosynthesis while oxygen concentrations decreased during night indicating net respiration

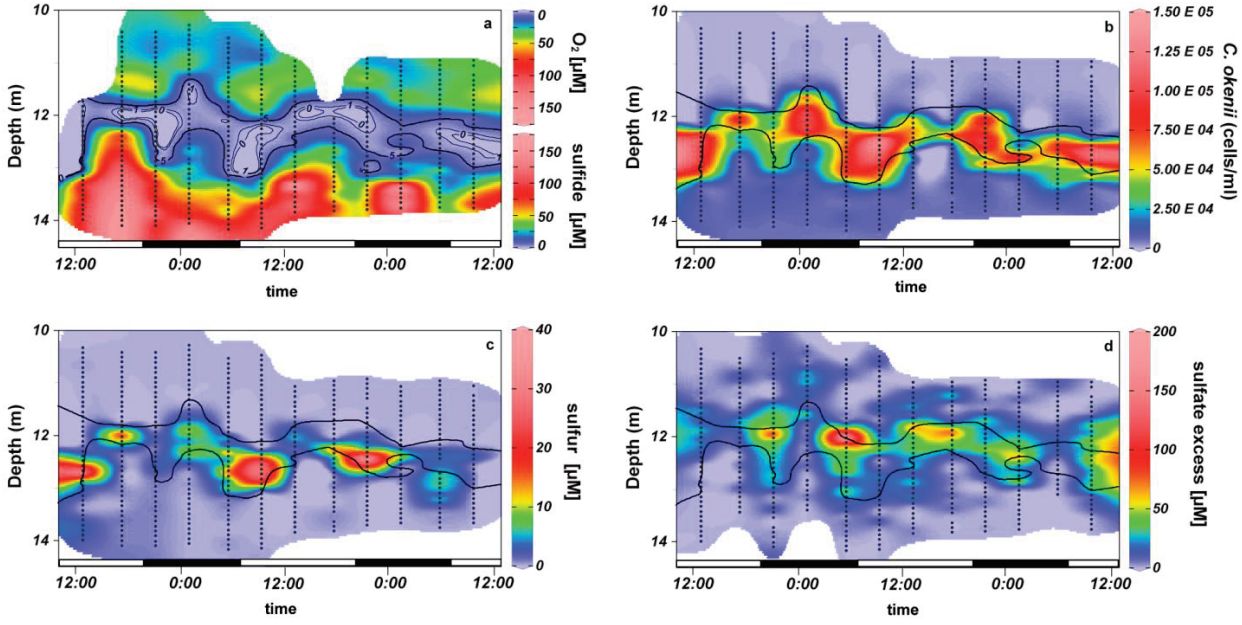

Figure 1: (a) Combined oxygen and sulfide profiles from 2015 revealing the persistence of an oxygen- and sulfide- free zone over a period of 48 hours, with contour lines delimiting sulfide concentrations. The bold contour lines delimiting the region with < 5 µM sulfide were used to define the chemocline in parallel profiles of *C. okeniii* cell counts (b), particulate sulfur (c), and sulfate excess (d). Black dots represent sampling points for all parameters except O_2 which was measured continuously with a microsensor. Shaded boxes represent dark periods between sunset at ~20:50 and sunrise at ~6:10. Original profiles from which the time plots were interpolated are provided in Fig S1.

(Fig 1a). Because the lake is meromictic, these stratified conditions were also relatively stable from year to year (see Fig S2 for 2013 and 2014 profiles) with some small differences. In 2015, the 0.5-1 m wide chemocline was located around 11-12 m depth, with the exact location varying over the day due to the action of internal waves (Egli et al., 1998). In previous years, the chemocline was up to 2 m wide (Fig S2) and remained completely sulfide-free in the dark. Conservative properties such as temperature and conductivity in the chemocline were constant (Fig S1&2) which is evidence of intense mixing. The mixing regime within the chemocline has apparently changed from year to year. Stable conductivity profiles revealed very strong mixing of the chemocline in 2013 and 2014 (Fig S2) whereas the reduced or absent region of constant conductivity revealed much weaker mixing of the chemocline in 2015 (Fig S1).

In the Lake Cadagno chemocline, a dense layer of anoxygenic phototrophic bacteria thrives on opposing gradients of sunlight and sulfide (e.g. Tonolla et al., 1999; Musat et al., 2008). The water in this layer owes its purple coloration to large numbers of the PSB *Chromatium okenii*, which were enumerated by flow cytometry (Fig 1b). Though other, smaller purple and green sulfur bacteria were also present, *C. okenii* was the most significant microorganism in the chemocline in terms of biomass and carbon fixation (Musat et al., 2008). Even higher densities of *C. okenii* were present in 2014 ($10^6 \cdot ml^{-1}$) than in 2015 ($10^5 \cdot ml^{-1}$). *C. okenii* is extremely motile, swimming at speeds of ~50 $\mu m \cdot s^{-1}$ (Vaituzis and Doetsch, 1969), and has been hypothesized to drive the convection and mixing of the chemocline (Wüest, 1994). The most numerically abundant anoxygenic PSB was *Lamprocystis* sp. (Tonolla et al., 2005) which is also motile via a single flagellum. These PSB migrate between gradients of sulfide, light, and oxygen by photo- and chemotaxis (Pfennig et al., 1968). We observed a presumably phototactic response

immediately after sunrise (9:00) when *C. okenii* cells aggregated at the top of the chemocline as evidenced by a peak in cell numbers there (Fig S1).

The oxidation of sulfide by these anoxygenic phototrophs proceeds via the formation of S^0 as an obligate intermediate (Mas and Van Gemerden, 1995). Zero-valent sulfur was measured as particulate sulfur on 0.7 µm filters and may comprise intracellular sulfur stored in the PSB *Chromatiaceae* and extracellular sulfur adhering to the GSB *Chlorobiaceae* (Tonolla et al., 2005). The highest concentrations of sulfur (Fig 1c) coincided with the highest *C. okenii* cell numbers (Fig 1b) in the chemocline. From the relatively good correlation (r^2 max = 0.78) between the two (Fig S3), we can presume that the majority of the S^0 was contained inside the large *C. okenii* and other co-localized PSB cells which together constitute the majority of the total microbial biovolume in the chemocline (Bosshard et al., 2000). It is also likely that some of this S^0 was present in the form of polysulfides formed by the reaction of free sulfide with intra- and extracellular sulfur, as has previously been suggested in other euxinic lakes (Overmann, 1997). Our analytical method for total sulfur did not distinguish between polysulfides and other types of S^0. However, we could confirm the presence of polysulfides inside live *C. okenii* cells in environmental samples using Raman spectroscopy (Fig 2). The Raman spectrum with two weak peaks at 152 and 218 and a prominent peak at 462 cm^{-1}

Figure 2: (a) Light microscope image of *Chromatium okenii* cells with intracellular sulfur inclusions. Scale bar is 10 µm. (b) Raman spectrum of a sulfur inclusion from a living *C. okenii* cell in an environmental sample. Exposure time was 0.5 sec.

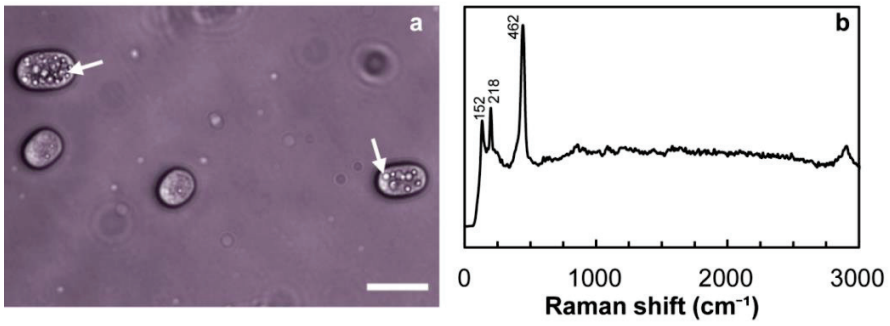

is characteristic of linear polysulfide species (Janz et al., 1976; Khan et al., 2011). The Raman peak at ~2900 cm^{-1} corresponds to the CH_2 and CH_3 stretching vibrations (Socrates, 2004), and its co-occurrence with polysulfide peaks may be evidence that the sulfur chains are terminated by organic end groups as reported by Prange et al (1999).

Sulfate originating from the dissolution of gypsum rocks enters the monolimnion of Lake Cadagno via underwater springs (Del Don et al., 2001). This leads to high sulfate (1-2 mM) concentrations at the lake bottom which decrease upwards through the water column. These background sulfate concentrations obscure small concentration changes induced by sulfate reduction and sulfide oxidation processes. In order to identify regions of sulfate production in and around the chemocline, deviations from the linear sulfate-conductivity mixing line were determined (Fig S4). These, differences between the measured sulfate concentration and the sulfate concentration predicted based on measured conductivity represent excess sulfate, which can be attributed to biological sulfate production:

$$\text{excess } [SO_4^{2-}] = \text{measured } [SO_4^{2-}] - \text{expected } [SO_4^{2-}]$$

Biogenic (excess) sulfate plotted over two diurnal cycles in 2015 (Fig 1d) exhibited a peak just below the oxycline at the top of the chemocline above the region of maximum *C. okenii* cell density. Due to the overlap of sulfate and oxygen under both light and dark conditions, sulfate production appeared related to the availability of oxygen. In contrast, sulfate production in 2014 (Fig 3) occurred within the maximum turbidity layer where the *C. okenii* were located and appeared related to the availability of photosynthetically active radiation (PAR), as the peak in biogenic sulfate corresponded with the sharp decrease in PAR to <1 $\mu E \cdot cm^{-1}$. The sulfate excess

of up to 125 µM in 2014 was much higher than in 2015 (25 µM). Whereas no changes were visible between light and dark sulfate production in 2015, biogenic sulfate measured in the dark profile in 2014 (Fig 3, 6:00) was significantly lower (30-40 µM) than in the light. The broad distribution of this excess sulfate peak in the dark may indicate that sulfate production occurred within a narrow zone during the day, and at night this sulfate was mixed into surrounding waters.

We also measured sulfate reduction rates (SRR) at several depths within the water column. No sulfate reduction was detected in the chemocline in 2014 or 2015. In 2014 SRR in the sulfidic monolimnion were about 235 $nM \cdot d^{-1}$ and 214 $nM \cdot d^{-1}$ at 14 and 15 m depth, respectively. SRR

Figure 3: Lake Cadagno profiles from Aug 2014 at midday (16:00), sunset (19:00), and just before sunrise (6:00), highlighting zones of sulfide consumption, sulfur production, and sulfate production in relation to oxygen and maximum turbidity. Sulfate excess was calculated as the difference between the measured sulfate concentration and the sulfate concentration predicted based on the measured conductivity. The sulfate production zone appears related to photosynthetically active radiation (PAR).

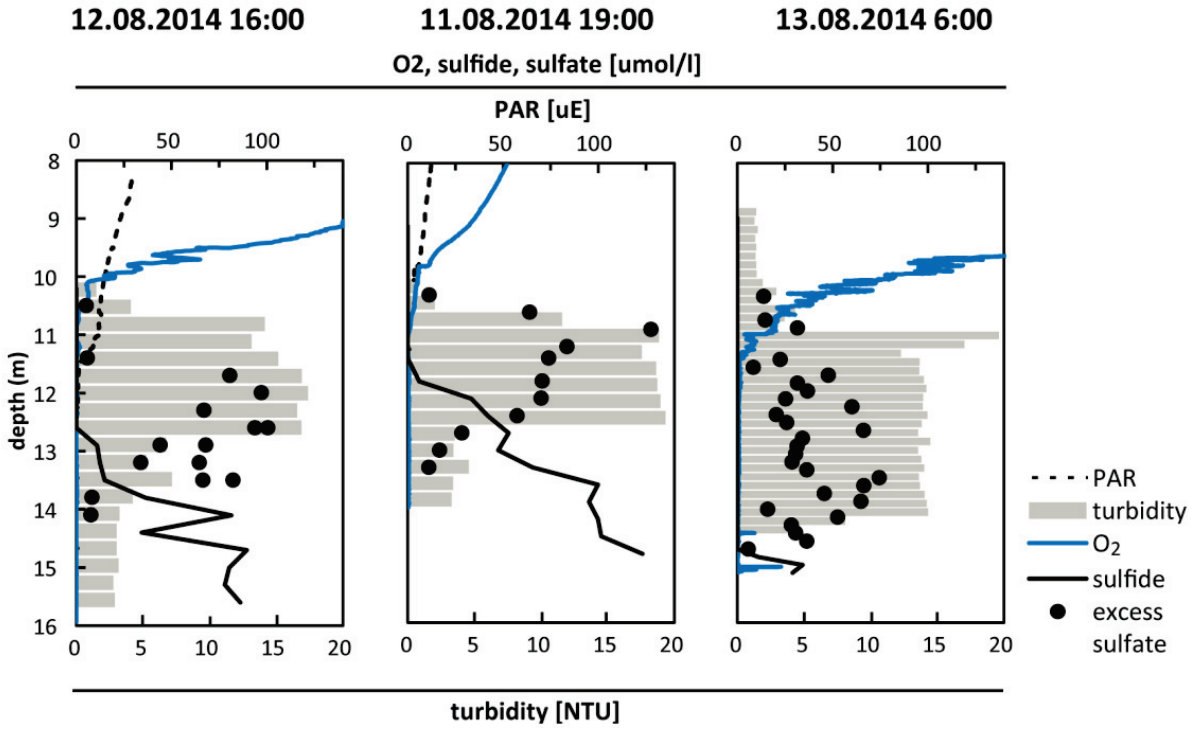

measured in the monolimnion in 2015 were in the same range (375 $nM \cdot d^{-1}$). Most of the sulfate reduction in Lake Cadagno occurs within the sediments (e.g. Del Don et al., 2001; Dahl et al., 2010) and the resulting sulfide diffuses upwards into the water column. These rate measurements indicate that sulfate reduction within the chemocline does not contribute significantly to the sulfide accumulated there.

The low concentrations of sulfide measured in the chemocline during the night in 2015 may actually represent a significant amount of total unconsumed sulfide diluted in the well-mixed waters. We therefore quantified this unconsumed sulfide at each time point of sampling by integrating sulfide concentrations over the chemocline (bold contour lines, Fig 1). The total sulfide inventory in the chemocline showed a clear diurnal trend, increasing in the dark and decreasing in the light (Fig 4a). The rate of sulfide accumulation in the chemocline could be calculated for each 4-h sampling interval (Fig S5a). It is evident that sulfide accumulated steadily at night and was most rapidly consumed during the first 3 hours of daylight.

In contrast, the sulfur inventory in the chemocline (Fig 4b) varied independently of light-dark changes, both increasing and decreasing in the light and in the dark. Changes in sulfur concentration over time (Fig S5b) reflect the dynamic balance between the two oxidation steps involved in the complete oxidation of sulfide, where positive S^0 accumulation rates indicate the predominance of sulfide oxidation to sulfur (equation 1) and negative S^0 accumulation rates indicate the predominance of sulfur oxidation to sulfate (equation 2).

(1) $O_2 + 2H_2S \rightarrow 2H_2O + 2S^o$

(2) $2H_2O + 2S^o + 3O_2 \rightarrow 4H^+ + 2SO_4^{2-}$

The two reactions can be summed up as:

(3) $2O_2 + H_2S \rightarrow 2H^+ + SO_4^{2-}$

Assuming that the two hours of remaining daylight between 17:05 and 21:00 may have contributed to the increase in S^0 at the beginning of the second dark period, sulfur accumulated most rapidly in the light at a rate of 0.18 $\mu mol \cdot cm^{-2} h^{-1}$ (Fig S5b). Sulfur also decreased most rapidly in the light at a rate of 0.32 $\mu mol \cdot cm^{-2} h^{-1}$ (Fig S5b). In the dark, an unexpected increase in total sulfur was observed at four time points (Fig 4b).

The inventory of biogenic sulfate in the chemocline (Fig 4c) was two orders of magnitude greater than the sulfur inventory (Fig 4b), and up to three orders of magnitude greater than the sulfide inventory (Fig 4a). This implies that the oxidation of sulfide would not be detected as a net concentration change in the very large background sulfate pool. The sulfur pool was also relatively insignificant compared to the excess sulfate pool, indicating that sulfur accumulation was only transient and most sulfide was completely oxidized to sulfate. No trends in excess sulfate accumulation were apparent over the light-dark periods.

To quantify biological sulfide consumption over time, we partitioned the total sulfide flux (Fig S5c) into two fractions: biologically consumed sulfide and accumulated sulfide in the chemocline. The consumed sulfide flux (Fig 4d) was calculated by subtracting the rate of sulfide accumulation (Fig S5a) from the total sulfide flux (Fig S5c). Variations in the consumed sulfide flux between 0.03 and 0.22 $\mu mol \cdot cm^{-2} h^{-1}$ (Fig 4d) were independent of light-dark cycles and could have been induced by internal waves, as mentioned above. Interestingly, the consumed

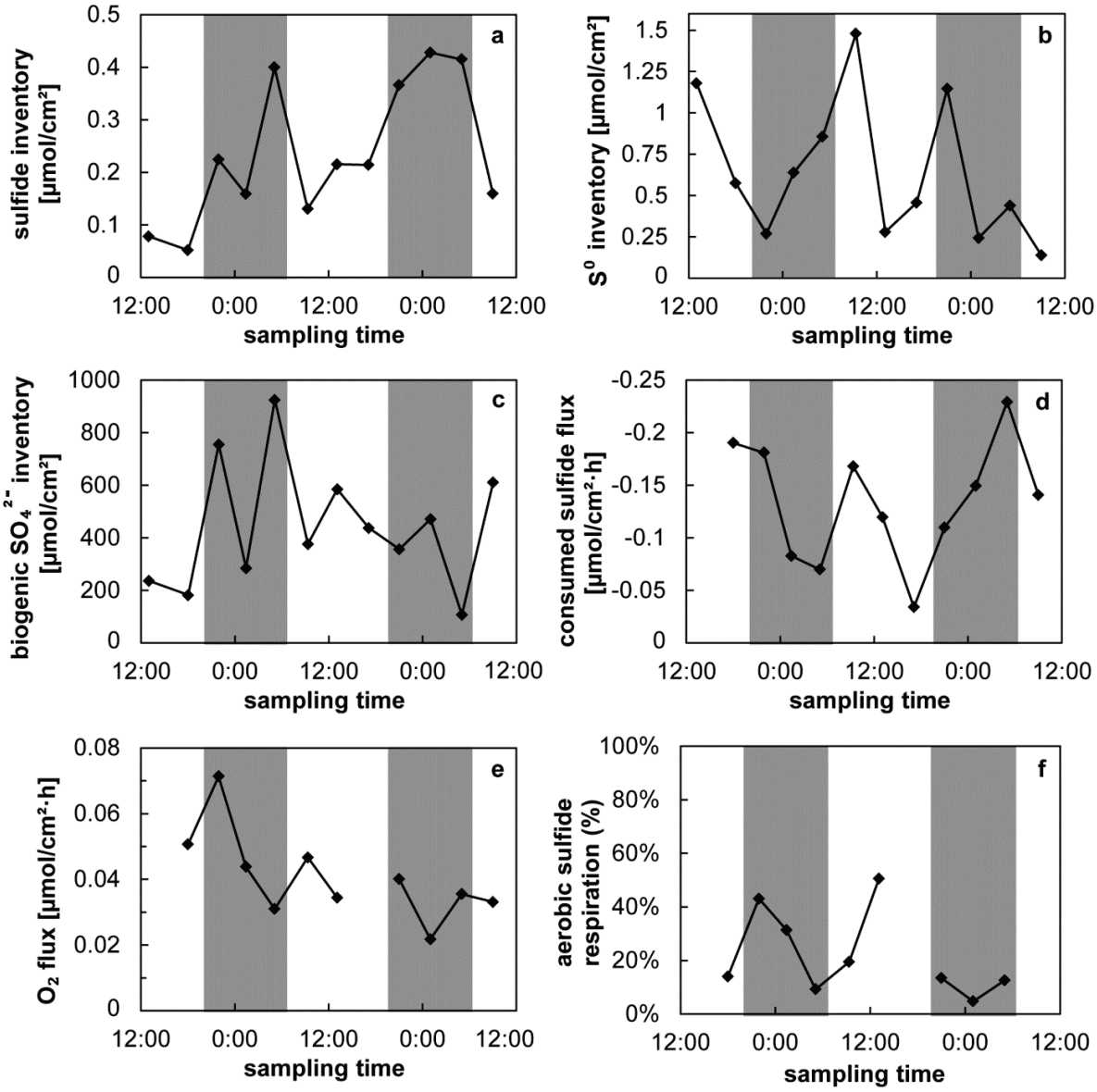

Figure 4: Light-dark dynamics of compounds in the Lake Cadagno chemocline measured at 4-h intervals over 48 hours. Total sulfide, particulate sulfur, and excess sulfate concentrations were integrated over the depth of the mixed layer to calculate the sulfide (a), sulfur (b), and sulfate (c) inventories, respectively. (d) The consumed sulfide flux was calculated by subtracting the sulfide accounted for by accumulation in the chemocline from the total sulfide flux into the mixed layer. (b) The downwards oxygen flux into the chemocline was used to estimate the maximum % of sulfide aerobically respired (f), assuming the complete oxidation of sulfide to sulfate. Shaded regions represent dark periods.

sulfide flux in the dark was well above zero, indicating that although some sulfide accumulated in the chemocline, sulfide oxidation continued in the dark. Moreover, sulfide consumption was not necessarily greater in the light than in the dark and rather depended on the total sulfide flux. In comparison, the upwards flux of sulfide in previous years was slightly lower, or 0.011-0.024 μmol·cm^{-2}h^{-1} in 2013 and 0.031-0.040 μmol·cm^{-2}h^{-1} in 2014.

It was not possible to compare the sulfide and sulfur budgets in Lake Cadagno because the sulfur fluxes are not in steady state. Sulfur is actively transported by the motile purple sulfur bacteria during chemo- and phototaxis (Pfennig et al., 1968) rather than by diffusive processes. Nonetheless, biogenic sulfate could be measured as the end product of sulfide oxidation in a distinctive zone overlapping with the base of the oxycline (Fig 1d). The total (upwards and downwards) biogenic sulfate flux in this region was roughly equivalent to the sulfide flux and followed a similar trend (Fig S5d). This implies that we were able to close the sulfur budget and account for all the sulfide oxidation as sulfate.

In the absence of light, electron acceptors such as NO_x^-, Fe^{3+}, Mn^{4+}, or O_2 can be utilized for sulfide oxidation. Nitrate and nitrite concentrations in the Lake Cadagno chemocline, however, are negligible (Milucka et al., 2015; Halm et al., 2009). Fluxes of Fe and Mn were too low to account for all the sulfide oxidized (Berg et al, submitted), and the formation of Fe- or Mn-oxides would ultimately involve oxygen or nitrate. We therefore calculated the oxygen flux into the chemocline (Fig 4e), which varied slightly between 0.022-0.071 μmol·cm^{-2}h^{-1} over the period of 48 h. Oxygen fluxes measured in 2013 and 2014 were in the same range, or 0.013-0.048 μmol·cm^{-2}h^{-1} and 0.037-0.073 μmol·cm^{-2}h^{-1}, respectively. In order to relate these oxygen fluxes to sulfide fluxes, we assumed that sulfide was oxidized with oxygen using a 1:2

stoichiometry (equation 3). The highest amount of sulfide oxidation accounted for by oxidizing equivalents available from oxygen in 2015 was represented as the maximum % aerobic sulfide respiration (Fig 4f). In the light, the remaining 40-80% of sulfide oxidation could be attributed to anoxygenic photosynthesis and/or aerobic sulfide oxidation fueled by *in situ* oxygen production by photosynthesic algae. At four time points in the dark, however, we could not explain the disappearance of roughly 60-90% of the sulfide. We plotted temperature/conductivity profiles to detect anomalies indicative of lateral transport processes, but the relatively smooth profiles did not reveal any intrusions of water masses as a possible oxygen source (Fig S6). In contrast, calculated oxygen fluxes in 2013 and 2014 were in all cases sufficient to account for the sulfide oxidized in the dark.

Incubations with anoxygenic phototrophs from Lake Cadagno

We monitored microbial activity linked to sulfide oxidation processes in the light and in the dark using lake water incubations with stable isotope labels. The uptake of ^{13}C-DIC and $^{15}NH_4^+$ was monitored alongside sulfide, sulfur, and oxygen under red light and dark conditions. Oxygen concentrations remained below detection limits throughout the incubations. In a sterile control, no detectable amounts of oxygen were found to leak into the incubation flasks for 3 days. Over a light period of 10 h, 42 µmol·l^{-1} sulfide was consumed with the concomitant assimilation of 9.1 µmol·l^{-1} CO_2 and 1.1 µmol·l$^{-1}NH_4^+$ (Fig 5a). This is equivalent to a sulfide oxidation rate of 4.1 µmol·l^{-1}·h^{-1}, a CO_2 fixation rate of 840 nmol C·l^{-1}·h^{-1}, and an NH_4^+ assimilation rate of 107 nmol N·l^{-1}·h^{-1}. These do not represent *in situ* rates because the light quality at depth may be different than the > 750 nm light used to prevent oxygenic photosynthesis in our experiments. During

anoxygenic photosynthesis, sulfide oxidation is stoichiometrically coupled to the reduction of CO_2 as first observed by van Niel (1932).

(4) $CO_2 + 2H_2S \rightarrow 2S^o + \text{“}CH_2O\text{”} + 2H_2O$

(5) $3CO_2 + 2S^o + 5H_2O \rightarrow 4H^+ + 2SO_4^{2-} + 3\text{“}CH_2O\text{”}$

These partial reactions can be summed up in the overall equation:

(6) $2CO_2 + H_2S + 2H_2O \rightarrow 2H^+ + SO_4^{2-} + 2\text{“}CH_2O\text{”}$

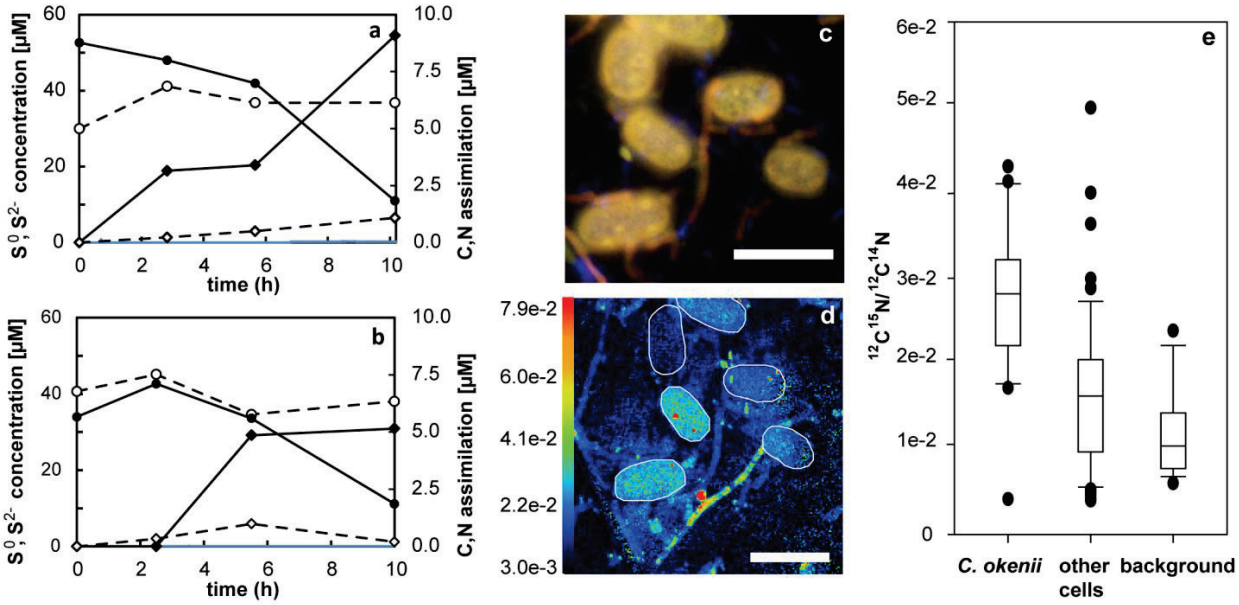

Figure 5. Light (a) and dark (b) *in situ* incubations from the Lake Cadagno chemocline showing sulfide (●) and S^o (○) species and CO_2 (♦) and NH_4^+ (◊) assimilation. An epifluorescence image (c) of autofluorescent phototrophic cells and other cells stained with DAPI from the end of the dark incubation and the parallel nanoSIMS image (d) showing $^{12}C^{15}N/^{14}N^{12}C$ ratios normalized to the natural abundance of ^{15}N. Scale bars are 10 µm. (e) Box-and-whisker plots showing $^{12}C^{15}N/^{14}N^{12}C$ ratios in *Chromatium okenii* and other cells in the sample. Background levels of ^{15}N are higher than natural abundance because ammonium adhered to the filter. The horizontal line within the box indicates the mean, boundaries of the box indicate the 25th- and 75th -percentile, and the whiskers indicate the highest and lowest values of the results, excluding outliers which are represented by black circles.

In our light incubation experiments, the CO_2 to sulfide ratio observed was about 1:4, which is lower than the theoretical ratios of partial and complete phototrophic sulfide oxidation. Ammonium was simultaneously assimilated at a C:N ratio of 8:1.

During the 10 h dark period, 23 $\mu mol \cdot l^{-1}$ sulfide was consumed and 5.2 $\mu mol \cdot l^{-1}$ CO_2 and 0.2 µM NH_4^+ were assimilated (Fig 5b). The dark rate of sulfide oxidation was approximately half (2.6 µM $H_2S \cdot h^{-1}$) of the light oxidation rate, but no known electron acceptors such as O_2, NO_x, or light were available. The corresponding CO_2 fixation rate was 600 nmol $C \cdot l^{-1} \cdot h^{-1}$ and the NH_4^+ assimilation rate was 25 nM $NH_4^+ \cdot h^{-1}$. It is possible that this dark carbon fixation was linked to dark sulfide oxidation, also resulting in a CO_2 to sulfide ratio of 1:4. The ratio of C:N assimilated in the dark was 24:1, or three times the light C:N assimilation ratio. The mechanism driving these dark reactions is not yet known. No significant change in sulfur concentration could be detected in the light or the dark incubations implying that sulfide was either oxidized to a colloidal sulfur pool passing through a 0.7 µm filter, or to sulfate.

In order to determine which bacteria were responsible for the dark carbon fixation and ammonium uptake observed, we performed single-cell nanoSIMS measurements of the light and the dark-incubated bacteria. Individual microbial cells could be identified based on DAPI staining, whereas phototrophic organisms were identified based on thee morphology of autofluorescent cells (Fig 5c). Cellular enrichment with ^{13}C was insignificant in both our light and dark experiments (data not shown), which is in contrast to the high ^{13}C enrichment measured previously (Musat et al., 2008). It is likely that due to the very low ^{13}C labeling percentage used (5%) and the low dark carbon fixation rates observed, the small amount of ^{13}C incorporated into individual cells was insufficient to detect using nanoSIMS. The uptake of $^{15}NH_4^+$ (100% labeled)

was measured as $^{15}N^{14}N/^{14}N$ and could also be used as a proxy for microbial activity. Phototrophic bacteria incorporated $^{15}NH_{4+}$ in the light (data not shown) and the dark (Fig 5d) into localized regions resembling granules within cells. Such localized assimilation is characteristic for storage compounds. Based on morphology, it appeared that the large *C. okenii*, coccoid-shaped *Lamprocystis* sp., and some filamentous GSB were highly active in the dark.

Cultivation of anoxygenic phototrophs from Lake Cadagno

We also attempted to study the anoxygenic phototrophs responsible for sulfide oxidation under controlled conditions by mimicking the Lake Cadagno environment with agar-stabilized sulfide gradients. Tubes of semi-solid agar containing a sulfidic bottom agar plug were inoculated with water from the chemocline. After a month of incubation in the light, dense communities of PSB developed between the gradient of upwards-diffusing sulfide and the surface colonies of photosynthetic algae (Fig S7). Microsensor profiles revealed that sulfide was completely consumed at the base of the PSB layer, but, unlike in the lake, as soon as the light was turned off, the sulfide gradient migrated slowly upwards through the agar into the zone of purple bacteria. Restricted bacterial motility in the agar and diffusion-limited conditions may have accounted for the differences observed between our cultures and *in situ* sulfide consumption.

Metagenomic insights into Lake Cadagno

We sequenced a metagenome (Fig S8) from the Lake Cadagno chemocline to obtain an overview of the metabolic potential of organisms in the oxygen and sulfide-free zone. Because the anoxygenic phototrophs appear to remain active in the dark, we searched in particular for

evidence of dark sulfide respiration mechanisms such as different types of terminal oxidases which indicate the potential for use of oxygen or other compounds as terminal electron acceptors. Although *Chromatium okenii* represent a large proportion of the biomass in the chemocline, they constitute only a minor fraction of total cell numbers (F. Danza, personal communication; Musat et al., 2008), explaining the low abundance of *Chromatium*-related sequences in our metagenome assembly. However, we were able to recover a genomic bin of a *Lamprocystis* species and two genomic bins of *Chlorobiaceae*, allowing us to investigate the genomic potential of other, more abundant anoxygenic phototrophs known to inhabit the chemocline of Lake Cadagno. Metagenomic data indicates that a *Pelodictyon clathratiforme*-like GSB is most abundant, with a ten-fold higher genome coverage compared to other genome bins of anoxygenic phototrophs (*Lamprocystis* sp. and a second pangenomic *Chlorobiaceae* bin). These results correspond well to the previously reported numerical dominance of *P. clathratiforme*, and the occurrence of *Lamprocystis* sp. and *Chlorobium phaeobacteroides* populations in Lake Cadagno (Tonolla et al., 2005).

In addition to the expected photothiotrophic machinery (genes encoding components of the SOX pathway, the reverse dissimilatory sulfite reductase [rDSR] pathway, and the adenylyl-sulfate reductase [APS] for sulfur oxidation, a PSII-like photosystem and RuBisCO), genes encoding both subunits of the cytochrome bd respiratory oxygen oxidoreductase were present in the *Lamprocystis* sp. genome bin, as well as several genes involved in the biosynthesis of cbb3 type cytochrome c oxidase. Both cytochrome bd and cytochrome *c* type cbb_3 are expressed in bacteria under microoxic conditions (Mouncey and Kaplan, 1998; Otten et al., 2001; Swem and Bauer, 2002) and have extremely high reported affinities for oxygen in the range of 3-8 nM

(D'Mello et al., 1996) and 7-40 nM (Preisig et al., 1996; Jackson et al., 2007), respectively. A variety of genes involved in oxidative stress defense (e.g. catalase, superoxide dismutase) were also detected. Furthermore, the presence of a gene repertoire encoding for glycogen metabolism indicates glycogen as a putative storage component in this PSB population.

DISCUSSION

The predominance of anoxygenic phototrophic bacteria in the chemocline and the large spatial separation between oxygen and sulfide gradients appears to suggest that the oxidative sulfur cycle in Lake Cadagno is light-driven. We would therefore expect a diurnal cycling of sulfur compounds such as sulfide, sulfur, and sulfate. However, our high-resolution profiles revealed that sulfide consumption in the chemocline occurred not only in the light but also in the dark. A dark mechanism of sulfide removal has not yet been described for the anoxic zone in the Lake Cadagno water column, nor has the dark metabolism of the dominant anoxygenic phototrophs been investigated *in situ*. From our assessment of possible alternative electron acceptors used to oxidize the flux of upwards-diffusing sulfide, we concluded that only the supply of oxygen was sufficient to account for up to almost half of the sulfide flux consumed in the dark (Fig 4f). These sulfide and oxygen fluxes were similar to previous years (2013 and 2014). The apparent deficit in the oxygen budget may have been supplemented by horizontal intrusions of oxygenated water masses into the chemocline or by an unknown electron acceptor (discussed below). Although temperature/conductivity profiles revealed no evidence of lateral intrusions, anomalies indicative of such horizontal mixing may have been obscured by the intense convection within the chemocline. In fact, the Lake Cadagno water column is not in steady state,

and the compression and expansion of water masses by internal waves could have influenced our calculations of the sulfide and oxygen budgets.

It is indeed surprising that aerobic sulfide oxidation should be the dominant sulfide oxidation process in an anoxic water layer. The storage and transport of intermediates, *i.e.* zero-valent sulfur, appears to play a key role in the coupling of electron donors from the monoliminion with electron acceptors from the epilimnion. The sequential occurrence of sulfide, sulfur, sulfate, and oxygen gradients revealed that sulfide was first oxidized to sulfur near the base of the chemocline and then transported to the base of the oxycline where it was oxidized to sulfate. Most of this sulfur was likely accumulated intracellularly during sulfide oxidation by *C. okenii* which is known to store more sulfur under light limiting conditions (Van Gemerden et al., 1990), such as those occurring at the base of the Lake Cadagno chemocline. Our Raman measurements suggest that some of the sulfur detected in the chemocline was in the form of linear polysulfides which are likely the more reactive, bioavailable stored sulfur species (Berg et al., 2014). In contrast to other environmental PSB populations which sediment out of the water column as they accumulate S^0 and increase their buoyant density (e.g. van Gemerden et al., 1985), *C. okenii* cells full of S^0 migrated upwards, especially in the early morning in response to the first rays of sunlight. In fact, the highest sulfide consumption rates were detected at this time when large numbers of *C. okenii* aggregated at the top of the chemocline, depleting the dark-accumulated sulfide within the first 3 h of daylight (Fig 4a,b). This indicates that sulfide was limiting in the chemocline for the remainder of the day. It is therefore likely that *C. okenii* and possibly other motile PSB also actively swim downwards to replenish their sulfur reserves, as shown by (Pfennig et al., 1968), rather than passively sinking.

While zero-valent sulfur served as an important intermediate in sulfide oxidation to sulfate, we could not determine what fueled the initial oxidation of sulfide to sulfur in the dark. We therefore hypothesize that dark sulfide oxidation in the Lake Cadagno chemocline is driven by the transport of electron donors and acceptors (*i.e.* O_2) in the well-mixed, turbulent chemocline. However, it is still not clear whether oxidizing and reducing equivalents (other than S^0) are stored intracellularly or whether dissolved compounds are simply carried by advected water masses. It is likely that bacteria are responsible for this mixing (Wüest, 1994; Egli et al., 1998), and directly benefit from the enhanced advective transport. Our microcosm experiments in agar tubes supported this theory that bacterial motility and mixing were necessary conditions for continued dark sulfide oxidation when sulfide and oxygen gradients were spatially separated. A weakening of the mixing regime in 2015 may have signified a breakdown of this transport mechanism and contributed to the accumulation sulfide in the chemocline.

Oxygen-dependent sulfate production in 2015 was evidenced by a peak in excess sulfate at the oxycline under both light and dark conditions (Fig 1d). In 2014, sulfate production was instead related to PAR intensity (Fig 2), indicating that sulfur could either have been oxidized aerobically within the chemocline using *in situ*-produced oxygen (Milucka et al., 2015) or phototrophically at some threshold light intensity in the upper half of the chemocline. Many of the PSB are known to switch to aerobic sulfide oxidation in the dark (e.g. Kampf and Pfennig, 1980; de Witt and van Gemerden, 1990). Our profiles show that PSB in Lake Cadagno are well adapted to fluctuating light/dark and oxic/anoxic conditions, surviving in both dark and light by respiring aerobically. This is in contrast to laboratory findings showing that PSB continue to grow

phototrophically under fluctuating oxic/anoxic conditions as long as they are provided with light (de Witt and van Gemerden, 1990).

It is interesting that oxygen should play a major role in sulfide oxidation in the anoxic chemocline of Lake Cadagno. Dissolved oxygen and sulfide may be entrained into the chemocline and consumed so rapidly that they remain below their respective detection limits of 50-100 nM (Kirf et al., 2014) and 0.5 µM (Reese et al., 2011) with the methods used. Biochemical evidence suggests that anoxygenic phototrophic bacteria could respire on such low, nanomolar concentrations of oxygen and sulfide. Several species of the *Chromatiaceae* described in the literature have a respiratory chain with a high affinity for O_2 (K_m= 0.3-0.9 µM) and sulfide (K_m=0.46 µM (Overmann and Pfennig, 1992). Genes for both the type *cbb*$_3$ and *bd* enzyme were identified in our *Lamprocystis* sp. metagenome bin as well as in the genome of *Thiodictyon syntrophicum*, another PSB isolated from Lake Cadagno (S. Luedin, personal communication) indicating a potential for aerobic metabolism under low oxygen conditions. In contrast, the bd cytochromes identified in our GSB metagenome bins likely has a similar function to bd cytochromes in the sulfate reducing bacteria, which play a role the defense against oxidative stress (Dolla et al., 2006). The biochemical limits to oxygen utilization are thus far below current definitions of *anoxia* and demonstrate that aerobic respiration is possible in the "anoxic" chemocline.

According to our carbon fixation measurements, light-independent carbon fixation activity may account for up to half of total primary production in the chemocline. The 1:4 stoichiometry of carbon fixation coupled to reduced sulfur oxidation measured in our incubations also suggests that the Lake Cadagno microbial community performs predominantly chemotrophic rather than

phototrophic sulfide oxidation under both light and dark conditions. In chemolithoautotrophic sulfide oxidation, H_2S serves not only as the energy source but also as the electron donor for the reduction of CO_2 leading to varied energy conservation efficiencies dependent on the enzymatic sulfur oxidation pathway utilized (Klatt and Polerecky, 2014). A low CO_2 fixation efficiency may thus indicate that processes other than anoxygenic photosynthesis oxidize sulfide not only in the dark but also in the light. Although aerobic respiration could be an alternative sulfide oxidation mechanism in the lake, no oxygen was present in our incubations to account for the approximately 20 µmol of sulfide oxidized in the dark. Moreover, the calculated oxygen fluxes could in general account for less than 50% of dark sulfide consumption in the lake. We can therefore not exclude the possibility that an additional, yet-unknown electron acceptor is utilized for sulfide oxidation.

The majority of the active microorganisms identified under both light and dark conditions were anoxygenic phototrophs which are known to accumulate a variety of carbon storage compounds in addition to S^0 in the light (Mas and Van Gemerden, 1995). Although filamentous GSB actively assimilated NH_4^+ in the dark (Fig 5d), we presumed that sulfur oxidation and CO_2 assimilation was dominated by purple sulfur bacteria based on a previous study (Storelli et al., 2013). Some PSB are known to reduce stored S^0 with glycogen in the dark (Van Gemerden, 1968; Del Don et al., 1994), but this type of glycogen fermentation as observed in laboratory cultures may be rather inefficient for bacteria in complex and fluctuating environments where other electron acceptors become transiently available. It is conceivable that a carbon compound of higher oxidation state than sulfide (-2) could instead be utilized for reduced sulfur oxidation. However,

the diel cycling of PHB or glycogen, the major storage compounds known for PSB, remains to be investigated.

Figure 6: Schematic model of sulfide oxidation in the Lake Cadagno chemocline.

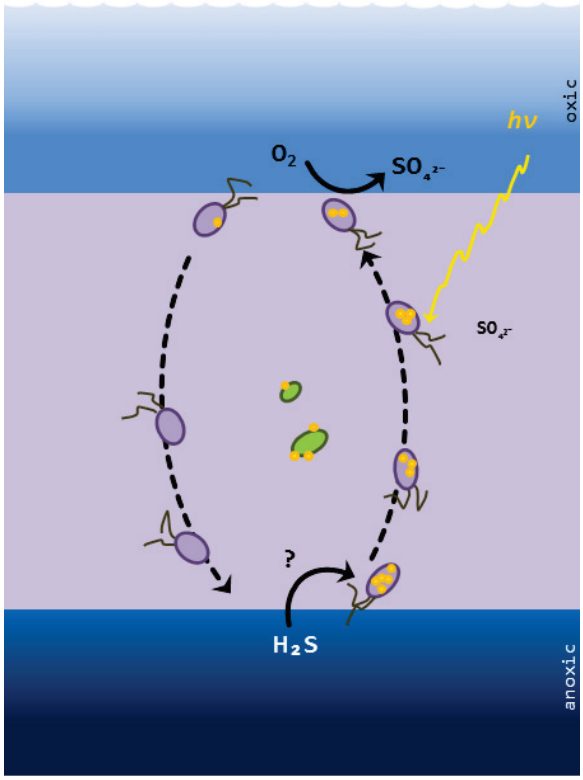

Taken together, our results could be used to construct a model (Fig 6) illustrating how sulfide is respired aerobically by anoxygenic, phototrophic bacteria in the oxygen- and sulfide-free chemocline of Lake Cadagno. Motile purple sulfur bacteria like *C. okenii* transport electron donors from the sulfidic zone as S^0 upwards to the oxycline where it is further oxidized to sulfate with light or O_2. It is possible that as the bacteria actively swim downward to replenish their internal sulfur, they entrain oxygenated water into the chemocline or that they store an unknown compound intracellularly. Although the insufficient supply of oxygen suggests that another, possibly organic, compound is involved in dark sulfide oxidation, such a compound has yet to be identified.

CONCLUSIONS

Sulfur-oxidizing bacteria have previously been reported to bridge distances between electron donor and acceptor supply by storing and transporting S^0 and NO^{3-} between redox zones (Fossing et al., 1995; Jørgensen and Gallardo, 1999) or even transferring electrons along nanowires (Pfeffer et al., 2012), but the sulfide oxidation processes in Lake Cadagno represent a new mechanism of electron transport by motile bacteria. The discovery of such novel storage

and transport processes may provide insight into sulfide oxidation in other anoxic environments such as the Black Sea where the mechanism of sulfide removal is not completely understood. The detection of significant light-independent sulfide oxidation linked to carbon fixation may also reshape our understanding of primary production at oxic-anoxic interfaces within the photic zone. These unexpected insights into the ecophysiology of the purple sulfur bacteria in Lake Cadagno demonstrate the importance of studying these versatile bacteria *in situ* using culture-independent methods to understand their function in the environment.

EXPERIMENTAL PROCEDURES

Sampling

The meromictic Lake Cadagno is situated in the Piora Valley in the Swiss Alps at an altitude of 1921 m. Data presented here were collected during field campaigns in September 2013, August 2014, June 2015 and August 2015. In 2013 and 2014 *in situ* measurements were performed with a profiling ion analyzer (PIA; see Kirf et al., 2014 for description) lowered from a platform anchored at the deepest part of the lake (20.7 m). Conductivity, turbidity, depth (pressure), temperature and pH were measured with a multi-parameter probe (XRX 620, RBR). Dissolved oxygen was recorded online with a type PSt1 normal (detection limit 125 nM) micro-optode and a type TOS7 trace (reliable detection limit 50-100 nM) micro-optode (PreSens). The oxygen sensors were calibrated by parallel Winkler titrations. Water samples for chemical analyses and cell counts were collected with a rosette syringe sampler equipped with twelve 60-ml syringes triggered online at selected depths. Due to a technical failure of the PIA, the 6 AM profile in August 2014 and all subsequent profiles in 2015 were measured with a SBE 19 plus V2 CTD probe (Sea-Bird Electronics, WA, USA) equipped with sensors for pressure, temperature and

conductivity, and with additional sensors for turbidity (WET Labs Eco), oxygen (SBE 43), pH (18-I) and two fluorescence wavelengths (WET Labs ECO-AFL, FL, USA). The detection limit of the SBE 43 oxygen probe was about 1 µmol/l. In parallel with *in situ* measurements, water for chemical analyses was pumped to the surface through Neoprene tubing attached to the CTD and filled into 60-ml syringes (rinsed 2 X with in situ water) on board. Two parallel metal plates of diameter ~15 cm attached to the submersed end of the tubing (see Materials and Methods for illustration) served to channel water horizontally, resulting in more discrete vertical profiling.

Water samples in syringes were aliquoted on board immediately after collection. Samples for sulfate analyses were filtered (0.22 µm pore size) directly into sterile Eppendorf vials. Sulfide samples were fixed with Zn-acetate to a final concentration of 0.1 % (w/v). Biomass was concentrated onto glass fiber filters (0.7 µm pore size) and stored at -20°C for analyses of intracellularly stored elemental sulfur and organic carbon compounds. Filtrate (0.22 µm pore size) was also collected and frozen at -20°C for metabolome analysis of dissolved compounds. Samples for fluorescence *in situ* hybridization were immediately fixed with 2% (v/v) formaldehyde. Samples for DNA analysis were collected on polycarbonate filters (0.22 µm pore size) on site and frozen at -20°C until further processing.

Chemical Analyses

Sulfide was measured using the colorimetric method of Cline (1969). Sulfate was measured on a 761 Compact ion chromatograph (Metrohm, Filderstadt, Germany) equipped with a Metrosep A SUPP 5 column. Intracellular sulfur on filters was extracted by sonication in methanol for 15 min in an ice bath and measured on an Acquity H-Class UPLC system (Waters Corporation, USA) with an Acquity UPLC BEH C18 column coupled to a photodiode array (PDA) detector. Analytical

conditions are further described in the supplementary methods. Data was acquired and processed using the Empower III software.

Sulfate reduction rates were measured by adding the radiotracer $^{35}SO_4^{2-}$ (5 MBq) to anoxic lake water in 50-ml glass syringes and incubated in the dark. A solution of unlabeled Na_2S was added to a final concentration of ~50 µmol·l^{-1} as a background sulfide pool in case of sulfide re-oxidation. At each sampling point, 10 ml of sample was dispensed into 5 ml of 20% (w/v) Zn-acetate. Reduced sulfur species (e.g. sulfur and sulfide as ZnS) were separated out via the chromium distillation method described in (Kallmeyer et al., 2004) and the radioactivity per sample was determined via scintillation counting (Packard 2500 TR).

Flux Calculations

Turbulent fluxes (J) of sulfide, sulfur, sulfate, and oxygen at the chemocline were calculated assuming steady state by applying Fick's first law: $J=-D\partial C/\partial x$. For sulfide, sulfate, and oxygen we used the turbulent diffusion coefficient (D) of $1.6 \times 10^{-6}\,m^2\,s^{-1}$ from (Wüest, 1994) corresponding to turbulence at the Lake Cadagno chemocline boundaries. For sulfur gradients within the well-mixed chemocline the coefficient $D = 1.5 \times 10^{-5}\,m^2\,s^{-1}$ (Wüest, 1994) was used. The change in concentration (∂C) was computed for each species over the depths with the steepest gradients. Oxygen and sulfide fluxes were determined for the regions immediately above and below the chemocline, defined as the zone of constant conductivity.

DNA extraction, sequencing, and analysis

Environmental DNA was extracted from polycarbonate filters with the MoBio PowerSoil DNA kit (MoBio Laboratories, Carlsbad, USA) according to the manufacturer's protocol with the following modification: the bead beating step was reduced to 30 sec followed by incubation on

ice for 30 sec, repeated 4x. The DNA was gel-purified using SYBR Green I Nucleic Acid Gel Stain (Invitrogen) and the QIAquick Gel Extraction Kit (Qiagen) according to the accompanying protocols. DNA concentration was determined fluorometrically at 260 nm, using the Qubit 2.0 Fluorometer and the Qubit dsDNA HS Assay KIT (Invitrogen) and sent to the Max Planck-Genome Centre (Cologne, Germany) for sequencing. The metagenome was sequenced (100 bp paired end reads) by Illumina HiSeq (Illumina Inc., USA) sequencing following a TruSeq library preparation. Metagenomic reads were adapter- and quality-trimmed (phred score 15, bbduk function of the BBMap package, https://sourceforge.net/projects/bbmap/) and paired-end reads were *de novo* assembled with the uneven depth assembler IDBA-UD (Peng et al., 2012). The metagenome assembly was binned based on tetranucleotide frequencies, coverage, taxonomic classification, paired=end read mapping and conserved single-copy gene profiles with the Metawatt binning software (version 3.5.2; Strous et al., 2012). Bins classified as known PSB or GSB and assessed as more the 25% complete based on conserved single-copy gene profiles were automatically annotated with the RAST annotation pipeline (Aziz et al., 2008) and manually screened for the presence of genes of interest to this study.

Stable isotope incubations

Water collected in 1-L Duran bottles was bubbled with N_2 gas for 15 min to remove any oxygen contamination. Labeled ^{13}C- HCO_3^- was added to a final concentration of 200 µM to achieve a final labeling percentage of approximately 10 atm % ^{13}C. Sulfide was added to a final concentration of 50 µM. Water was aliquoted anoxically into 50-ml Winkler bottles and sealed with no headspace. Bottles were incubated in a water bath with a constant temperature (4-6°C) for 12 h. Half the bottles were exposed > 750 nm filtered (red) light and half the bottles were

wrapped in aluminium foil to keep them dark. Dissolved O_2 concentrations were monitored in the last bottle of each incubation series using trace optode spots (TROXSP5, Pyroscience) fixed to the inner surface of the incubation bottles connected to a FireSting O_2 oxygen logger (Pyroscience). Bottles were sampled destructively at each time point by concentrating ^{13}C-labeled biomass onto precombusted (6 h at 600 °C) GF/F filters (Whatman, St Louis, MO, USA). Sub-samples were also fixed with 2 % (v/v) formaldehyde at 4°C for no more than 24 hours before filtration onto 0.2 µm Au/Pd-sputtered polycarbonate filters (Millipore) for subsequent nanoSIMS analyses. At the beginning of the experiment, a water sample was sterile-filtered into a glass HPLC vial to verify the ^{13}C-DIC labeling percentage. Samples for sulfide, intracellular sulfur, and sulfate were collected and processed as described above.

Mass spectrometry isotope uptake analysis

The incorporation of $^{13}CO_2$ and $^{15}NH_4^+$ into biomass was measured by combustion of particulate organic carbon collected on GF/F filters. Filters were first decalcified by exposure to 37% fuming HCl for > 12 h, dried in an oven at 60°C, and packed into tin capsules for combustion analysis. The C- and N-isotopic composition of particulate organic carbon in these experiments was determined on an automated elemental analyser (Thermo Flash EA, 1112 Series) coupled to a Delta Plus XP IRMS (Thermo Finnigan, Dreieich, Germany). Instrument accuracy and precision of C and N measurements were estimated at 1.066223 ± 0.006581 ^{13}C atom% and 0.366426 ± 0.005328 ^{15}N atom%, respectively, based on the mean and 3 standard deviations of caffeine standards measured in parallel with the samples. The labeling % of $^{13}CO_2$ was determined from 1 ml of culture filtrate transferred into a 12 ml Exetainer (Labco Limited, High Wycombe, UK) with a He headspace. Samples were subsequently acidified with the addition of ~100 µl

concentrated H_3PO_4. Outgassed $^{13}CO_2$ was analyzed using a GasBench II coupled to a Delta Plus isotope ratio mass spectrometry (IRMS; Thermo Finnigan, Dreieich, Germany).

NanoSIMS

Cells on Au/Pd-sputtered filters were stained with 4',6-diamidino-2-phenylindole (DAPI, 1 µg ml^{-1}) and areas of interest were marked using a Laser Micro Dissection (LMD) microscope 6500 (Leica, Berlin, Germany). Marked areas were imaged in parallel using a Nikon ECLIPSE Ci microscope using a DAPI excitation filter to detect total cells and green (cy3) and red (FITC) excitation filters to detect autofluorescent phototrophic cells. Prepared filters were analyzed using a nanoSIMS 50L (CAMECA, Gennevilliers Cedex, France) at the Max Planck Institute for Marine Microbiology in Bremen. Each measurement area was first pre-sputtered with a Cs^+ primary ion beam of 300 pA. Then a primary Cs^+ ion beam with a current between 1.0 and 1.2 pA and a beam diameter smaller than 100 nm was rastered across the cells for analysis. Secondary ion images of $^{12}C^-$, $^{13}C^-$, $^{12}C^{14}N^-$, $^{12}C^{15}N^-$, $^{32}S^-$ and $^{31}P^-$ were recorded simultaneously, using 5 electron multipliers. Analysis areas ranged between 10 x 10 µm to 50 x 50 µm in size, corresponding to an image size of 256 x 256 and 512 x 512 pixels. For every area of interest, 40 planes were recorded using a dwell time of 1 ms per pixel. The proprietary CAMECA WinImage processing software and the Mathlab based Look@NanoSIMS software (Polerecky et al., 2012) was used for images and data processing. All planes of measurement were corrected for possible stage and source drift during the measurement and accumulated after the correction.

ACKGNOWLEDGEMENTS

We are grateful to the 2014 and 2015 Cadagno Field Expedition Teams from EAWAG and MPI Bremen for assistance in the field, and to the Alpine Biology Center Foundation (Switzerland) for

use of its research facilities. We would especially like to thank Dolma Michellod, Kirsten Oswald, Daniela Tienken and Samuel Luedin for technical support. Funding was provided by the International Max Planck Research School of Marine Microbiology, the Max Planck Society, and the Deutsche Forschungsgemeinschaft (through the MARUM Center for Marine Environmental Sciences).

REFERENCES

Aziz, R.K., Bartels, D., Best, A.A., DeJongh, M., Disz, T., Edwards, R.A. et al. (2008) The RAST Server: rapid annotations using subsystems technology. *BMC Genomics* **9**: 1.

Berg, J.S., Schwedt, A., Kreutzmann, A.-C., Kuypers, M.M., and Milucka, J. (2014) Polysulfides as Intermediates in the Oxidation of Sulfide to Sulfate by Beggiatoa spp. *Applied and Environmental Microbiology* **80**: 629-636.

Bosshard, P.P., Stettler, R., and Bachofen, R. (2000) Seasonal and spatial community dynamics in the meromictic Lake Cadagno. *Archives of Microbiology* **174**: 168-174.

Cline, J.D. (1969) Spectrophotometric determination of hydrogen sulfide in natural waters. *Limnology and Oceanography* **14**: 454-458.

Dahl, T.W., Anbar, A.D., Gordon, G.W., Rosing, M.T., Frei, R., and Canfield, D.E. (2010) The behavior of molybdenum and its isotopes across the chemocline and in the sediments of sulfidic Lake Cadagno, Switzerland. *Geochimica et Cosmochimica Acta* **74**: 144-163.

De Wit, R., Jonkers, H.M., Van Den Ende, F.P., and Van Gemerden, H. (1989) In situ fluctuations of oxygen and sulphide in marine microbial sediment ecosystems. *Netherlands Journal of Sea Research* **23**: 271-281.

De Witt, R., and van Gemerden, H. (1990) Growth of the phototrophic purple sulfur bacterium Thiocapsaroseopersicina under oxic/anoxic regimens in the light. *FEMS microbiology ecology* **6**: 69-76.

Del Don, C., Hanselmann, K.W., Peduzzi, R., and Bachofen, R. (1994) Biomass composition and methods for the determination of metabolic reserve polymers in phototrophic sulfur bacteria. *Aquatic Sciences* **56**: 1-15.

Del Don, C., Hanselmann, K.W., Peduzzi, R., and Bachofen, R. (2001) The meromictic alpine Lake Cadagno: orographical and biogeochemical description. *Aquatic Sciences* **63**: 70-90.

D'mello, R., Hill, S., and Poole, R.K. (1996) The cytochrome bd quinol oxidase in Escherichia coli has an extremely high oxygen affinity and two oxygen-binding haems: implications for regulation of activity in vivo by oxygen inhibition. *Microbiology* **142**: 755-763.

Dolla, A., Fournier, M., and Dermoun, Z. (2006) Oxygen defense in sulfate-reducing bacteria. *Journal of Biotechnology* **126**: 87-100.

Egli, K., Wiggli, M., Klug, J., and Bachofen, R. (1998) Spatial and temporal dynamics of the cell density in a plume of phototrophic microorganisms in their natural environment. *Doc Ist Ital Idrobiol* **63**: 121-126.

Findlay, A.J., Bennett, A.J., Hanson, T.E., and Luther, G.W. (2015) Light-dependent sulfide oxidation in the anoxic zone of the Chesapeake Bay can be explained by small populations of phototrophic bacteria. *Applied and Environmental Microbiology* **81**: 7560-7569.

Fossing, H., Gallardoi, V., Jorgensen, B., Hiittel, M., Nielsenl, L., Schulz, H. et al. (1995) Concentration and transport of nitrate by the mat-forming sulphur bacterium Thioploca. *Nature* **374**: 20.

Halm, H., Musat, N., Lam, P., Langlois, R., Musat, F., Peduzzi, S. et al. (2009) Co-occurrence of denitrification and nitrogen fixation in a meromictic lake, Lake Cadagno (Switzerland). *Environmental Microbiology* **11**: 1945-1958.

Jackson, R.J., Elvers, K.T., Lee, L.J., Gidley, M.D., Wainwright, L.M., Lightfoot, J. et al. (2007) Oxygen reactivity of both respiratory oxidases in Campylobacter jejuni: the cydAB genes encode a cyanide-resistant, low-affinity oxidase that is not of the cytochrome bd type. *Journal of Bacteriology* **189**: 1604-1615.

Janz, G., Downey Jr, J., Roduner, E., Wasilczyk, G., Coutts, J., and Eluard, A. (1976) Raman studies of sulfur-containing anions in inorganic polysulfides. Sodium polysulfides. *Inorganic Chemistry* **15**: 1759-1763.

Jørgensen, B.B., and Des Marais, D.J. (1986) Competition for sulfide among colorless and purple sulfur bacteria in cyanobacterial mats. *FEMS Microbiology Ecology* **2**: 179-186.

Jørgensen, B.B., and Gallardo, V.A. (1999) Thioploca spp.: filamentous sulfur bacteria with nitrate vacuoles. *FEMS Microbiology Ecology* **28**: 301-313.

Jørgensen, B.B., Kuenen, J.G., and Cohen, Y. (1979) Microbial transformations of sulfur compounds in a stratified lake (Solar Lake, Sinai) 1. *Limnology and Oceanography* **24**: 799-822.

Jørgensen, B.B., Fossing, H., Wirsen, C.O., and Jannasch, H.W. (1991) Sulfide oxidation in the anoxic Black Sea chemocline. *Deep Sea Research Part A Oceanographic Research Papers* **38**: S1083-S1103.

Kallmeyer, J., Ferdelman, T.G., Weber, A., Fossing, H., and Jørgensen, B.B. (2004) A cold chromium distillation procedure for radiolabeled sulfide applied to sulfate reduction measurements. *Limnology and Oceanography Methods* **2**: 171-180.

Kampf, C., and Pfennig, N. (1980) Capacity of Chromatiaceae for chemotrophic growth. Specific respiration rates of Thiocystis violacea and Chromatium vinosum. *Archives of Microbiology* **127**: 125-135.

Khan, S.A., Hughes, R.W., and Reynolds, P.A. (2011) Raman spectroscopic determination of oxoanions in aqueous polysulfide electrolyte solutions. *Vibrational Spectroscopy* **56**: 241-244.

Kirf, M.K., Dinkel, C., Schubert, C.J., and Wehrli, B. (2014) Submicromolar oxygen profiles at the oxic–anoxic boundary of temperate lakes. *Aquatic Geochemistry* **20**: 39-57.

Klatt, J.M., and Polerecky, L. (2014) Assessment of the stoichiometry and efficiency of CO2 fixation coupled to reduced sulfur oxidation. *Frontiers in Microbiology* **6**.

Kühl, M., and Jørgensen, B.B. (1992) Microsensor measurements of sulfate reduction and sulfide oxidation in compact microbial communities of aerobic biofilms. *Applied and Environmental Microbiology* **58**: 1164-1174.

Lavik, G., Stührmann, T., Brüchert, V., Van der Plas, A., Mohrholz, V., Lam, P. et al. (2009) Detoxification of sulphidic African shelf waters by blooming chemolithotrophs. *Nature* **457**: 581-584.

Mas, J., and Van Gemerden, H. (1995) Storage products in purple and green sulfur bacteria. In *Anoxygenic Photosynthetic Bacteria*: Springer, pp. 973-990.

Milucka, J., Kirf, M., Lu, L., Krupke, A., Lam, P., Littmann, S. et al. (2015) Methane oxidation coupled to oxygenic photosynthesis in anoxic waters. *The ISME Journal*.

Mouncey, N.J., and Kaplan, S. (1998) Oxygen Regulation of the ccoN Gene Encoding a Component of the cbb 3 Oxidase in Rhodobacter sphaeroides 2.4. 1T: Involvement of the FnrL Protein. *Journal of Bacteriology* **180**: 2228-2231.

Musat, N., Halm, H., Winterholler, B., Hoppe, P., Peduzzi, S., Hillion, F. et al. (2008) A single-cell view on the ecophysiology of anaerobic phototrophic bacteria. *Proceedings of the National Academy of Sciences* **105**: 17861-17866.

Niel, C.v. (1932) On the morphology and physiology of the purple and green sulphur bacteria. *Archives of Microbiology* **3**: 1-112.

Otten, M.F., Stork, D.M., Reijnders, W.N., Westerhoff, H.V., and Van Spanning, R.J. (2001) Regulation of expression of terminal oxidases in Paracoccus denitrificans. *European Journal of Biochemistry* **268**: 2486-2497.

Overmann, J. (1997) Mahoney Lake: a case study of the ecological significance of phototrophic sulfur bacteria. In *Advances in Microbial Ecology*: Springer, pp. 251-288.

Overmann, J. (2001) Phototrophic consortia: a tight cooperation between non-related eubacteria. In *Symbiosis*: Springer, pp. 239-255.

Overmann, J., and Pfennig, N. (1992) Continuous chemotrophic growth and respiration of Chromatiaceae species at low oxygen concentrations. *Archives of Microbiology* **158**: 59-67.

Overmann, J., Cypionka, H., and Pfennig, N. (1992) An extremely low-light adapted phototrophic sulfur bacterium from the Black Sea. *Limnology and Oceanography* **37**: 150-155.

Pedrós-Alió, C., and Guerrero, R. (1993) Microbial ecology in lake Cisó. In *Advances in Microbial Ecology*: Springer, pp. 155-209.

Peng, Y., Leung, H.C., Yiu, S.-M., and Chin, F.Y. (2012) IDBA-UD: a de novo assembler for single-cell and metagenomic sequencing data with highly uneven depth. *Bioinformatics* **28**: 1420-1428.

Pfeffer, C., Larsen, S., Song, J., Dong, M., Besenbacher, F., Meyer, R.L. et al. (2012) Filamentous bacteria transport electrons over centimetre distances. *Nature* **491**: 218-221.

Pfennig, N., Höfling, K.-H., and Kusmierz, H. (1968) *Chromatium okenii (Thiorhodaceae)-Biokonvektion, aero-und phototaktisches Verhalten*: IWF.

Polerecky, L., Adam, B., Milucka, J., Musat, N., Vagner, T., and Kuypers, M.M. (2012) Look@ NanoSIMS–a tool for the analysis of nanoSIMS data in environmental microbiology. *Environmental Microbiology* **14**: 1009-1023.

Prange, A., Arzberger, I., Engemann, C., Modrow, H., Schumann, O., Trüper, H.G. et al. (1999) In situ analysis of sulfur in the sulfur globules of phototrophic sulfur bacteria by X-ray absorption near edge spectroscopy. *Biochimica et Biophysica Acta (BBA)-General Subjects* **1428**: 446-454.

Preisig, O., Zufferey, R., Thöny-Meyer, L., Appleby, C.A., and Hennecke, H. (1996) A high-affinity cbb3-type cytochrome oxidase terminates the symbiosis-specific respiratory chain of Bradyrhizobium japonicum. *Journal of Bacteriology* **178**: 1532-1538.

Reese, B.K., Finneran, D.W., Mills, H.J., Zhu, M.-X., and Morse, J.W. (2011) Examination and refinement of the determination of aqueous hydrogen sulfide by the methylene blue method. *Aquatic geochemistry* **17**: 567-582.

Socrates, G. (2004) *Infrared and Raman Characteristic Group frequencies: Tables and Charts*: John Wiley & Sons.

Stal, L.J., van Gemerden, H., and Krumbein, W.E. (1985) Structure and development of a benthic marine microbial mat. *FEMS Microbiology Ecology* **1**: 111-125.

Storelli, N., Peduzzi, S., Saad, M.M., Frigaard, N.-U., Perret, X., and Tonolla, M. (2013) CO_2 assimilation in the chemocline of Lake Cadagno is dominated by a few types of phototrophic purple sulfur bacteria. *FEMS Microbiology Ecology* **84**: 421-432.

Strous, M., Kraft, B., Bisdorf, R., and Tegetmeyer, H. (2012) The binning of metagenomic contigs for microbial physiology of mixed cultures. *Frontiers in Microbiology* **3**: 410.

Swem, D.L., and Bauer, C.E. (2002) Coordination of ubiquinol oxidase and cytochrome cbb3 oxidase expression by multiple regulators in Rhodobacter capsulatus. *Journal of Bacteriology* **184**: 2815-2820.

Tonolla, M., Peduzzi, R., and Hahn, D. (2005) Long-term population dynamics of phototrophic sulfur bacteria in the chemocline of Lake Cadagno, Switzerland. *Applied and Environmental Microbiology* **71**: 3544-3550.

Tonolla, M., Demarta, A., Peduzzi, R., and Hahn, D. (1999) In situ analysis of phototrophic sulfur bacteria in the chemocline of meromictic Lake Cadagno (Switzerland). *Applied and Environmental Microbiology* **65**: 1325-1330.

Vaituzis, Z., and Doetsch, R. (1969) Motility tracks: technique for quantitative study of bacterial movement. *Applied Microbiology* **17**: 584-588.

Van Gemerden, H. (1968) On the ATP generation by Chromatium in darkness. *Archiv für Mikrobiologie* **64**: 118-124.

Van Gemerden, H., and Mas, J. (1995) Ecology of phototrophic sulfur bacteria. In *Anoxygenic Photosynthetic Bacteria*: Springer, pp. 49-85.

Van Gemerden, H., Visscher, P.T., and Mas, J. (1990) Environmental control of sulfur deposition in anoxygenic purple and green sulfur bacteria. In *Novel Biodegradable Microbial Polymers*: Springer, pp. 247-262.

van Gemerden, H., Montesinos, E., Mas, J., and Guerrero, R. (1985) Diel cycle of metabolism of phototrophic purple sulfur bacteria in Lake Ciso(Spain). *Limnology and Oceanography* **30**: 932-943.

Van Gemerden, H., Tughan, C.S., De Wit, R., and Herbert, R. (1989) Laminated microbial ecosystems on sheltered beaches in Scapa Flow, Orkney Islands. *FEMS Microbiology Ecology* **5**: 87-101.

Wieland, A., Zopfi, J., Benthien, M., and Kühl, M. (2005) Biogeochemistry of an iron-rich hypersaline microbial mat (Camargue, France). *Microbial Ecology* **49**: 34-49.

Wüest, A. (1994) Interactions in lakes: Biology as source of dominant physical forces. *Limnologica Jena* **24**: 93-104.

SUPPLEMENTARY FIGURES

Figure S1: Profiles of the Lake Cadagno water column from 2015 taken every ~4 hrs for 48 hrs. Sunset was at 20:53 and sunrise at 6:11. Some sulfide accumulates in the chemocline in the dark and presumably reacts with S^0 to form polysulfides which is detected as sulfide by the Cline method. S^0 was measured as particulate (intra- and extracellular) sulfur on 0.7 um filters and included polysulfides which would have spontaneously oxidized during filtration. Oxygen data was not available for profiles 1 and 8.

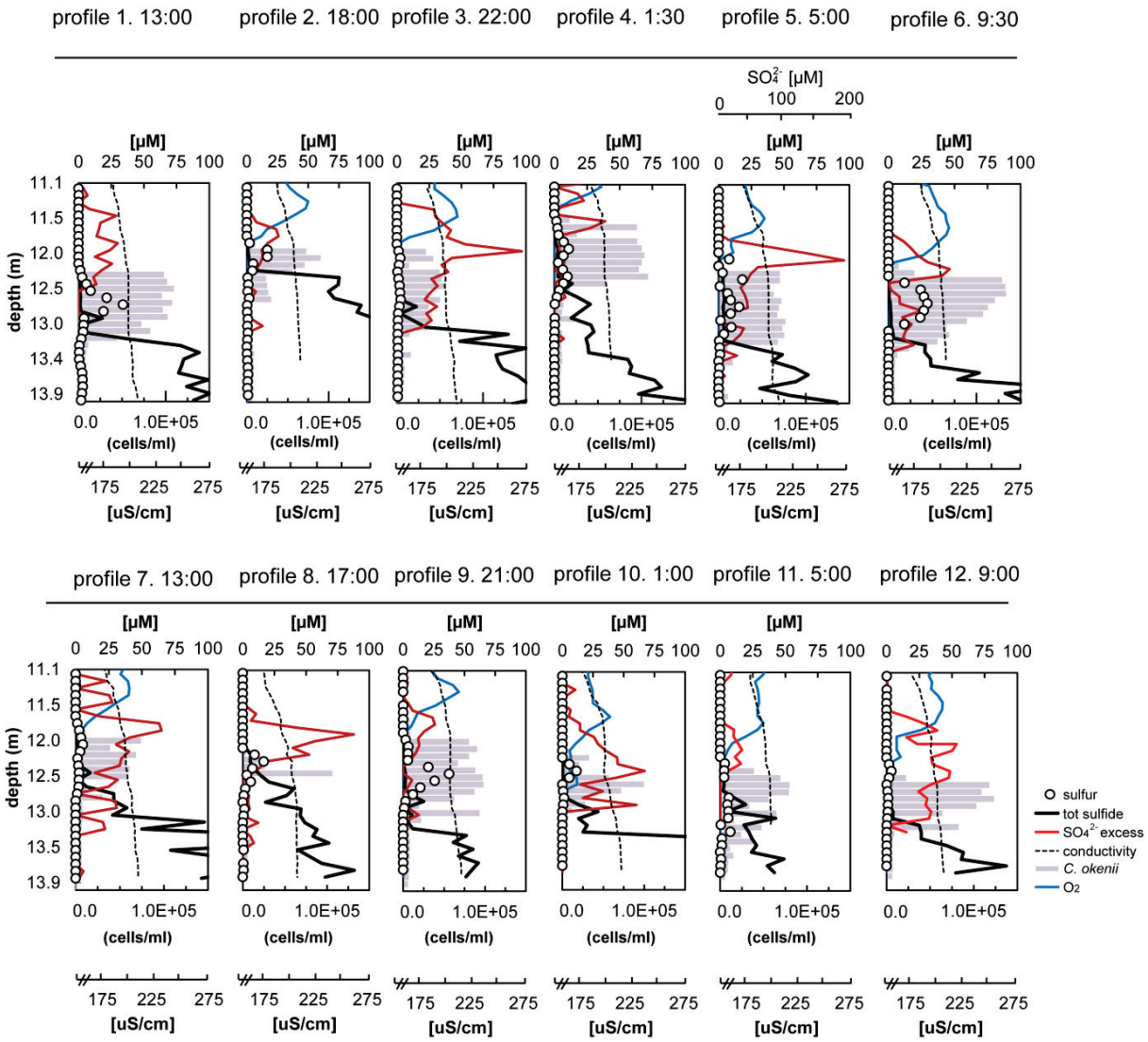

Figure S2: Profiles of the Lake Cadagno water column in Sept 2013 and Aug 2014. September 2013 profiles were taken at midday (12:00), sunset (19:00) and after 1 h (20:00) and 4 h (23:00) of darkness. August 2014 profiles were taken in full sun (16:00) and just before sunrise after a full period of darkness (6:00). Turbidity units were multiplied by a factor of 5.

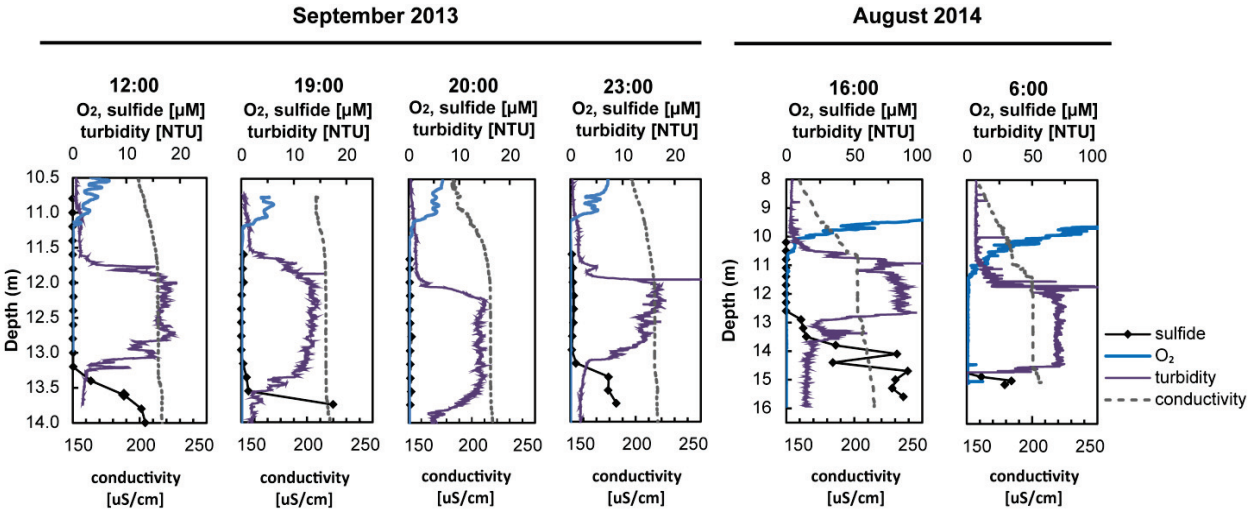

Figure S3: Zero-valent sulfur concentration plotted against *C. okenii* numbers at each depth for some representative profiles from 2015.

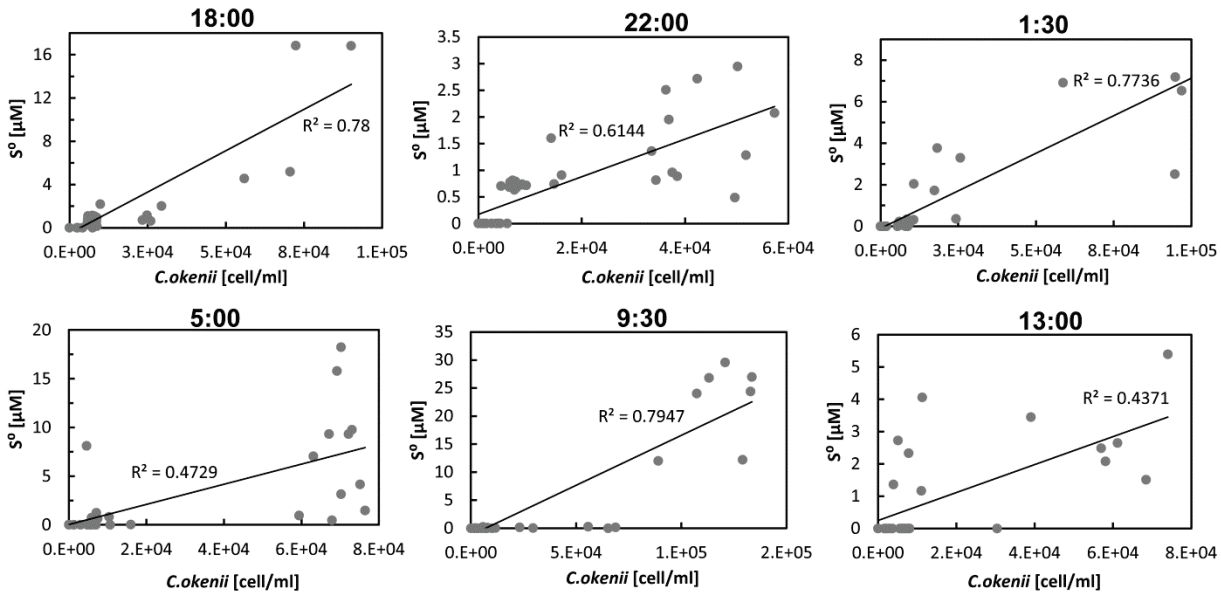

Figure S4: Sulfate versus conductivity profiles values plotted for Lake Cadagno profiles from Aug 2014 at midday (16:00), sunset (19:00), and just before sunrise (6:00).

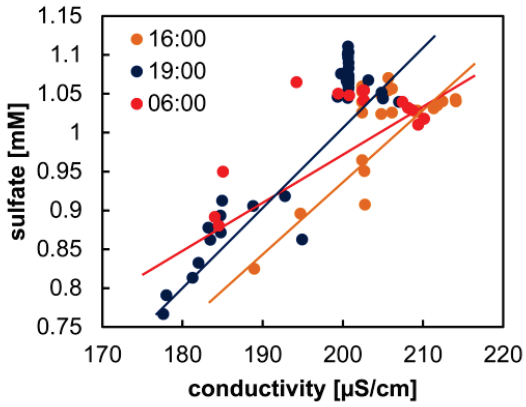

Figure S5: Graphs showing the light-dark dynamics of sulfur compounds in the Lake Cadagno chemocline measured at 4-h intervals over 48 hours: (a) the rate of sulfide accumulation is the change in the sulfide inventory over time. (b) The change in the sulfur inventory over time, (c) the original sulfide flux, and (d) the total (upwards and downwards) flux of biogenic sulfate. Shaded regions represent dark periods.

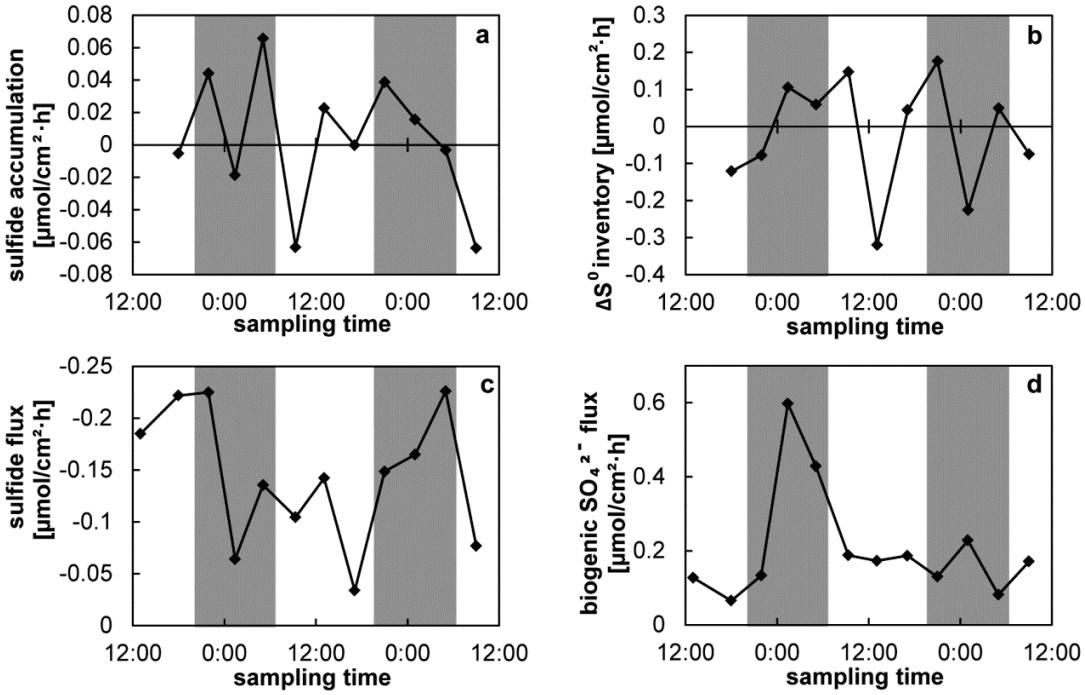

Figure S6: Temperature/conductivity and oxygen profiles from Lake Cadagno measured at 4-h intervals over 48 h in 2015. The shaded region represents the chemocline.

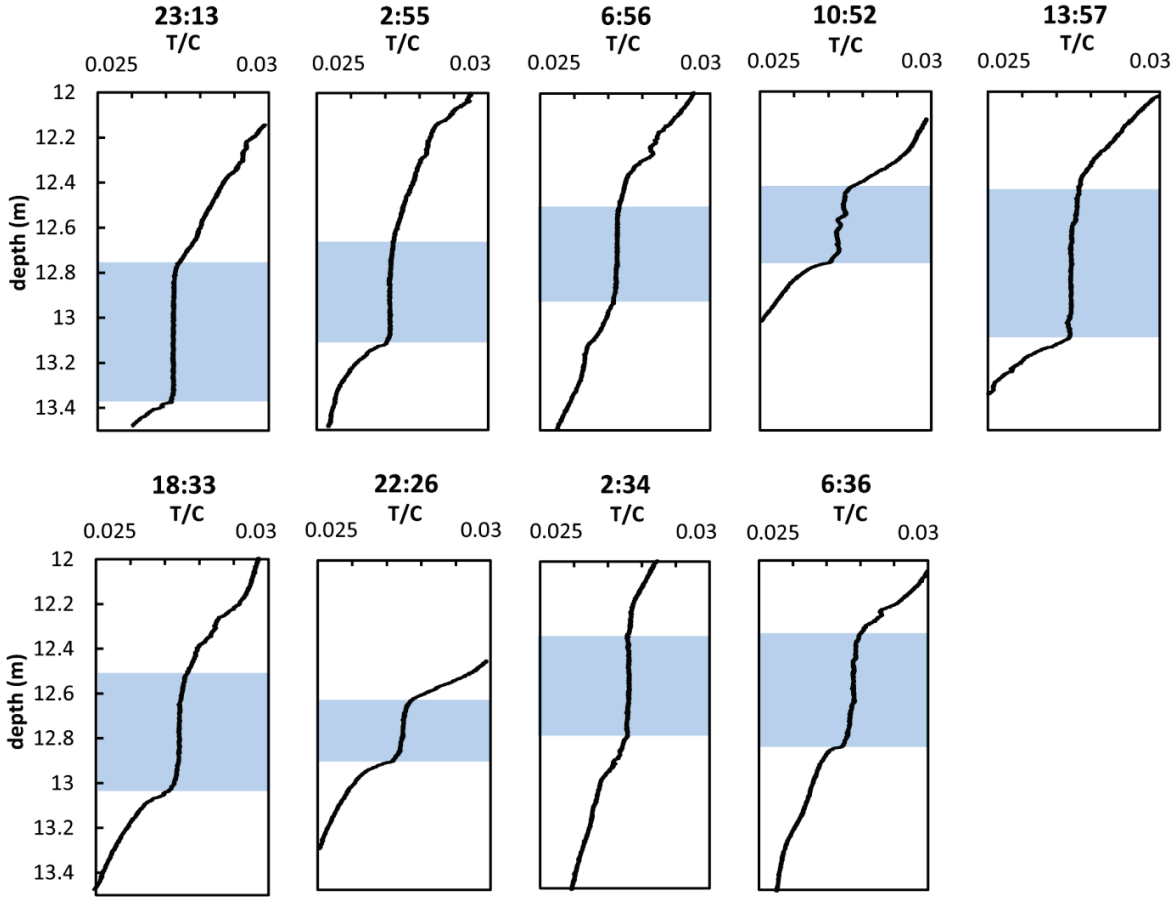

Figure S7: Agar-stabilized gradient tubes inoculated with Lake Cadagno water, in which swimming motility of *C. okenii* is reduced. The layer of *C. okenii* established itself between opposing gradients of sulfide (diffusing from below), light (provided from above), and oxygen (produced by some algae colonies above) and is visible as the dark pink coloration. Presence of *C. okenii* and other purple sulfur bacteria was also verified under the microscope. Microsensors were used to measure H_2S, pH, and O_2. The pH-adjusted sulfide profiles are shown in the light at 0 h (black line), and after 3 h (dashed line) and 6 h (dotted line) of darkness.

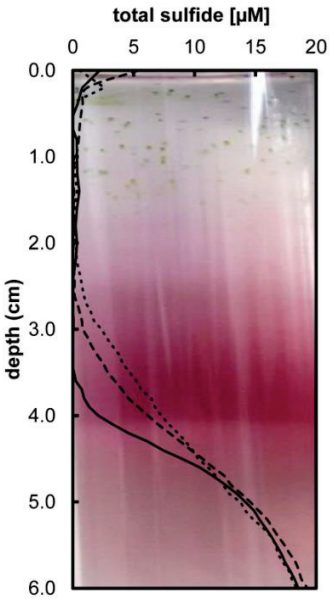

Figure S8: Contigs >10,000 kB from the Lake Cagadno chemocline bulk assembly are plotted by GC content (in %) versus sequencing coverage (fold). Contigs with coverage over 100x were excluded here. Each is represented by an elipse of equal size, independent of the contig size. Larger clusters and clouds signify that multiple/many contigs are located in that region. Contours of the main bins of interest were highlighted in color, and bin coverage information is summarized in the table below.

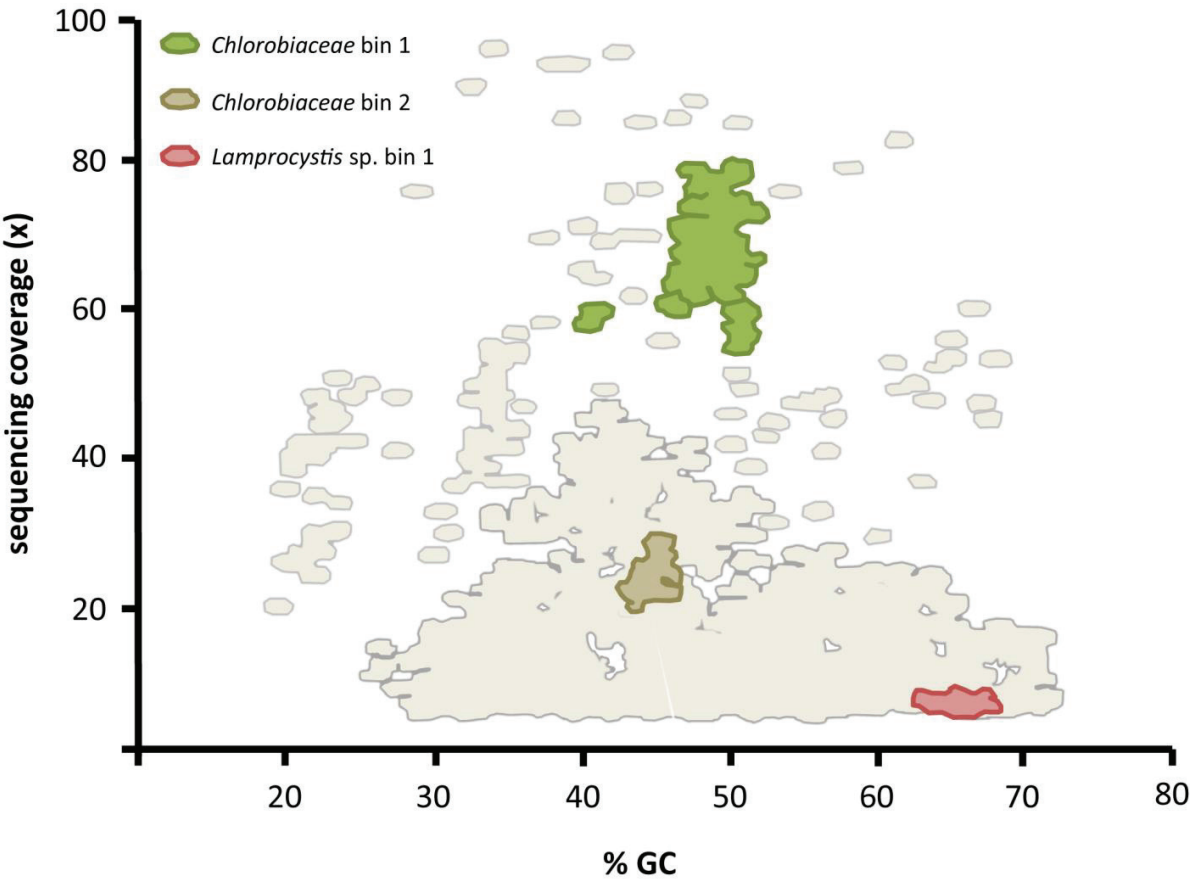

Bin	Mb	N (contigs)	N50	N (tRNA)	coverage	completeness	duplication
Chlorobiaceae bin 1	2.36	108	39948	36	67.7	80.2	1.0 x
Chlorobiaceae bin 2	4.16	727	17628	42	10.9	86.9	1.2 x
Lamprocystis sp. bin 1	8.91	2016	6141	46	6.9	75.9	1.5 x

Intracellular silver deposition as a tool for targeted detection and chemical analyses of uncultured bacteria

Jasmine S. Berg[1], Daniela Tienken[1], Alexander Khachikyan[1], Sten Littmann[1], Marcel M. M. Kuypers[1], Jana Milucka[1]

[1]Department of Biogeochemistry, Max Planck Institute for Marine Microbiology, Celsiustrasse 1, 28359, Bremen, Germany.

Submitted: *The ISME Journal*

doi:-

Author contributions: JM and MMMK designed the research project. JSB, AK, DT, SL performed the research. JSB, AK, DT, SL, MMMK and JM analyzed data. JSB and JM wrote this manuscript.

ABSTRACT

Despite two centuries of effort in cultivating microorganisms, the vast majority of environmental bacteria remain uncultured. Our knowledge of their physiology and metabolic capacities therefore strongly depends on methods capable of analyzing single cells. Bacterial identification is a key step required by all currently used single-cell imaging techniques and is typically performed by means of fluorescent labeling. Yet, fluorescence cannot be visualized by ion- and electron microscopy and only enables correlative, and thus indirect, cell identification. Here we present a new method of bacterial identification by *in situ* hybridization coupled to deposition of silver (silver-DISH). We show that hybridized cells containing silver can be directly visualized by scanning electron microscopy, energy dispersive X-ray spectroscopy, secondary ion mass spectrometry (nanoSIMS), and confocal Raman micro-spectroscopy. Silver-DISH altered the isotopic (^{13}C and ^{15}N) and elemental composition of stable-isotope probed cells considerably less than other available hybridization methods, making silver-DISH suitable for broad applications in stable-isotope labeling studies. Additionally, we demonstrate that silver-DISH can induce a surface-enhanced Raman scattering (SERS) effect, amplifying the Raman signal of biomolecules inside bacterial cells. This makes silver-DISH the only currently available method that is capable of delivering a SERS-active substrate inside specifically-targeted microbial cells.

INTRODUCTION

The recent emergence of single-cell technologies in the form of light-, ion-, laser- and electron microscopy has enabled important discoveries regarding the contributions of microorganisms to biogeochemical element cycling. For example, nano-scale secondary mass spectrometry (nanoSIMS) has been used to reveal the ecophysiology of uncultured bacteria (Musat *et al.,* 2008), metabolic heterogeneity within microbial communities

(Lechene *et al.,* 2007) and inter-species nutrient transfer (Thompson *et al.,* 2012). Scanning electron and atomic force microscopy have brought new insights into the mechanisms of e. g. bacterial-mineral interactions (Kato *et al.,* 2012) and aided visualization of uncultured environmental bacteria (Pfeffer *et al.,* 2012). The application of Raman spectroscopy has additionally proven useful for rapid, non-destructive characterization of single cells and their storage compounds (Li *et al.,* 2012; Berg *et al.,* 2014; Strola *et al.,* 2014; Berry *et al.,* 2015). Nonetheless, combining cell identification with these multiple analytical techniques remains a challenge.

The identification of bacteria in environmental samples generally relies on fluorescence *in situ* hybridization (FISH) combined with fluorescence microscopy (for review see e.g. Pernthaler *et al.,* 2002). A combination of FISH with catalyzed reporter deposition (CARD) is the gold standard for environmental samples where signal amplification is often necessary due to low ribosome content of slow-growing bacteria or background autofluorescence of pigmented microorganisms. Fluorescent labeling is, however, not ideal for use with other single-cell methods because it is invisible under the electron microscope and nanoSIMS, and it interferes with spectral acquisition under the Raman microscope. Labeling methods with halogen atoms compatible with nanoSIMS are available [HISH (Musat *et al.,* 2008), EL-FISH (Behrens *et al.,* 2008), or SIMSISH (Li *et al.,* 2008)], but the presence of halogenated minerals in soils or marine sediments can cause high background during halogen detection with SIMS. Therefore, recently, heavy elements such as gold and silver have obtained much interest as viable alternatives for environmental cell detection [Gold-FISH (Schmidt *et al.,* 2012) and Gold-ISH (Kubota *et al.,* 2014)]. Gold and silver are exogenous to living organisms and do not occur in most environmental systems. Detection and visualization of these elements is possible with a variety of methods, TEM (Danscher 1981), SEM (Gérard *et al.,* 2005), energy

dispersive X-ray spectroscopy (EDS; Schmidt *et al.,* 2012), Raman spectroscopy (Efrima and Zeiri 2009), and nanoSIMS (Milucka *et al.,* 2012), but mostly only after an enhancement reaction to reach a critical mass or concentration above detection limits.

Here we present silver deposition *in situ* hybridization (silver-DISH) as an alternative to existing *in situ* hybridization techniques for bacterial identification. We demonstrate the compatibility of this method on pure cultures of *Escherichia coli* and environmental samples from Lago di Cadagno, Switzerland. We demonstrate that successful silver deposition can be easily visualized with optical and scanning electron microscopy, Raman microscopy and nanoSIMS and can thus serve for direct cell identification using these methods. Moreover, we show that this method has the potential for targeted deposition of silver inside bacterial cells which leads to an intracellular surface-enhanced Raman scattering (SERS) effect.

RESULTS AND DISCUSSION

Our silver-DISH protocol was developed, optimized, and evaluated using pure cultures of *E.coli* (Supporting Information). We found a concordance between silver-DISH and CARD-FISH with respect to efficiency and pattern of staining (Fig. S1), which is to be expected considering that both protocols use identical oligonucleotide probes and thus are only limited by the quality of probe binding. Therefore, the silver-DISH protocol can be used in the same manner as CARD-FISH for cell identification and counting. Such agreement between fluorescent (FISH) and autometallographic methods has also been shown previously (e.g. Kenzaka *et al.,* 2005). Environmental application of silver-DISH was demonstrated on a water sample from Lago di Cadagno. Here, the purple sulfur bacterium *Chromatium okenii* contributes substantially to the microbial biomass at the chemocline and accounts for up to 70% of the total carbon fixation though constituting only 0.3% of total

microbial cell numbers (Musat *et al.,* 2008). These bacteria were chosen as candidates for testing the application of silver-DISH in a complex environmental sample as they are large and autofluorescent, and thus easily recognizable within the sample. First, *Chromatium spp* were targeted with the species-specific oligonucleotide probe Cmok453 (Tonolla *et al.,* 1999), stained with silver following our protocol and investigated with optical microscopy.

Inspection of silver-DISH hybridized *Chromatium* spp. under an optical microscope revealed dense, sharply-defined, black outlines of the *Chromatium* cells (Fig S1a). The intensity of the black color varied among individual cells, suggesting varying amount of deposited silver. Such heterogeneous appearance of staining was not restricted to the use of silver-DISH, but was also observed during CARD-FISH with the same oligonucleotide probe (Fig S1b). We speculate that these differences in the staining intensity might be intrinsic to the hybridization technique as the degree of fluorescence somewhat reflects the ribosome content of the cell which naturally varies among more to less active cells (e.g. Dortch *et al.,* 1983; DeLong *et al.,* 1989; Kemp *et al.,* 1993). Non-specific silver deposition associated with other cells or organic material was not apparent (Fig S1a). However, it is conceivable that the visual quality control using optical microscopy may be hindered in samples containing refractive or opaque particles. Additionally, presence of surface-charged minerals might catalyze non-specific deposition of silver. However, in nanoSIMS or EDX analyses these abiotic silver deposits in the sample should be discernible from silver-labeled cells by the absence of biologically relevant elements (C, N, P, S).

Silver-DISH enables direct cell identification under SEM/EDS

Microbial cell identification in environmental samples under the SEM typically relies on morphology. This becomes problematic when cells are altered in size and shape by sample

Figure 1: (a) A combined secondary electron and fluorescence image of a Lago di Cadagno water sample containing *Chromatium* cells stained by silver-DISH and *Deltaproteobacteria* stained by CARD-FISH. Signals from autofluorescence (red), DAPI (blue), and Oregon Green (green) were overlain. Regions with overlapping signals appear white. (b) The EDX map from the same field of view shows the distribution of silver (blue) and carbon (yellow). (c) A silver-stained *Chromatium* cell imaged with the back-scattered electron detector (BSE) at 5 keV with a beam deceleration of 3 keV, showing mainly surface topographical information. Heavy elements such as silver appear brighter. The white square indicates the region from which BSE images at 5 keV (d) and 20 keV (e) were collected, revealing silver nanoparticles inside the cell.

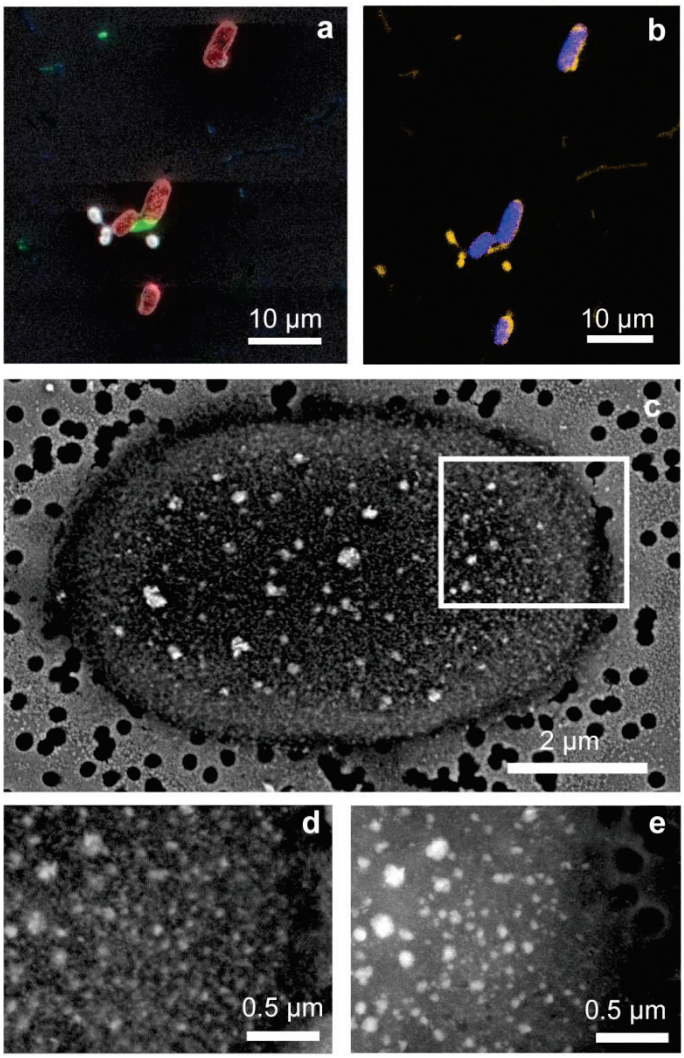

preparation or, as is the case for most bacteria, are simply not morphologically conspicuous. Direct labeling of cells for visualization under SEM presents an advantage over the current practice of correlative imaging of fluorescently labeled cells. Cell labeling by means of heavy element deposition has been previously successfully applied for SEM and SXM imaging (Gérard *et al.,* 2005; Kenzaka *et al.,* 2005; Ménez *et al.,* 2007; Schmidt *et al.,* 2012; Almstrand *et al.,* 2015). We therefore investigated the applicability of silver-DISH for cell identification and visualization by SEM-EDX. We could successfully visualize autofluorescent *Chromatium* cells from a Lago di Cadagno water sample directly using an integrated correlative light and electron microscope (SECOM) after labeling via silver-DISH (Fig 1a). The simultaneous identification of *Chromatium* by silver-

DISH and *Deltaproteobacteria* by normal CARD-FISH in the same sample (Fig 1a&b) demonstrates that silver-DISH can be combined with standard fluorescent FISH techniques for a multi-probe labeling approach. EDX images confirmed that only *Chromatium* cells contained silver (Fig 1b) whereas other, even closely associated, cells stained with DAPI (Fig 1a) did not. Labeled *Chromatium* were also distinguishable from other bacterial cells in backscattering electron (BSE) images (Fig 1c), where higher mass elements such as silver appear brighter. At higher electron voltage, the electron beam penetrates deeper into the cell, collecting information from a larger sample volume. Thus, the BSE images at 5 keV (Fig 1d) and 20 keV (Fig 1e) revealed that these bright silver grains were indeed deposited inside the cell. The presence of silver in the *Chromatium* cells was confirmed by EDS which showed a heterogeneous but high silver content of 50.35 ± 6.68 (median ± median absolute deviation) normalized atomic % concentration using a 1:2 dilution. The size and shape of deposited metal nanoparticles depended on the concentrations of staining reagent used (Fig S2a). The highest reagent concentration (20% or 1:5 dilution) promoted the formation of large crystalline grains (average grain size of 101 nm; Fig S2b), whereas lower concentrations promoted the nucleation of smaller ca. 30 nm, rounded grains (Fig S2c). Co-occurring microorganisms such as other small purple sulfur bacteria and *Deltaproteobacteria* (Fig 1a) contained up to 1.8 atomic % silver at the highest staining reagent concentrations (50% or 1:2 dilution). The background content of silver decreased with decreasing reagent concentration and dropped below 1% with a 1:20 dilution. In *Chromatium* cells, other biological elements, such as carbon, were measured and mapped alongside silver (Fig 1b).

Considering the very high cellular silver content of hybridized cells, we further investigated the possibility that the introduction of silver into the cell affected the elemental composition of the original cell material. *Chromatium* cells differ naturally in their cellular carbon,

phosphorus and sulfur content due to presence of intracellular storage inclusions (i.e. zero-valent sulfur, PHB and polyphosphate) and we therefore used pure cultures of *E.coli* for testing. We applied different dilutions of the EnzMet developing reagents and measured the resulting elemental composition (represented as normalized atomic % concentration) of the cells. The C:N and N:P ratios from *E. coli* stained with silver-DISH were then compared to those of unlabeled, unhybridized *E. coli* cells (Fig S3). The silver content of hybridized *E. coli* decreased proportionally to increasing reagent dilution, reaching 18.26 ± 5.95 atomic % silver at a 1:5 (low) dilution and 3.89 ± 1.33 atomic % at a 1:20 (high) dilution. At low dilution, the median C to N ratio (14.6:1) was significantly different from an untreated sample (10.4:1) (Mann-Whitney test; $p=0.004$) but no significant difference was observed in the median C to N ratio of the untreated sample compared to high dilution (11.8:1). The median N to P ratio of untreated cells (30.2:1) was significantly higher (Mann-Whitney test; $p<0.001$) than that of cells incubated at low reagent dilution (13.9:1) but not significantly different from that of cells at high reagent dilution (26.1:1). It is conceivable that some nitrogen-containing cellular components were lost during hybridization. Alternatively, lower cellular N:P ratios of hybridized cells could result from the tendency of phosphate to adsorb to silver metal (Niaura *et al.,* 1997). This is supported by our measurements that showed slightly higher median phosphorus concentrations in silver-labeled (0.34 ± 0.12 atomic %) versus unlabeled (0.31 ± 0.08 atomic %) cells. A sufficient amount of silver is necessary for intracellular Au/Ag detection by SEM/EDS (Gérard *et al.,* 2005; Schmidt *et al.,* 2012) but our results show that at high silver concentrations, the elemental composition of microbial cells may be strongly affected. This can be simply circumvented by decreasing the amount of deposited silver. For example, at a dilution of 1:20, silver concentrations could still be measured via EDS but little to no differences in C:N:P ratios were observed before (259:28:1)

and after (282:26:1) silver-DISH (Fig S3). Any further dilution of the developing reagents tested resulted in silver levels not significantly different from the background. We thus concluded that cell labeling via silver-DISH is a viable approach for identification of environmental bacteria using SEM-EDS imaging.

Silver-DISH compatibility with single-cell nanoSIMS analyses

Nanoscale secondary ion mass spectrometry (nanoSIMS) is a powerful method for investigating metabolic activities of single microbial cells in the environment. Before analysis, cells of interest are typically identified using fluorescent imaging and the boundaries of fields of view must be outlined, e.g. with laser markings (Alonso *et al.,* 2012). Unambiguous identification of cells can be compromised by cellular autofluorescence which interferes with the CARD-FISH signal. This can be partially circumvented using nanoSIMS-optimized CARD-FISH protocols. In HISH (Musat *et al.,* 2008), EL-FISH (Behrens *et al.,* 2008), or SIMSISH (Li *et al.,* 2008) the use of halogenated tyramides or oligonucleotide probes complements the fluorescent signal with fluorine (^{19}F) or bromine (^{80}Br) which can be detected with nanoSIMS. However, for cells with high or fluctuating endogenous fluorine or bromine levels, respectively, this method may not provide correct identification. Additionally, halogen-containing minerals (e.g. fluoro-apatite) occurring in soils, sediments and other environmental samples create background signals which can interfere with sample analysis. In contrast, silver-DISH relies on the deposition of an element which is rare in most habitats and is virtually absent from microbial cells. The use of silver (detected as $^{107}Ag^-$) presents a technical advantage over available gold labeling methods, because its relatively low mass allows it to be measured simultaneously with biologically relevant ions (e.g. C, N, P, S and their isotopes) without a time-consuming shift of the magnetic peak.

Figure 2: NanoSIMS images of silver ($^{107}Ag/^{12}C_2$) deposited by silver-DISH in ^{13}C-enriched *Chromatium* cells. (a) Two *Chromatium* cells (outlined) are discernible based on $^{107}Ag/^{12}C_2$ ratios. Also visible are unspecifically deposited silver particles which differ from cells in size and in the absence of carbon. Intracellular carbon storage granules visible in the (b) $^{13}C^{12}C$ /$^{12}C_2$ image confirm that silver signal was recorded from inside *Chromatium* cells. Other, non-hybridized, cells are visible both in (b) the $^{13}C^{12}C$ /$^{12}C_2$ and (c) $^{32}S/^{12}C_2$ images. Scale bar is 3 µm.

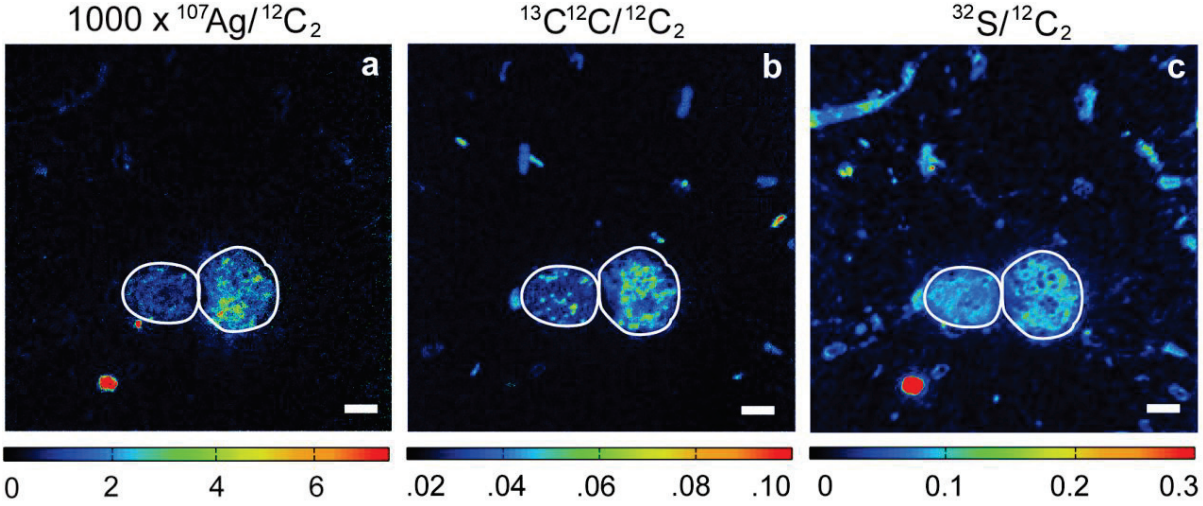

As a proof-of-principle we combined silver-DISH with nanoSIMS as an alternative to HISH-SIMS for imaging the heterotrophic growth of *E.coli* with ^{13}C-labeled glucose and ^{15}N-labeled ammonium (Fig S4) and the photoautotrophic growth of *Chromatium* spp with ^{13}C-DIC (Fig 2). Identification of *Chromatium* under the nanoSIMS was performed by recording the $^{107}Ag^-$ ion, corresponding to deposited elemental silver (details of analysis are included in the Material and Methods) (Fig 2a). Because nanoSIMS imaging physically erodes the sample surface we conclude that the detection of $^{107}Ag^-$ signal in *Chromatium* cells can be used as additional evidence that silver was deposited intracellularly. Dimer ions $^{13}C^{12}C^-$ and $^{12}C^{12}C^-$ ($^{12}C_2^-$) rather than single ions were measured to reduce the mass range between the trolleys ^{107}Ag and ^{12}C and to increase the space between the trolleys used for measurement of $^{13}C^{12}C^-$ and $^{12}C^{12}C^-$ in the multi-collection system. Although it is unconventional to measure the C_2^- dimers (as mass 24 and 25) in environmental microbiology, they are in fact more compatible with the CN species due to the tuning effect of the E0S lens and thus result in a

more precise isotopic analysis (Pett-Ridge and Weber 2012). As the $^{13}C^{12}C/^{12}C^{12}C$ ratio is *ca.* 2-fold higher than the corresponding $^{13}C/^{12}C$ ratio (see Materials and Methods for exact formula) measuring C_2^- dimers appears particularly suitable for samples with low ^{13}C content. The ^{13}C-enrichment of *Chromatium* cells (Fig 2b) is evidence for light-driven carbon fixation by these bacteria, and the patchy distribution of ^{13}C in these large cells suggests that ^{13}C-DIC was incorporated as a storage product. Although this purple sulfur bacterium is also known to store zero-valent sulfur, the intracellular distribution of sulfur did not resemble the morphology of sulfur globules (Fig 2c). It is possible that sulfur was simply respired by bacteria before fixation, or that elemental sulfur volatilized under the ultra-high (10^{-10} hPa) vacuum in the nanoSIMS chamber. Abundant ^{32}S measured in surrounding cells could be attributed to sulfur-containing organic substances (e.g exopolymers) produced by some bacteria (Braissant *et al.,* 2007). A large diversity of non-silver labeled, active (^{13}C-enriched) cells was also visible in the $^{13}C^{12}C$ ratio image (Fig 2b).

All current *in situ* hybridization protocols (mono-FISH, CARD-FISH and presumably also EL- or HISH) influence the isotopic composition of hybridized cells (Musat *et al.,* 2014). We therefore evaluated a potential isotope dilution effect by measuring the change of the isotopic ^{13}C and ^{15}N ratios in *E. coli* cells after treatment with silver-DISH. We found that silver-DISH also altered the isotopic composition of the hybridized cells but to a lesser degree than fluorescent ISH methods. Interestingly, the degree of dilution was proportional to the initial isotopic enrichment (Fig S4). The median decrease of $^{13}C/^{12}C$ was 0.0018 at low enrichment and 0.0431 at high enrichment. Expressed as atom % ^{13}C the median decrease in ^{13}C after silver-DISH was negligible in low enriched cells (0.17 atom % ^{13}C) but reached ca. 2.5 atom % ^{13}C in highly enriched cells. Silver-DISH treatment alone had a significant effect on ^{13}C loss as did the degree of enrichment alone (permutation-based two-way ANOVA; p<

0.001). The interaction of the two factors, silver-DISH and degree of enrichment, also significantly affected cellular ^{13}C content (p= 0.001). In comparison to ^{13}C, silver staining had a more pronounced effect on nitrogen isotopic content. The median $^{15}N/^{14}N$ enrichment decreased from 0.053 (5.05 atom % ^{15}N) in untreated *E. coli* cells to 0.007 (0.73 atom % ^{15}N) after silver-DISH. In other words, silver-DISH caused a significant 4.32 % loss in the ^{15}N fraction of enriched cells (one-way ANOVA; p< 0.001). Overall, silver-DISH affected the ^{13}C or ^{15}N content of the cells less than mono-FISH (decrease of 13% and 37% in ^{13}C and ^{15}N, respectively) and CARD-FISH (decrease of 30% and 43% in ^{13}C and ^{15}N, respectively; Musat *et al.,* 2014). This is due in part to the extremely high enrichment of cells tested by Musat and colleagues (2014), which has a more pronounced effect on the isotopic loss. We speculate that an additional reason for this difference might be that apart from the oligonucleotide probe and HRP no additional organic molecules containing C and N (such as tyramides) are introduced into the cell during silver-DISH. Thus silver-DISH is a viable method for single-cell nanoSIMS imaging and quantitative analyses of substrate uptake by use of stable isotope labeling.

Deposited silver nanoparticles induce a targeted intracellular SERS effect

Silver deposited by silver-DISH can also be visualized by means of Raman micro-spectroscopy. The contribution of silver-DISH is particularly powerful for this technique as currently used fluorescent ISH protocols severely interfere with spectral acquisition under the Raman microscope. Our measurements of silver-labeled *Chromatium* using a 532 nm laser revealed complex Raman spectra, containing a putative silver peak along with peaks belonging to cell components (Fig 3). The spectrum of silver exhibits a weak, rounded peak at ~200 cm^{-1} (Fig S5) and lies in a cell-silent spectral region, thus not interfering with analysis of biological samples. Interestingly, even when measured with the same settings, the spectra

Figure 3: Raman spectra from a silver-labeled *Chromatium* cell. The spectra were collected successively (bottom to top) from a single spot with 1 sec exposure and 0.03 mW laser power. Dashed lines correspond to peak positions of elemental silver (yellow), HRP (green) and some selected cellular compounds: carbohydrates, proteins, and amino acids (black) and carotenoids (purple). a.u. stands for arbitrary units.

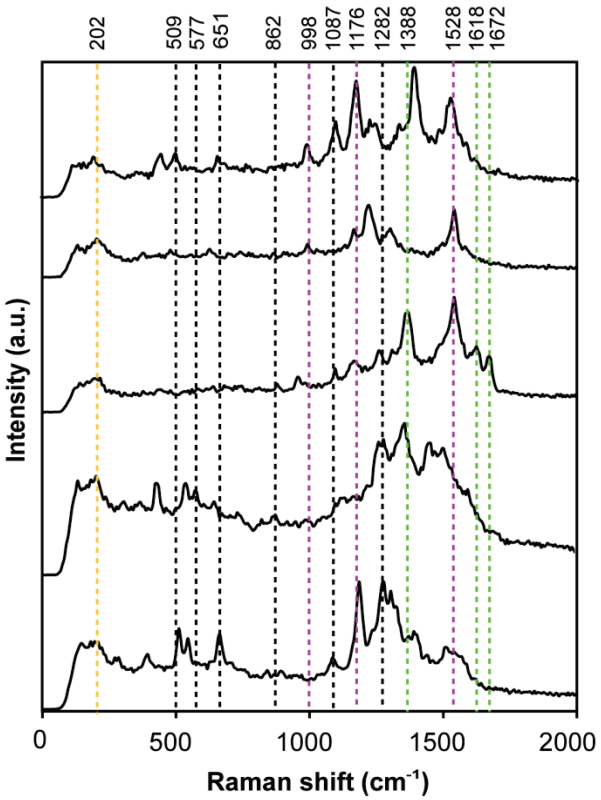

recorded from the same point were not identical; peaks appeared to shift both in position and in height during continuous 1-second measurements (Fig 3). This "blinking" phenomenon is typically not observed in normal Raman spectra but was described to occur in surface-enhanced Raman spectra (SERS) due to intermittent, single-molecule spectra enhancement (Krug *et al.,* 1999). The SERS effect occurs when a metallic nanostructure interacts with incident photons, generating an enhanced electric field in the vicinity of the metal surface. The majority of reported SERS studies of bacteria rely on extracellular interaction of silver colloids with bacterial cells or via silver-coated surfaces onto which analyzed microorganisms are immobilized (Grow *et al.,* 2003). These studies have therefore been limited to amplification of molecules from the cell wall and its immediate vicinity such as (flavins, PDA, lysozyme, EPS) which tend to be amplified (Cowcher *et al.,* 2013, Zeiri *et al.,* 2002, Zhang *et al.,* 2005). Bacteria have also been successfully infused with metal colloids (Efrima and Bronk 1998), but this non-targeted approach cannot discriminate between various organisms. Silver-DISH deposits silver nanoparticles intracellularly (Fig 1d&e), inducing a SERS effect within specifically targeted bacterial cells. To our knowledge, this is the only approach reported so

far which allows for the controlled deposition of SERS-active substrate inside bacterial cells. Another advantage of silver-DISH is that the silver nanoparticles are synthesized within the bacteria (as opposed to simple mixing with pre-fabricated colloids) allowing a more intimate contact between the metal and bacterial components. This is advantageous as the SERS effect only acts in the immediate vicinity of the metal surface.

Silver-stained *Chromatium* cells exhibited rich SERS spectra with various peaks (Fig. 3) Peaks observed at 675, 840, 1300 and 1644 cm^{-1} were tentatively attributed to nucleic acids (e.g. De Gelder *et al.,* 2007). Spectra were also characterized by putative HRP peaks at approximately 1388, 1618, and 1672 cm^{-1} and exhibiting large (up to 10 cm^{-1}), temporal fluctuations as also reported by Bjerneld *et al.* (2002). The co-occurring peaks at 998, 1176, and 1528 cm^{-1} were typical of the carotenoid pigments of *Chromatium* (Koyama *et al.,* 1982). Peaks at 930 and 1400 cm^{-1} (usually assigned to carboxylate stretching modes of alpha amino acids) and around 1123 cm^{-1} [assigned to C-C or C-N or phosphate vibration in DNA or =C-C= or unsaturated fatty acids (Zhang *et al.,* 2005; Cowcher *et al.,* 2013)] observed in silver-infused cells by Efrima and Zeiri (2009) were also detected. In general, our SERS spectra were very different from non-SERS Raman spectra from *Chromatium* cells (Fig S6) which are typically dominated by the resonance peaks of carotenoids (Koyama *et al.,* 1982) that mask all other biological Raman peaks. This is in agreement to previous suggestions that the majority of normal Raman bands might be absent in the SERS spectrum (Efrima and Zeiri 2009). For example, our SERS spectra did not contain the phenylalanine peak which appears characteristic of normal Raman spectra of whole cells (Huang *et al.,* 2007, Schuster *et al.,* 2000).

Raman mapping of *Chromatium* cells revealed a variable degree of signal enhancement throughout the cell (Fig 4a) which can be attributed to the heterogeneous deposition of

Figure 4: (a) A Raman map of three silver-stained *Chromatium* spp. cells (outlined) showing signal intensity in the 1100-1900 cm^{-1} "biological" region. High signal intensity, represented in white, is due to the silver-induced SERS effect. (b) Representative SERS spectra from *Chromatium* cells treated with different dilutions of silver-staining reagents. A normal Raman spectrum from a cell not treated with silver-DISH (no silver) is provided for reference. All spectra were recorded with different cells but with same settings (0.03 mW, 1 sec exposure). Intensity of the Raman signal is depicted in arbitrary units (a.u.), however, all spectra were scaled proportionally to original signal intensity. For orientation purposes, baseline-corrected Raman counts of the highest peaks in the 1:20 dilution (23678 cps) were ca. 20-fold higher than in non-labeled cells (no silver; 1137 cps).

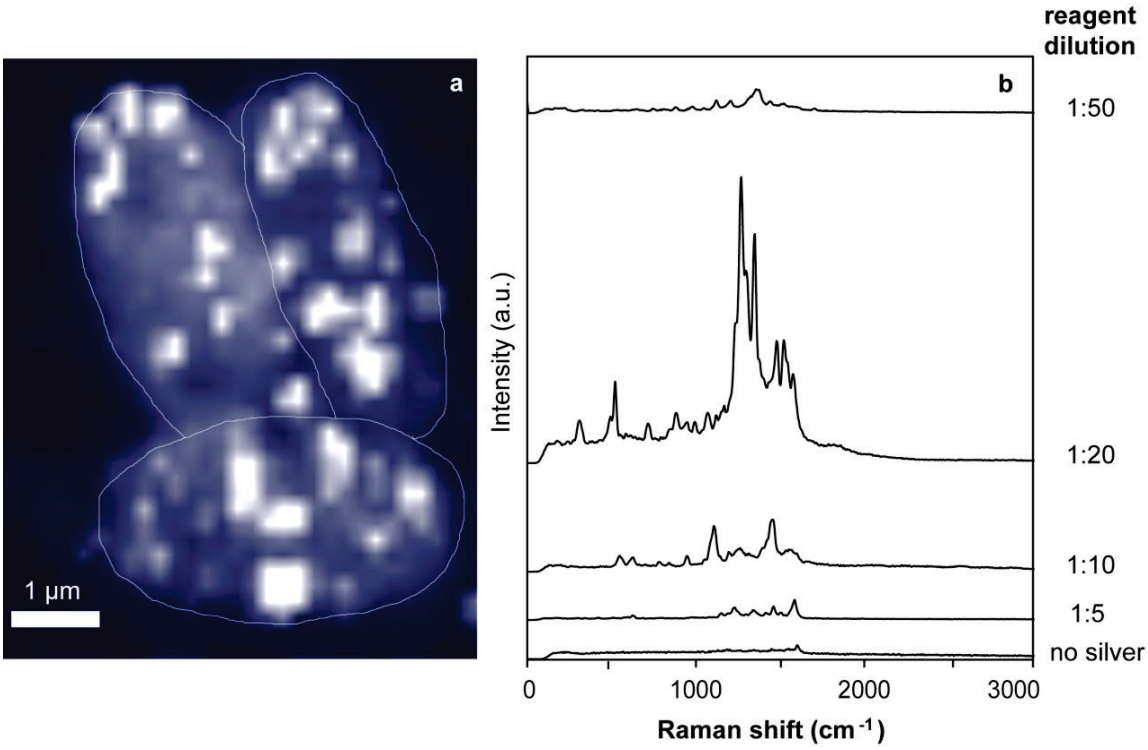

silver or the 'hot-spot' effect of SERS (Maher 2012). This might be a consequence of a patchy distribution of cell constituents, such as ribosomes, and, consequently, the hybridized probes. A spectrum from a region with no detectable silver peak was very similar to a spectrum from a cell not hybridized with the probe (non-SERS) in that no silver or HRP peaks were visible and the spectrum intensity was relatively weak (Fig 4b, bottom spectrum). In the same cell, the spectrum from a region of high signal intensity (with a strong silver peak at 212 cm^{-1} and biological peaks at 700-1650 cm^{-1}) was up to 10-fold stronger than a non-SERS spectrum. Indeed, it is understood that nanoparticle size, shape, and inter-particle distance influence the SERS enhancement effect (e.g. Kerker and Blatchford 1982, Stamplecoskie *et*

al., 2011). Because of the variability in peak enhancement across both a spectrum and a sample, we defined the enhancement factor simply as the maximum peak intensity in a SERS spectrum, divided by the maximum peak intensity of a non-enhanced, non-resonance Raman spectrum. We then calculated the average SERS enhancement factor from >30 random spectra from samples with different average silver grain sizes. In agreement with literature reports, grain-size dependent SERS enhancement followed a normal distribution with an optimal grain size of approximately 43 nm (Fig S7), corresponding to a reagent dilution of 1:20 (Fig S2). At this reagent concentration, the average enhancement factor was about 5-fold, but enhancement of up to 50-fold was observed. Although such silver metal nanoparticles with a large surface area are prone to oxidation, the SERS effect was still observed after 2 and 3 days (Fig S8) demonstrating that silver nanoparticles are stable enough for short-term storage under normal atmosphere. As expected, we did not observe any SERS amplification with an excitation wavelength of 785 nm, which is too far from resonance with the surface plasmons of silver colloids.

CONCLUSIONS AND OUTLOOK

In this study we present an alternative *in situ* hybridization method which allows for direct cell identification with all tested single-cell imaging techniques (nanoSIMS, SEM, EDX and Raman micro-spectroscopy). Due to its broad range compatibility, silver-DISH allows for correlative use of these methods on complex environmental samples. We demonstrate that silver-DISH had a substantially smaller effect on the cellular isotopic and elemental composition and thus might enable a more precise quantification of uptake of isotopically-labeled substrates by nanoSIMS than other currently available hybridization techniques. Silver-DISH is also compatible with elemental cell analysis by EDX spectroscopy as it does not significantly alter the C:N and N:P ratios of hybridized cells. Detection of silver in silver-DISH

hybridized cells by Raman micro-spectroscopy is facilitated by a SERS phenomenon induced by the deposition of silver colloids in microbial cells. This is, to our knowledge, the only method so far reported that overcomes the limitation of delivering a SERS-active substrate into bacterial cells. Consequently, silver-DISH enables a targeted amplification of Raman spectra from biomolecules inside specific cells and opens new possibilities for the application of confocal Raman microscopy in microbiology. Signal amplification resulting from the SERS effect may enable Raman investigation of biological compounds which are weak Raman scatterers or otherwise masked by background fluorescence. The shorter integration times required for Raman analysis could be relevant for single-cell manipulation techniques such as laser tweezers or flow sorting for subsequent analyses.

METHODS

Cultivation and sampling

Competent *Escherichia coli* were maintained at 37°C on minimal media containing per L distilled water 6.0 g Na_2HPO_4, 3.0 g KH_2PO_4, 1.0 g NH_4Cl, 0.5 g NaCl, 0.12 g $MgSO_4 \cdot 6H_2O$, 1.1 g $CaCl_2 \cdot 2H_2O$, and 18.0 g glucose. For labeling experiments, cells were transferred into medium containing ^{13}C-labeled glucose ($^{13}CC_5H_{12}O_6$; 99 atom % ^{13}C, Sigma-Aldrich, St. Louis, MO, USA) and ^{15}N-labeled ammonium sulfate [$(^{15}NH_4)_2SO_4$; 98 atom % ^{15}N; Sigma-Aldrich, St. Louis, MO, USA] to reach final labeling percentage in the medium of *ca.* 100 atom % ^{13}C and 62 atom % ^{15}N. Low- and high-enriched *E. coli* were obtained by sub-sampling at different time points (after ca. 1.5 and 12 hours). The ^{13}C and ^{15}N uptake in *E. coli* cells was confirmed by combustion of bulk biomass samples followed by isotope ratio mass spectrometry. Samples were fixed 45-60 min at room temperature in 2% (v/v) formaldehyde and resuspended in 1X PBS.

Environmental samples of *Chromatium okenii* were collected in the summer of 2014 from the chemocline (15.1 m depth) of Lago di Cadagno, Switzerland and stored at 4°C in the dark for up to two weeks until further processing. Lake water was incubated in sealed, anoxic serum bottles for 8 days in the light with 20 atom % added $H^{13}CO_3^-$. All samples were fixed 45-60 min at room temperature in 2% (v/v) formaldehyde.

Cell hybridization

Liquid CARD-FISH was performed on *E. coli* samples following the protocol of Pernthaler *et al.* (2002). For each 500 µl of cell suspension, 1 ml of 0.01 M HCl was added and incubated for 10 min at room temperature to inactivate endogenous peroxidases. Cells were subsequently pelleted by centrifugation for 10 min at 5000 RCF. Cells were permeabilized by digestion with lysozyme (Sigma-Aldrich), 10 mg ml^{-1}, for 30 min (*E. coli*) at 37°C, and subsequently washed in MilliQ for 10 min. Hybridization was performed using 2 µl of horseradish peroxidase(HRP)-labeled oligonucleotide probe mix per 600 µl of hybridization buffers containing 35% (vol/vol) formamide at 46°C for 2.5 h. A 1:1:1 mix of EUB338, EUB338-II and EUB338-III (Daims *et al.,* 1999) was used for *E.coli* cells in pure culture. Cells were washed in 1 ml wash buffer at 48°C for 15 min, 1xPBS for 10 min and then with MilliQ for 5 min. Silver labeling of hybridized cells was achieved using the EnzMet™ HRP Detection Kit (Nanoprobes Inc, Yaphank, New York, USA) which is designed for sensitive, high-resolution visualization of target proteins or nucleic acids. The accompanying EnzMet™ protocol was followed, with a few modifications. Solutions A, B, and C were diluted 1:5 and the 10 min silver staining step with solution C was performed in the dark to avoid photoreduction of Ag^+ and random Ag deposition. Finally, cells were filtered directly onto gold-palladium sputtered polycarbonate filters (GTTP type; pore-size 0.22 µm; Millipore,

Eschborn, Germany). *E. coli* samples used for SEM detection limit determinations were prepared on commercial gold filters (APC, Eschborn, Kernporenfilter, 0.2 µm pore size, 40 nm gold layer above and 20 nm gold layer on backside) using the following dilutions of the EnzMet Kit reagents: 1:2, 1:5, 1:20, 1:50, and 1:100. Fixed, unlabeled *E. coli* were filtered directly on top of silver-labeled *E. coli*.

Cells from environmental samples were collected on gold-palladium sputtered polycarbonate filters (GTTP type; pore-size 0.22 µm; Millipore, Eschborn, Germany) or glass slides and processed using the above-described CARD-FISH protocol. Best results were obtained with an additional 1 min incubation step in 0.1M HCl for peroxidase deactivation and a 60 min lysozyme permeabilization step. Centrifugation steps were omitted and volumes of all solutions except the hybridization buffer/probe mix were increased to 50 ml. The probe Cmok453 (Tonolla *et al.,* 1999) was used to target *Chromatium okenii* in environmental samples. EnzMet Kit reagents A, B, and C were diluted 1:5 and staining was performed for 10 min in the dark. Excess silver halide was removed by washing filters one minute in a stop bath of 01.M citric acid and one minute in a wash bath of 0.1M Na-thiosulfate. To demonstrate multi-probe labeling, samples were subsequently incubated in 0.1M HCl to deactivate HRP before performing normal CARD-FISH using the probe Delta42a (Loy *et al.,* 2002) targeting most *Deltaproteobacteria*.

NanoSIMS

Hybridized filters were analyzed using a nanoSIMS 50L (CAMECA, Gennevilliers Cedex, France) at the Max Planck Institute for Marine Microbiology in Bremen, Germany. $AgNO_3$ dried onto a polycarbonate filter was used for tuning of the instrument to detect heavy silver ions. On filtered samples, areas of interest were pre-sputtered with a Cs^+ primary ion beam

of 300 pA. For the analyses, a primary Cs^+ ion beam with a beam current between 1.0 and 1.2 pA and a beam diameter of 100 nm was rastered across the cells. With our nanoSIMS 50L system (at the Max-Planck-Institute in Bremen) it was not possible to record the ^{12}C and ^{13}C ions simultaneously with ^{107}Ag even though it might be theoretically feasible on other nanoSIMS instruments. We could record ^{12}C together with carbon and nitrogen dimers and ^{107}Ag (Fig 2 and Fig S9). More specifically, secondary ion images of $^{12}C^-$, $^{12}C_2^-$, $^{12}C^{14}N^-$, $^{32}S^-$ and $^{107}Ag^-$ were recorded simultaneously, using 5 electron multipliers from analysis areas ranging from 10 x 10 µm to 50 x 50 µm in size, and corresponding to an image size of 256 x 256 and 512 x 512 pixels, respectively, using a dwell time of 1 ms per pixel. For ^{13}C- and ^{15}N-enriched cells, we also recorded $^{13}C^{12}C^-$ and $^{12}C^{15}N^-$. ^{13}C was recorded together with ^{12}C and carbon and nitrogen dimers, but without ^{107}Ag, in a parallel run. For every area of interest 40 planes were recorded. All planes of measurement were corrected for possible stage and source drift during the measurement and accumulated after the correction. Images and data were processed using the proprietary CAMECA WinImage processing software and the Matlab-based Look@NanoSIMS software (Polerecky *et al.,* 2012).

To assess a possible dilution effect of silver-DISH on isotopic signals, we compared $^{13}C^{12}C/^{12}C^{12}C$ ratios in *E. coli* from four different treatment conditions: low ^{13}C-enriched unlabeled, low ^{13}C-enriched Ag-labeled, high ^{13}C-enriched unlabeled, high ^{13}C-enriched Ag-labeled *E.coli* cells. Ratios of $^{13}C^{12}C/^{12}C^{12}C$ were converted to $^{13}C/^{12}C$ using a conversion formula $R_{(13C/12C)} = -0.1488*R^2_{(13C12C/12C12C)} + 0.4751*R_{(13C12C/12C12C)} + 0.0008$. We also compared $^{15}N/^{14}N$ ratios in ^{15}N-enriched unlabeled and Ag-labeled *E.coli* cells. The fraction (*D*) of ^{13}C or ^{15}N per cell was calculated from the ratios *R* of $^{13}C/^{12}C$ and $^{12}C^{15}N/^{12}C^{14}N$ using the equation: $D = \frac{R}{R+1} \times 100$.

Scanning electron microscopy (SEM) and energy dispersive X-ray spectroscopy (EDS)

Filter pieces with Ag-labeled cells were mounted on electrically conductive, adhesive tags (Leit-Tab; Plano GmbH, Wetzlar, Germany). Specimens were investigated with a FEI environmental field emission SEM Quanta 250 FEG (FEI, Eindhoven, Netherlands) at an acceleration voltage of 1 keV using an Everhart-Thornley secondary electron detector (ETD). Back-scattered electron images were measured at 5 keV, 5 keV with a beam deceleration of 3 keV, and 20 keV using a concentric backscattered electron detector (CBS). EDS measurements were carried out using the Quanta 250 FEG instrument equipped with an EDS system Quantax 400 with a XFlash 6/30 double detector system (Bruker Nano GmbH, Berlin, Germany). The detectors have an energy resolution of < 123 eV at MnKα. The EDS measurements were performed at an acceleration voltage of 10 keV.

For correlative fluorescent imaging, samples were prepared on Indium-Tin-Oxide (ITO) coated coverslips instead of filters. The FEI Quanta 250 FEG was combined with a SECOM platform (DELMIC, Delft The Netherlands) to perform fluorescence microscopy directly within the scanning electron microscope. The SECOM platform was equipped with a four-channel LED excitation source and a multi-band fluorescence filter set. The signals for DAPI, Oregon Green, and autofluorescence were measure at 390/22 nm, 485/25 nm, and 648/20 nm excitation wavelengths, respectively. The exposure time for all three lines was 300 milliseconds. A Nikon CFI Plan Apo 40x microscope objective (NA=0.95) was used in combination with an Andor Zyla 5.5 sCMOS camera with 2560 x 2160 pixels and a pixel size of 6.5 x 6.5 µm.

Raman Spectroscopy

Membrane filters were mounted on glass microscopy slides for Raman analysis. Colloidal Ag and $AgNO_3$ were measured for reference on CaF_2 slides and a summary of spectra is provided in Fig S6.

Raman spectra were acquired using an NTEGRA Spectra confocal spectrometer (NT-MDT, Eindhoven, Netherlands) coupled to an upright Olympus BX51 microscope. The excitation light from a 532-nm solid state laser was focused on the sample through an Olympus 100× (numerical aperture [NA], 0.9) air objective, resulting in a laser power of no more than 0.03 mW at the sample. The pinhole aperture was maintained at 55 µm, corresponding to a spatial resolution of 250 to 300 µm. Raman scattered light was dispersed with a 150-line·mm^{-1} grating and collected by an electron-multiplying charge-coupled device (EMCCD) camera (Andor Technology, Belfast, Northern Ireland) cooled to -70°C. Raman spectra were recorded between 0 and 4,500 cm^{-1} with a spectral resolution of 0.2 cm^{-1} using the software Nova_Px 3.1.0.0 (NT-MDT, Eindhoven, Netherlands). Full-spectrum maps were first background corrected and then exported to Adobe Photoshop CS2 for brightness/contrast adjustment.

ACKNOWLEDGMENTS

We thank Soeren Ahmerkamp for help with statistical calculations. This work was supported the Max Planck Society and the Deutsche Forschungsgemeinschaft (through the MARUM Center for Marine Environmental Sciences).

REFERENCES

Almstrand R, Drennan DM, Sharp JO (2015). Polygold-FISH for signal amplification of metallo-labeled microbial cells. *J Basic Microbiol*. **55:**798-802.

Alonso C, Musat N, Adam B, Kuypers MMM, Amann R (2012). HISH–SIMS analysis of bacterial uptake of algal-derived carbon in the Río de la Plata estuary. *Syst Appl Microbiol* **35:** 541-548.

Behrens S, Lösekann T, Pett-Ridge J, Weber PK, Ng W-O, Stevenson BS *et al.* (2008). Linking microbial phylogeny to metabolic activity at the single-cell level by using enhanced element labeling-catalyzed reporter deposition fluorescence in situ hybridization (EL-FISH) and NanoSIMS. *Appl Environ Microbiol* **74:** 3143-3150.

Berg JS, Schwedt A, Kreutzmann A-C, Kuypers MMM, Milucka J (2014). Polysulfides as intermediates in the oxidation of sulfide to sulfate by *Beggiatoa* spp. *Appl Environ Microbiol* **80:** 629-636.

Berry D, Mader E, Lee TK, Woebken D, Wang Y, Zhu D *et al.* (2015). Tracking heavy water (D_2O) incorporation for identifying and sorting active microbial cells. *Proc Natl Acad Sci USA* **112:** E194-E203.

Bjerneld EJ, Földes-Papp Z, Käll M, Rigler R (2002). Single-molecule surface-enhanced Raman and fluorescence correlation spectroscopy of horseradish peroxidase. *J Phys Chem B* **106:** 1213-1218.

Braissant O, Decho AW, Dupraz C, Glunk C, Przekop KM, Visscher PT (2007). Exopolymeric substances of sulfate-reducing bacteria: Interactions with calcium at alkaline pH and implication for formation of carbonate minerals. *Geobiology* **5:** 401-411.

Cowcher DP, Xu Y, Goodacre R (2013). Portable, quantitative detection of Bacillus bacterial spores using surface-enhanced Raman scattering. *Anal Chem* **85:** 3297-3302.

Daims H, Brühl A, Amann R, Schleifer K-H, Wagner M (1999). The domain-specific probe EUB338 is insufficient for the detection of all *Bacteria*: development and evaluation of a more comprehensive probe set. *Syst Appl Microbiol* **22:** 434-444.

Danscher G (1981). Histochemical demonstration of heavy metals. *Histochemistry* **71:** 1-16.

De Gelder J, De Gussem K, Vandenabeele P, Moens L (2007). Reference database of Raman spectra of biological molecules. *J Raman Spectrosc* **38:** 1133-1147.

DeLong EF, Wickham GS, Pace NR (1989). Phylogenetic stains: ribosomal RNA-based probes for the identification of single cells. *Science* **243:** 1360-1363.

Dortch Q, Roberts TL, Clayton JR, Ahmed SI (1983). RNA/DNA ratios and DNA concentrations as indicators of growth rate and biomass in planktonic organisms. *Mar Ecol Prog Ser* **13:** 61-71.

Efrima S, Bronk B (1998). Silver colloids impregnating or coating bacteria. *J Phys Chem B* **102:** 5947-5950.

Efrima S, Zeiri L (2009). Understanding SERS of bacteria. *J Raman Spectrosc* **40:** 277-288.

Gérard E, Guyot F, Philippot P, López-García P (2005). Fluorescence *in situ* hybridisation coupled to ultra small immunogold detection to identify prokaryotic cells using transmission and scanning electron microscopy. *J Microbiol Methods* **63:** 20-28.

Grow AE, Wood LL, Claycomb JL, Thompson PA (2003). New biochip technology for label-free detection of pathogens and their toxins. *J Microbiol Methods* **53:** 221-233.

Huang WE, Stoecker K, Griffiths R, Newbold L, Daims H, Whiteley AS *et al.* (2007). Raman-FISH: combining stable-isotope Raman spectroscopy and fluorescence in situ hybridization for the single cell analysis of identity and function. *Environ Microb* **9:** 1878-1889.

Kato S, Hashimoto K, Watanabe K (2012). Microbial interspecies electron transfer via electric currents through conductive minerals. *Proc Natl Acad Sci USA* **109:** 10042-10046.

Kemp P, Lee S, LaRoche J (1993). Estimating the growth rate of slowly growing marine bacteria from RNA content. *Appl Environ Microbiol* **59:** 2594-2601.

Kenzaka T, Ishidoshiro A, Yamaguchi N, Tani K, Nasu M (2005). rRNA sequence-based scanning electron microscopic detection of bacteria. *Appl Environ Microbiol* **71:** 5523-5531.

Kerker M, Blatchford C (1982). Elastic scattering, absorption, and surface-enhanced Raman scattering by concentric spheres comprised of a metallic and a dielectric region. *Phys Rev B* **26:** 4052.

Koyama Y, Kito M, Takii T, Saiki K, Tsukida K, Yamashita J (1982). Configuration of the carotenoid in the reaction centers of photosynthetic bacteria. Comparison of the resonance Raman spectrum of the reaction center of Rhodopseudomonas sphaeroides G1C with those of cis-trans isomers of β-carotene. *BBA-Bioenergetics* **680:** 109-118.

Krug JT, Wang GD, Emory SR, Nie S (1999). Efficient Raman enhancement and intermittent light emission observed in single gold nanocrystals. *J Am Chem Soc* **121:** 9208-9214.

Kubota K, Morono Y, Ito M, Terada T, Itezono S, Harada H *et al.* (2014). Gold-ISH: A nano-size gold particle-based phylogenetic identification compatible with NanoSIMS. *Syst Appl Microbiol*. **37:**261-266.

Lechene CP, Luyten Y, McMahon G, Distel DL (2007). Quantitative imaging of nitrogen fixation by individual bacteria within animal cells. *Science* **317:** 1563-1566.

Li M, Canniffe DP, Jackson PJ, Davison PA, FitzGerald S, Dickman MJ *et al.* (2012). Rapid resonance Raman microspectroscopy to probe carbon dioxide fixation by single cells in microbial communities. *ISME J* **6:** 875-885.

Li T, Wu TD, Mazéas L, Toffin L, Guerquin-Kern JL, Leblon G *et al.* (2008). Simultaneous analysis of microbial identity and function using NanoSIMS. *Environ Microb* **10:** 580-588.

Loy A, Lehner A, Lee N, Adamczyk J, Meier H, Ernst J *et al.* (2002). Oligonucleotide microarray for 16S rRNA gene-based detection of all recognized lineages of sulfate-reducing prokaryotes in the environment. *Appl Environ Microbiol* **68:** 5064-5081.

Maher RC (2012). SERS hot spots. *Raman spectroscopy for nanomaterials characterization*. Springer. pp 215-260.

Ménez B, Rommevaux-Jestin C, Salomé M, Wang Y, Philippot P, Bonneville A *et al.* (2007). Detection and phylogenetic identification of labeled prokaryotic cells on mineral surfaces using Scanning X-ray Microscopy. *Chem Geol* **240:** 182-192.

Milucka J, Ferdelman TG, Polerecky L, Franzke D, Wegener G, Schmid M *et al.* (2012). Zero-valent sulphur is a key intermediate in marine methane oxidation. *Nature* **491:** 541-546.

Musat N, Halm H, Winterholler B, Hoppe P, Peduzzi S, Hillion F *et al.* (2008). A single-cell view on the ecophysiology of anaerobic phototrophic bacteria. *Proc Natl Acad Sci USA* **105:** 17861-17866.

Musat N, Stryhanyuk H, Bombach P, Adrian L, Audinot J-N, Richnow HH (2014). The effect of FISH and CARD-FISH on the isotopic composition of ^{13}C-and ^{15}N-labeled *Pseudomonas putida* cells measured by nanoSIMS. *Syst Appl Microbiol*. **37:**267-276.

Niaura G, Gaigalas AK, Vilker VL (1997). Surface-enhanced Raman spectroscopy of phosphate anions: adsorption on silver, gold, and copper electrodes. *J Phys Chem B* **101:** 9250-9262.

Pernthaler A, Pernthaler J, Amann R (2002). Fluorescence in situ hybridization and catalyzed reporter deposition for the identification of marine bacteria. *Appl Environ Microbiol* **68:** 3094-3101.

Pett-Ridge J, Weber PK (2012). NanoSIP: NanoSIMS applications for microbial biology. *Microbial Systems Biology*. Springer. pp 375-408.

Pfeffer C, Larsen S, Song J, Dong M, Besenbacher F, Meyer RL *et al.* (2012). Filamentous bacteria transport electrons over centimetre distances. *Nature* **491:** 218-221.

Polerecky L, Adam B, Milucka J, Musat N, Vagner T, Kuypers MMM (2012). Look@ NanoSIMS–a tool for the analysis of nanoSIMS data in environmental microbiology. *Environ Microb* **14:** 1009-1023.

Schmidt H, Eickhorst T, Mußmann M (2012). Gold-FISH: a new approach for the in situ detection of single microbial cells combining fluorescence and scanning electron microscopy. *Syst Appl Microbiol* **35:** 518-525.

Schuster KC, Reese I, Urlaub E, Gapes JR, Lendl B (2000). Multidimensional information on the chemical composition of single bacterial cells by confocal Raman microspectroscopy. *Anal Chem* **72:** 5529-5534.

Stamplecoskie KG, Scaiano JC, Tiwari VS, Anis H (2011). Optimal size of silver nanoparticles for surface-enhanced Raman spectroscopy. *J Phys Chem C* **115:** 1403-1409.

Strola SA, Baritaux J-C, Schultz E, Simon AC, Allier C, Espagnon I *et al.* (2014). Single bacteria identification by Raman spectroscopy. *J Biomed Opt* **19:** 111610-111610.

Thompson AW, Foster RA, Krupke A, Carter BJ, Musat N, Vaulot D *et al.* (2012). Unicellular cyanobacterium symbiotic with a single-celled eukaryotic alga. *Science* **337:** 1546-1550.

Tonolla M, Demarta A, Peduzzi R, Hahn D (1999). In situ analysis of phototrophic sulfur bacteria in the chemocline of meromictic Lake Cadagno (Switzerland). *Appl Environ Microbiol* **65:** 1325-1330.

Zeiri L, Bronk B, Shabtai Y, Czege J, Efrima S (2002). Silver metal induced surface enhanced Raman of bacteria. *Colloid Surf. A-Physicochem. Eng. Asp.* **208:** 357-362.

Zhang X, Young MA, Lyandres O, Van Duyne RP (2005). Rapid detection of an anthrax biomarker by surface-enhanced Raman spectroscopy. *J Am Chem Soc* **127:** 4484-4489.

SUPPLEMENTARY INFORMATION

Silver-deposition* in situ *hybridization

The silver-DISH protocol introduced in this study was developed as a slight modification of a standard protocol for catalyzed reporter deposition FISH (Fig S10). Fixed microbial cells were first permeabilized and incubated in 0.01M hydrochloric acid to inactivate endogenous peroxidases, then hybridization was performed using HRP-conjugated oligonucleotide probes. The sole difference between the silver-DISH and CARD-FISH protocols lay in the amplification step after probe binding. In silver-DISH, amplification was performed at room temperature in the dark using a commercially available EnzMet® detection kit (Fig S10). The kit included three solutions, 'HRP Detect A', 'HRP Detect B', and 'HRP Detect C', which were consecutively applied to the sample. The development step took between 10 to maximum 30 minutes which is comparable to CARD amplification. After final wash in deionized water and drying, filters were ready for microscopic imaging. The exact chemical composition of the EnzMet™ kit solutions was not specified in the accompanying Product Information Data Sheet. However, we assume that the silver deposition reaction was analogous to other silver development techniques, where free silver(I) ions are reduced in the presence of hydrogen peroxide by some chemical developing solution and deposited as metallic silver(0) at sites of probe binding. The silver-DISH protocol is in principle similar to other so-far reported autometallographic ISH protocols (Gérard *et al.,* 2005); Kenzaka *et al.,* 2005; Schmidt *et al.,* 2012; Almstrand *et al.,* 2015), with the major difference that standard CARD-FISH oligonucleotide probes (HRP-conjugated) are employed and instead of a biotin-streptavidin system or antibodies. Additionally, as the silver is not directly conjugated to the oligonucleotide probes, the penetration of the probe into the cell and its binding to ribosomal DNA is not affected. Therefore, no changes in e.g. permeabilization or formamide

concentration are required and thus no additional testing is needed. To achieve optimal silver staining for different samples, parameters such as concentration of the development reagent and the deposition time might need to be modified as these control the amount and size of deposited silver grains (Fig S2).

SUPPLEMENTARY FIGURES

Fig S1: Light and fluorescence microscopy images of *Chromatium* cells after (a) silver-DISH, and (b) traditional CARD-FISH (in green) using the cMOK453 probe. The sample was counterstained with DAPI (blue). The different intensity of silver or fluorescent staining presumably reflects differences in the ribosomal content of the cells. Scale bars are 5 µm.

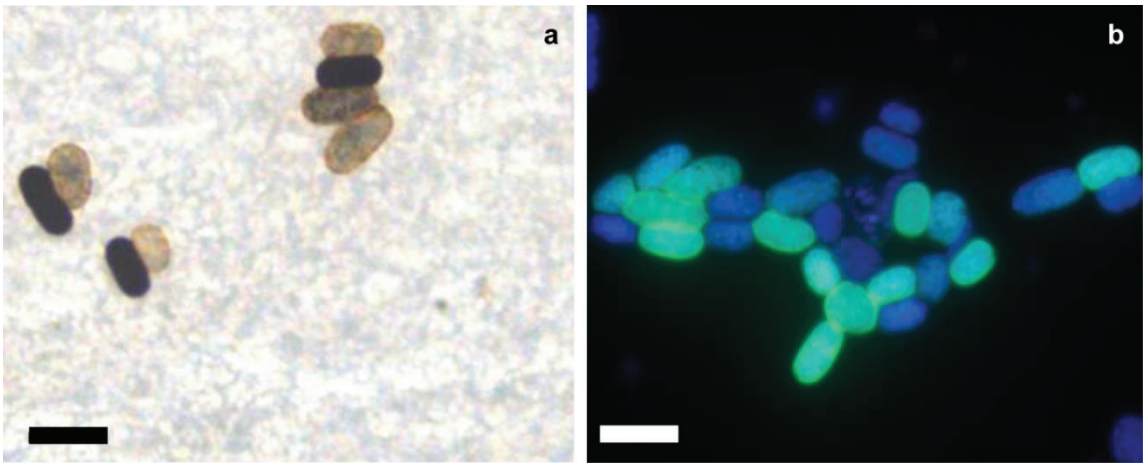

Fig S2: (a) Average diameter of silver nanoparticles as a function of silver staining reagent dilution showing an increasing, linear trend. Particles were measured with SEM. (b) Larger, crystalline grains were detected at high reagent concentration and (c) smaller, rounded particles were detected at low reagent concentration. Scale bar is 500 nm.

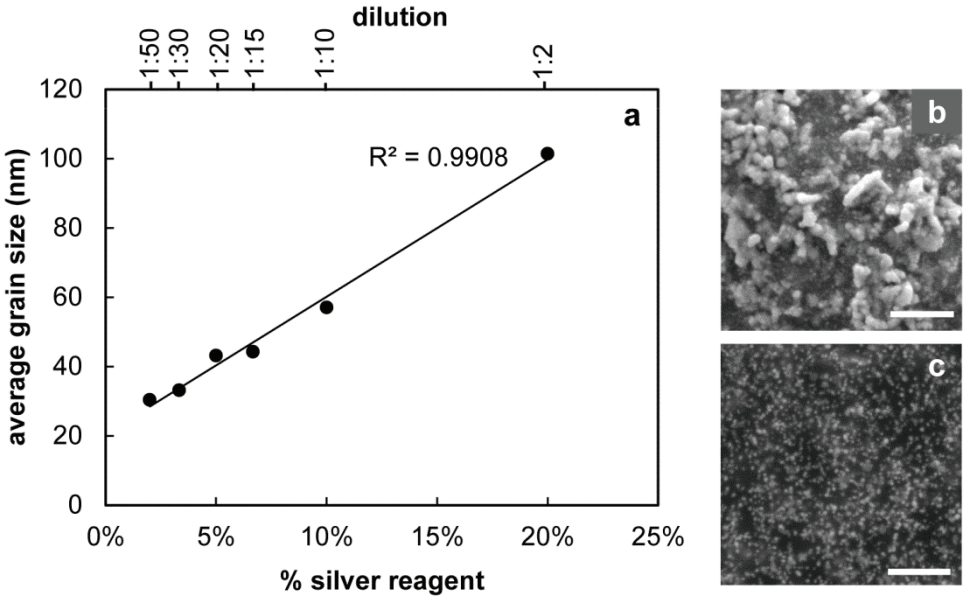

Fig S3: Box and whisker plot of C to N (left) and N to P (right) ratios of untreated, unhybridized *E. coli* cells and cells after silver-DISH treatment with a 1:5 and 1:20 dilution of staining reagents (n>44 for all treatments). Carbon, nitrogen, and phosphorus were quantified as normalized atomic % concentration by EDS. The horizontal line within the box indicates the median, boundaries of the box indicate the 25TH- and 75th -percentile, and the whiskers indicate the highest and lowest values of the results, excluding outliers which are represented by black circles.

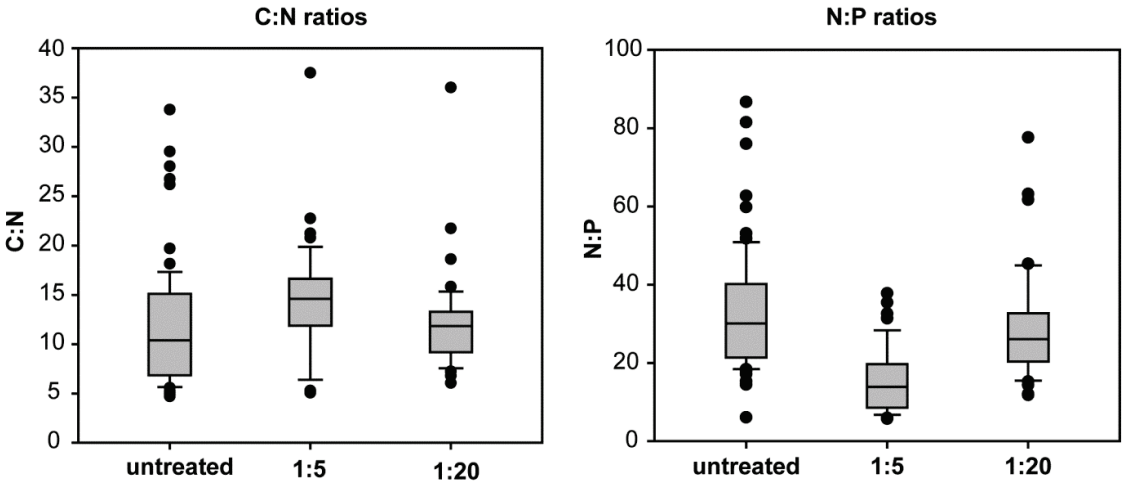

Fig S4: Box and whisker plots of the recalculated $^{13}C/^{12}C$ and $^{12}C^{15}N/^{12}C^{14}N$ ratios measured by nanoSIMS in untreated (NON) and silver-DISH treated (silver) *E. coli* cells. Low (top left) and high (top right) ^{13}C-enriched cells were compared (n>40), and only one degree of ^{15}N enrichment was measured (n>120; bottom left). The horizontal line within the box indicates the median, boundaries of the box indicate the 25TH- and 75th -percentile, and the whiskers indicate the highest and lowest values of the results, excluding outliers which are represented by black circles. (bottom right) NanoSIMS images corresponding to the *E. coli* cells measured in high ^{13}C treatment (top right). The $^{13}C^{12}C$ content of cells containing ^{107}Ag deposited via silver-DISH appears slightly lower than that of fixed, unlabeled *E. coli* cells. Scale bar is 2 µm.

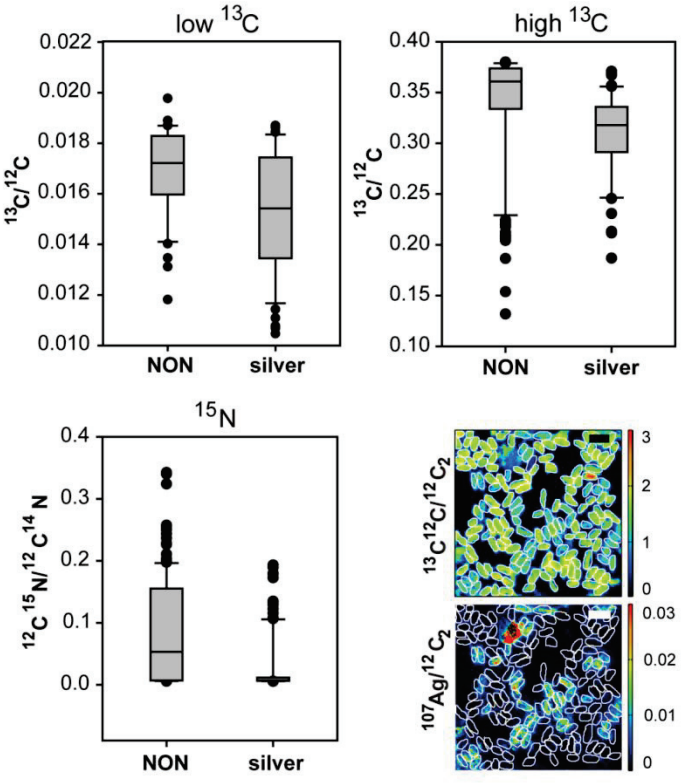

Fig S5: Raman spectra of silver compounds used for reference.

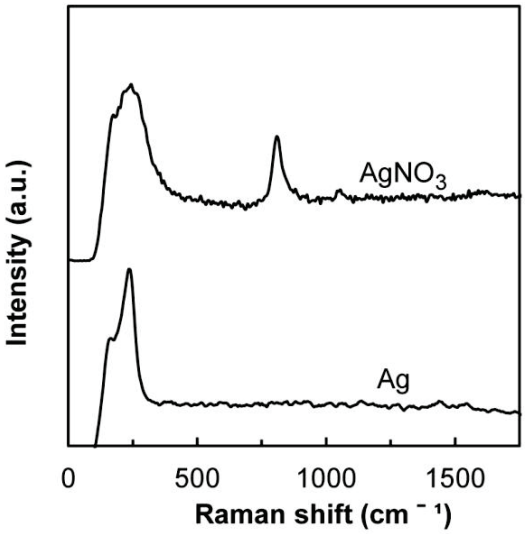

Fig S6: A normal Raman spectrum of a *Chromatium* cell not stained with silver exhibiting peaks characteristic of carotenoids

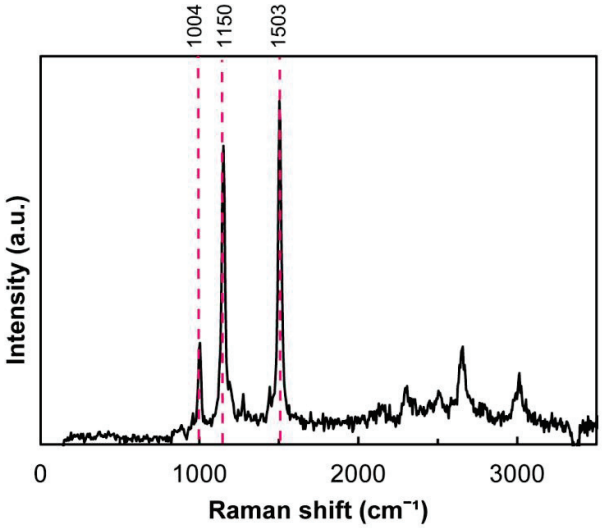

Fig S7: Plot of the calculated SERS enhancement factor as a function of grain diameter. The degree of enhancement of the Raman signals depends on the grain size and exhibits a normal distribution.

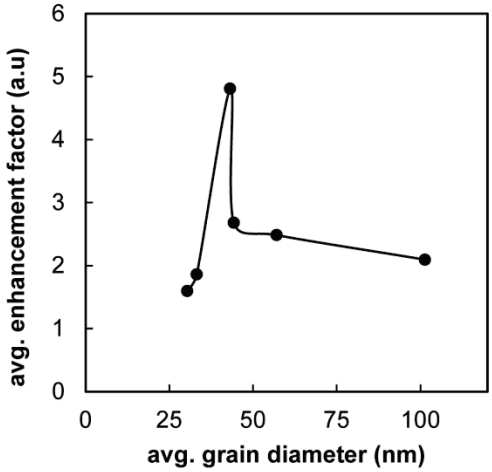

Fig S8: Raman spectra taken from a single cell, but different points, on day 1, day 2, and day 3 after silver staining. Significant SERS enhancement is still visible after sample storage for 3 days under normal atmosphere.

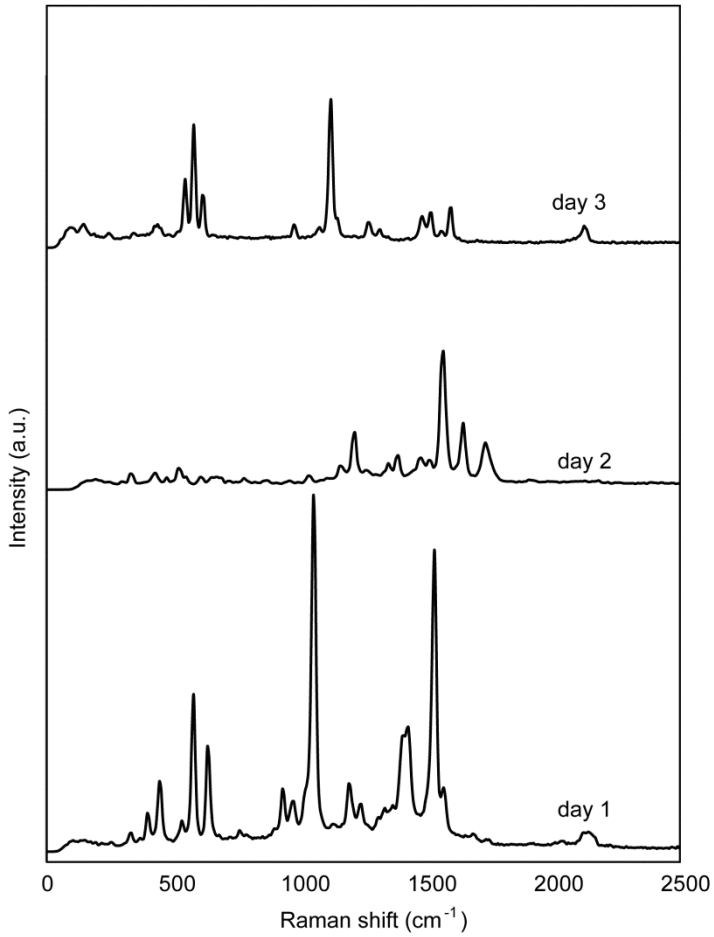

Fig S9: NanoSIMS image of $^{13}C/^{12}C$ in *Chromatium* cells from Fig 2 recorded in a separate run. In The $^{13}C^-$ and $^{12}C^-$ ions were measured in parallel with the $^{13}C^{12}C^-$ and $^{12}C^{12}C^-$ for comparison.

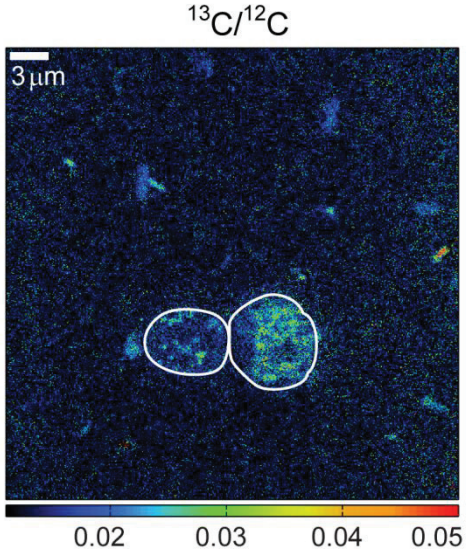

Fig S10: Schematic representation of silver-DISH protocol.

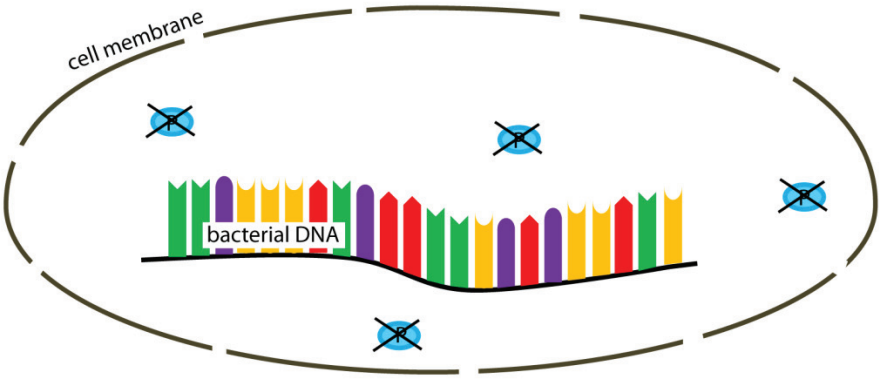

Step 1: Fixation, permeabilization, inactivation of endogenous peroxidases

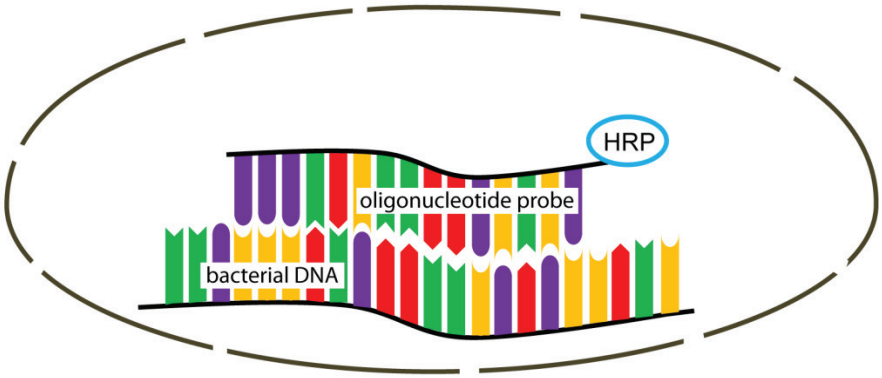

Step 2: In situ hybridization with HRP-labeled probe

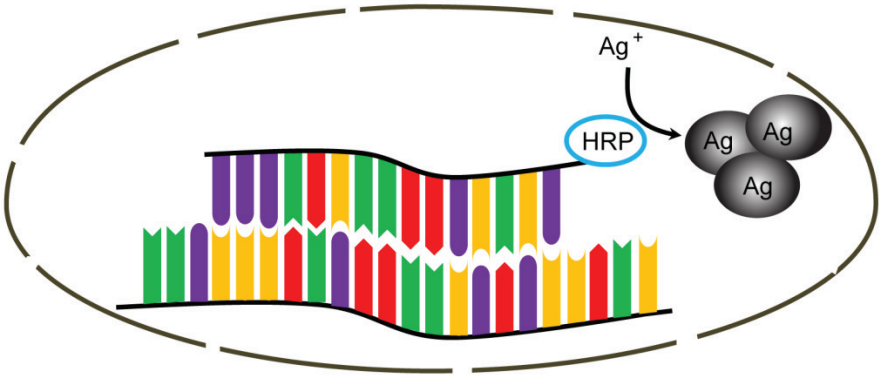

Step 3: HRP-catalyzed Ag^+ reduction and deposition of silver particles

CONTRIBUTED MANUSCRIPTS

Community shift from phototrophic to chemotrophic sulfide oxidation following anoxic holomixis in a stratified seawater lake

Petra Pjevac[1], Marino Korlević[2], Jasmine S. Berg[3], Elvira Bura-Nakićd[4], Irena Ciglenečki[5], Rudolf Amann[1], and Sandi Orlić[2,6]

[1]Department of Molecular Ecology, Max Planck Institute for Marine Microbiology, Bremen, Germany
[2]Center for Marine Research, Ruđer Bošković Institute, Rovinj, Croatia
[3]Department of Biogeochemistry, Max Planck Institute for Marine Microbiology, Bremen, Germany
[4]Division for Marine and Environmental Research, Ruđer Bošković Institute, Zagreb, Croatia
[5]Institute of Geochemistry and Petrology, Swiss Federal Institute of Technology, Zürich, Switzerland
[6]Division of Materials Chemistry, Ruđer Bošković Institute, Zagreb, Croatia

Published in: *Applied and Environmental Microbiology*

doi: 10.1128/AEM.02435-14

Author contributions: PP and SO developed concepts and ideas. PP conceived and wrote the manuscript, performed CARD-FISH experiments, construction and sequencing of soxB gene clone libraries, and analysis of all the sequence data. MK performed DNA isolation, constructed 16S rRNA gene clone libraries and CARD-FISH experiments. JSB performed Raman microscopy analyses. EB-N measured *in situ* chemical hydrographical data. SO collected samples and performed CARD-FISH experiments. MK, JSB, EB-N, IC, RA and SO edited the manuscript.

SUMMARY

Most stratified sulfidic holomictic lakes become oxygenated after annual turnover. In contrast, Lake Rogoznica, on the eastern Adriatic coast, has been observed to undergo a period of water column anoxia after water layer mixing and establishment of holomictic conditions. Although Lake Rogoznica's chemistry and hydrography have been studied extensively, it is unclear how the microbial communities typically inhabiting the oxic epilimnion and a sulfidic hypolimnion respond to such a drastic shift in redox conditions. We investigated the impact of anoxic holomixis on microbial diversity and microbially mediated sulfur cycling in Lake Rogoznica with an array of culture-independent microbiological methods. Our data suggest a tight coupling between the lake's chemistry and occurring microorganisms. During stratification, anoxygenic phototrophic sulfur bacteria were dominant at the chemocline and in the hypolimnion. After an anoxic mixing event, the anoxygenic phototrophic sulfur bacteria entirely disappeared, and the homogeneous, anoxic water column was dominated by a bloom of gammaproteobacterial sulfur oxidizers related to the GSO/SUP05 clade. This study is the first report of a community shift from phototrophic to chemotrophic sulfide oxidizers as a response to anoxic holomictic conditions in a seasonally stratified seawater lake.

Selective pressure of temperature on competition and cross-feeding within denitrifying and fermentative microbial communities

Anna Hanke[1], Jasmine Berg[1], Theresa Hargesheimer[1], Halina E. Tegetmeyer[2], Christine E. Sharp[3], and Marc Strous[1,2,3,*]

[1]Microbial Fitness Group, Max Planck Institute for Marine Microbiology, Bremen, Germany
[2]Center for Biotechnology, Institute for Genome Research and Systems Biology, University of Bielefeld, Bielefeld, Germany
[3]Energy Bioengineering Group, Department of Geoscience, University of Calgary, Calgary, AB, Canada
*Correspondence: Marc Strous; mstrous@uccalgary.ca

Published in: *Frontiers in Microbiology*

doi: 10.3389/fmicb.2015.01461

Author contributions: AH performed all experiments with help from JB and TH. HT performed next generation DNA sequencing, read quality control and assembly. MS performed binning, annotation, and read mapping. CS analyzed abundance of *Alpha*- and *Gammaproteobacteria* in environmental datasets. The manuscript was written by AH and MS with input from all other co-authors.

SUMMARY

In coastal marine sediments, denitrification and fermentation are important processes in the anaerobic decomposition of organic matter. Microbial communities performing these two processes were enriched from tidal marine sediments in replicated, long term chemostat incubations at 10 and 25°C. Whereas denitrification rates at 25°C were more or less stable over time, at 10°C denitrification activity was unstable and could only be sustained either by repeatedly increasing the amount of carbon substrates provided or by repeatedly decreasing the dilution rate. Metagenomic and transcriptomic sequencing was performed at different time points and provisional whole genome sequences (WGS) and gene activities of abundant populations were compared across incubations. These analyses suggested that a temperature of 10°C selected for populations related to Vibrionales/Photobacterium that contributed to both fermentation (via pyruvate/formate lyase) and nitrous oxide reduction. At 25°C, denitrifying populations affiliated with *Rhodobacteraceae* were more abundant. The latter performed complete denitrification, and may have used carbon substrates produced by fermentative populations (cross-feeding). Overall, our results suggest that a mixture of competition—for substrates between fermentative and denitrifying populations, and for electrons between both pathways active within a single population –, and cross feeding—between fermentative and denitrifying populations—controlled the overall rate of denitrification. Temperature was shown to have a strong selective effect, not only on the populations performing either process, but also on the nature of their ecological interactions. Future research will show whether these results can be extrapolated to the natural environment.

Candidatus Desulfofervidus auxilii, a hydrogenotrophic sulfate-reducing bacterium involved in the thermophilic anaerobic oxidation of methane

Viola Krukenberg[1]*, Katie Harding[1], Michael Richter[1], Frank Oliver Glöckner [1,2], Harald R. Gruber-Vodicka[1], Birgit Adam[1], Jasmine S. Berg[1], Katrin Knittel[1], Halina E. Tegetmeyer,[3,4] Antje Boetius[1,3,5] and Gunter Wegener[1,5]

[1]Max Planck Institute for Marine Microbiology, Bremen, Germany.
[2]Jacobs University Bremen GmbH, Bremen, Germany.
[3]Alfred Wegener Institute, Helmholtz Center for Polar and Marine Research, Bremerhaven, Germany.
[4]Center for Biotechnology, Bielefeld University, Bielefeld, Germany.
[5]MARUM, Center for Marine Environmental Sciences, University Bremen, Bremen, Germany.

Published in: *Environmental Microbiology*

doi: 10.1111/1462-2920.13283

Author contributions: VK, AB, and GW designed the study. Experiments were performed by VK, KH and HET. Data were analyses were performed by VK, KH, MR, FOG HG-V, KK and GW. Microscopic imaging was performed by VK, BA, JSB and HG-V. VK, AB and GW wrote the manuscript with contributions from all co-authors.

SUMMARY

The anaerobic oxidation of methane (AOM) is mediated by consortia of anaerobic methane-oxidizing archaea (ANME) and their specific partner bacteria. In thermophilic AOM consortia enriched from Guaymas Basin, members of the ANME-1 clade are associated with bacteria of the HotSeep-1 cluster, which likely perform direct electron exchange via nanowires. The partner bacterium was enriched with hydrogen as sole electron donor and sulfate as electron acceptor. Based on phylogenetic, genomic and metabolic characteristics we propose to name this chemolithoautotrophic sulfate reducer Candidatus Desulfofervidus auxilii. Ca. D. auxilii grows on hydrogen at temperatures between 50°C and 70°C with an activity optimum at 60°C and doubling time of 4–6 days. Its genome draft encodes for canonical sulfate reduction, periplasmic and soluble hydrogenases and autotrophic carbon fixation via the reductive tricarboxylic acid cycle. The presence of genes for pili formation and cytochromes, and their similarity to genes of Geobacter spp., indicate a potential for syntrophic growth via direct interspecies electron transfer when the organism grows in consortia with ANME. This first ANME-free enrichment of an AOM partner bacterium and its characterization opens the perspective for a deeper understanding of syntrophy in anaerobic methane oxidation.

3. DISCUSSION & OUTLOOK

DISCUSSION & OUTLOOK

At oxic-anoxic interfaces, the intersection of chemical gradients fuels intense biogeochemical cycling via a complex combination of abiotic and biotic reactions. Microorganisms compete with spontaneous chemical reactions to gain energy while influencing primary productivity and organic matter degradation. The aim of this thesis was to disentangle the microbial from the abiotic processes and determine their contribution to the redox cycling of Fe and S. In the preceding manuscripts, the application of modern, single-cell technologies to investigate biogeochemical cycling on the single-cell level enabled unprecedented insights into extremely rapid, even cryptic, microbial processes with transient intermediates. In the following section, the major findings are discussed in context of our current understanding of biogeochemical cycling and open questions are highlighted for future research.

3.1 Interaction of biogeochemical cycles: importance of oxygen in the anoxic zone

The investigations of biogeochemical cycling at the oxic-anoxic interface of Lake Cadagno in this thesis and in other works (e.g. Tonolla et al., 2004; Halm et al., 2009; Milucka et al., 2015) have revealed that diverse metabolic processes compete for light and oxygen within an ostensibly anoxic chemocline. The adaptation of phototrophs to specific light intensities and wavelengths has been well-studied (e.g. Abella et al., 1980; Parkin and Brock, 1980; Guerrero et al., 1985) and can explain the distribution of oxygenic and anoxygenic photosynthetic organisms over a wide depth range in the water column of Lake Cadagno. Surprisingly, the purple sulfur bacteria in Cadagno chemocline respired chemotrophically using O_2 as an electron acceptor, even in the

presence of light (Chapter 3). These bacteria are expected to grow phototrophically, but are apparently well-adapted to fluctuating environmental conditions and scavenge extremely low amounts of available oxygen. In fact, it was most astonishing that molecular oxygen was found to play a major role not only in the microbial oxidation of reduced sulfur (Chapter 3), but also of Fe^{2+} (Chapter 2), CH_4 (Milucka et al., 2015), and potentially $Mn^{2+/3+}$ (Chapter 2) in an anoxic water layer.

Molecular oxygen enters the Lake Cadagno chemocline via advection and diffusion of surface waters and *in situ* production by photosynthetic algae (Milucka et al., 2015), but it is so efficiently scavenged that concentrations remain below the detection limits of our instruments (the reliable detection limit of the trace optodes used is about 50-100 $nmol \cdot l^{-1}$). The diversity of microorganisms subsisting on this single limiting electron acceptor implies that competition for molecular oxygen is intense. Microorganisms have evolved various mechanisms to survive under oxygen-limiting conditions including physical associations with oxygenic phototrophs, high-affinity terminal oxidases, and intracellular storage compounds. Aerobic methanotrophs in Lake Cadagno have been observed to form associations with photosynthetic algae in the chemocline, securing them direct access to *in situ* produced oxygen (Milucka et al., 2015). In addition, the enzyme utilized in the first oxidation step of methane, methane monooxygenase, has a high affinity for O_2 with a K_m of 0.14 $\mu mol \cdot l^{-1}$ (Joergensen, 1985). Two high-affinity terminal oxidases, namely cytochrome bd quinol oxidase (Borisov et al., 2011) and a cytochrome *c* type *cbb3*, which has the highest affinity for O_2 (7 $nmol \cdot l^{-1}$) among all cytochrome oxidases (Preisig et al., 1996; Pitcher and Watmough, 2004), have been identified in the genomes of at least seven microaerophilic iron-oxidizing bacteria (Kato et al., 2012). These *cbb3* oxidases were also

identified in the genomes of some purple sulfur bacteria from Lake Cadagno including *Lamprocystis* sp. (Chapter 3) and *Thiodictyon* sp. (S. Luedin, personal communication) suggesting their involvement in aerobic sulfide oxidation there. The greatest advantage of the motile purple sulfur bacteria *Chromatium* sp. appears to be their ability to transport reducing or oxidizing equivalents in unknown form, bridging the distance between gradients of oxygen and sulfide. The outcome of this competition is governed by thermodynamics, with CH_4, Fe^{2+} and Mn^{2+} being consumed in order of decreasing energy yield (Fig 1). Sulfide oxidation proceeds before methane oxidation, out of thermodynamic order, because it can be consumed by low-light adapted purple and green sulfur bacteria, and possibly with an intracellular storage compound. Aerobic methanotrophs may also indirectly be inhibited by sulfide scavenging of Cu (e.g. Haraldsson and Westerlund, 1991), a trace metal necessary for synthesis of methane monoxygenase, but this was beyond the scope of this investigation.

Figure 1: A chemical profile of Lake Cadagno showing oxygen and a variety of different electron donors potentially involved in microaerobic processes in the chemocline (courtesy of C. Schubert).

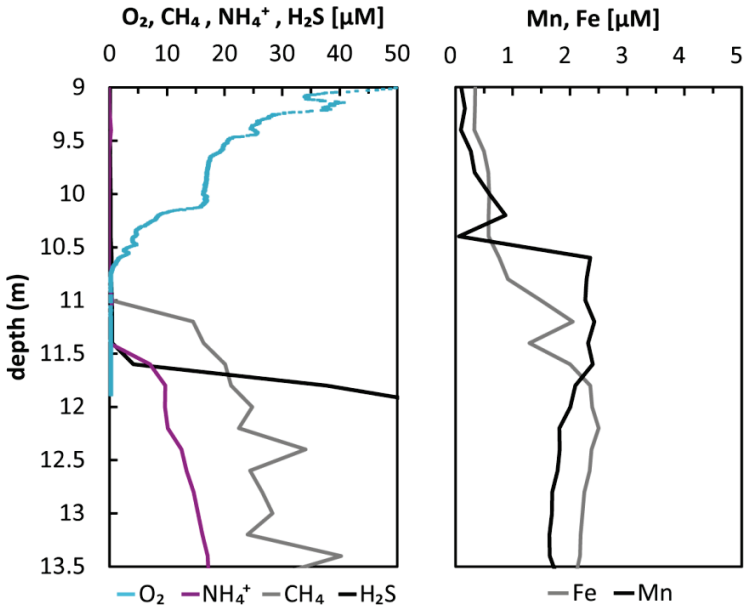

Overall, our results imply that aerobic metabolisms may abound in environments previously considered anoxic. Conversely, anaerobic processes such as iron reduction and anoxygenic photosynthesis appear to be reasonably oxygen tolerant as they occurred alongside aerobic

metabolisms. Aerobic methane oxidation under anoxic conditions has been demonstrated in other stratified systems such as Rotsee (Oswald et al., 2015), but has been linked to light-driven photosynthesis *in situ.* We found evidence for significant aerobic respiration by purple sulfur bacteria in the dark, stimulated by enhanced transport processes – either advection or bacterial swimming (Chapter 3). In the future, measuring and defining true anoxia, *i.e.* with STOX sensors (Revsbech et al., 2009), will be essential for understanding the biochemical limits of aerobic respiration, which currently occurs below the O_2 detection limits of conventional methods.

3.2 Overlooked cryptic cycles

Until now, iron redox cycling has been poorly studied in environments where it is scarce as an electron donor/acceptor. In this thesis, investigations into the iron cycle of Lake Cadagno revealed that despite relatively low iron concentrations, intense microbial iron cycling may substantially contribute to primary production and organic matter degradation at the chemocline. Our results imply that low abundance compounds could also be involved in significant biogeochemical cycling in other environments. In the Lake Cadagno water column, total iron concentrations are 1-2 $\mu mol \cdot l^{-1}$, which is significantly lower than in sediment where microbial iron cycling has been well-studied (e.g. Thamdrup et al., 1994; Thamdrup, 2000; Schippers and Jørgensen, 2002). This is still 2-3 orders of magnitude higher than in the ocean, but patterns of dissolved iron in oxygen minimum zones (OMZs) suggest that microbial activity may regulate the speciation and distribution of iron there. High subsurface respiration in OMZs leads to the depletion of O_2, and sequentially occurring gradients of reduced manganese and iron along with a coinciding nitrite peak have been cited as evidence of anaerobic remineralization and reduction processes (Landing and Bruland, 1987; Lewis and Luther, 2000;

Moffett et al., 2007; Vedamati et al., 2014). Similar mechanisms may also occur in other stratified aquatic environments with low iron concentrations, such as anoxic lakes and basins, which are widespread. Further studies are necessary to better understand the microbial impact on the iron cycle in modern surface waters and stratified anoxic lakes such as Lake Cadagno could thus serve as easily-accessible, model systems for this purpose.

Although iron cycling in high iron environments has been relatively well-studied, the microbial contribution to these processes may thus far have been underestimated. The abiotic reduction of iron oxide with sulfide occurs so rapidly that in sulfate-reducing environments, much of iron reduction has been attributed to indirect iron reduction by sulfide (Jørgensen, 1982; Thamdrup et al., 1994). While iron sulfides (FeS, FeS_2) have been considered a major sink for both iron and sulfur, the detection of active microbial re-oxidation of FeS in Lake Cadagno, implies that iron (and sulfur) can actually be recycled many times before burial, especially within the photic zone. This means that the contribution of iron-reducing bacteria to organic matter degradation could be underestimated if the recycling of FeS is not taken into account. In addition, we found that microorganisms were responsible for iron reduction in Lake Cadagno, even in the presence of high (1-2 $mmol \cdot l^{-1}$) sulfate concentrations. This is in contrast to the findings of Hansel et al., (2015) that despite thermodynamic predictions, sulfate reducers outcompete iron reducers even in low-sulfate, freshwater environments. The disagreement between our results and previous findings suggest that we do not yet fully understand the dynamics of the competition between iron- and sulfate-reducing bacteria. While sulfate reduction was dominant regardless of the crystalline form of the Fe(III) substrate provided to the microbial communities (Hansel et al., 2015), it is possible that other factors such as affinity for simple organic substrates or

sensitivity to light and oxygen may govern the competition between these bacteria. Further studies of iron-reducing and sulfate reducing-bacteria in co-cultures will be necessary to identify these determinant environmental factors.

Evidently, new methods are needed to detect cryptic cycles such as tightly coupled microbial iron oxidation and reduction processes. Although the discovery of biomarkers such as specific genes for iron metabolism could aid in the identification of iron cycling bacteria in the environment, intense activity driven by a rare and highly diverse biosphere would still be easily overlooked. In Lake Cadagno, for example, we used a specific CARD-FISH probe to search for the photoferrotroph *Rhodomicrobium* sp. enriched in Chapter 3 but detected no more than 3 cells in one milliliter of lake water. This implies that the highly diverse Fe-cycling bacteria detected in Lake Cadagno are low in numbers but highly active. In the future, elucidating cryptic cycles driven by the rare biosphere may simply require labor-intensive, multi-disciplinary approaches as well as increasingly sensitive methods to measure transient reactive intermediates at extremely low concentrations.

3.3 Dark sulfide oxidation: new processes and a missing oxidant

Our investigations into the dynamics of sulfide oxidation in Lake Cadagno revealed that a surprising biological mechanism driven by microbial storage and transport processes removes sulfide from the water column before it diffuses into oxic waters. The anoxygenic phototrophic bacteria primarily responsible for the oxidation of sulfide within the chemocline apparently respired aerobically both in the dark and in the light. The supply of electron donors and acceptors to these bacteria inhabiting a 1-2 m layer devoid of both oxygen and sulfide was enhanced by their constant swimming, which may have resulted in intracellular transport or

entrainment of oxidizing and reducing equivalents. However, it was not possible to close electron budgets (in the dark) in this non-steady state system as a large deficit in calculated oxygen fluxes was observed. We could also not explain how sulfide was oxidized to zero-valent sulfur at the base of the Cadagno chemocline where both light and oxygen gradients were absent. The possibility that an unidentified compound not among the known terminal electron acceptors for sulfide oxidation was involved could therefore not be excluded.

Because purple sulfur bacteria are known to accumulate not only zero-valent sulfur but also glycogen and polyhydroxyalkanoates, we considered stored carbon as an alternative oxidant for sulfide. In theory, a carbohydrate with an oxidation state (0), higher than that of H_2S (-2), could be utilized for dark sulfide oxidation. This would be contrary to previous reports that *Chromatium* utilize glycogen to reduce stored S^0 in the dark (Van Gemerden, 1968). Nonetheless, sulfide oxidation may be more efficient for energy generation than the sulfur reduction reaction which produces only 3 ATP per carboxyl unit broken down (Van Gemerden, 1968). The utilization of stored carbohydrates may have been coupled to dark sulfide oxidation and concomitant CO_2 and NH_4^+ assimilation observed in our bottle incubations which were cut off from *in situ* oxygen fluxes (Chapter 3, Fig 5). To confirm this theory, it will be essential to quantify glycogen and its transformation products over a full diel cycle, as well as the changes in glycogen concentration along light gradients over the depth of the chemocline.

Alternatively, redox reactions of sulfide with dissolved organic matter (DOM) may be important for sulfur cycling in the anoxic chemocline of Lake Cadagno. It has been previously shown that humic substances can accept electrons from sulfide (Heitmann and Blodau, 2006). DOM could thus serve as an electron shuttle, oxidizing and incorporating sulfide at the base of the

chemocline. The convection of the chemocline could naturally circulate reduced humic substances upwards to the oxycline where they could be reoxidized. It may even be possible for sulfide oxidizing bacteria to transfer electrons to humic acids similarly to *Geobacter* spp. which use humic acids as an electron shuttle during organic carbon reduction (Lovley et al., 1996). We therefore tested the abiotic electron accepting capacity of *in situ* filtered Lake Cadagno water and pasteurized (killed) controls. No decrease in sulfide concentrations was observed over time (Fig 2). Our experiments thus did not support the involvement of DOM in sulfide oxidation in Lake Cadagno.

Figure 2: Control experiments monitoring abiotic sulfide oxidation in pasteurized (1h at 72 C) and filtered (0.2µm) Lake Cadagno water. Incubations were performed in 50-ml Winkler bottles with no headspace and a replicate from the series was sampled destructively at each time point.

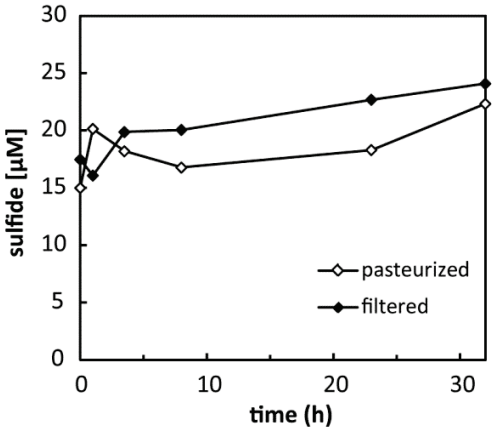

Although the storage and transport processes involved in sulfide oxidation in the Lake Cadagno chemocline are not yet fully understood, they represent a novel biological mechanism to bridge the gap between oxidants and reductants without nanowires (Pfeffer et al., 2012). The vertical migration of large sulfur bacteria storing sulfur and nitrate has already been described as an effective survival mechanism in stratified environments (Fossing et al., 1995; Jørgensen and Gallardo, 1999), but purple sulfur bacteria in Lake Cadagno appear to use unknown storage materials and advective transport. This novel microbial respiration mechanism could provide insights into other sulfidic environments within the photic zone, such as the Chesapeake Bay (Findlay et al., 2015) and the Black Sea (Jørgensen et al., 1991), where dark sulfide consumption processes are not completely understood.

3.4 Single-cell assessment of the ecophysiology of environmental bacteria

Our single-cell investigations of the Lake Cadagno bacterial community revealed surprising insights into the ecophysiology of the purple sulfur bacteria. With nanoSIMS, we found that these anoxygenic phototrophic bacteria in the environment fixed CO_2 in the dark. They thus behaved differently than these same bacteria in laboratory pure cultures, which respired stored organic compounds and sulfur in the dark (Van Gemerden, 1968). We also observed that the $^{15}NH_4^+$ assimilated by *Chromatium okenii* and smaller, round phototrophic cells (Chapter 3, Fig 5d) was incorporated into highly localized granules. The only nitrogen reserve compound thus far described is cyanophycin, which is unique to cyanobacteria (Obst and Steinbüchel, 2006), though gene homologs for cyanophycin synthesis have been found in heterotrophic bacteria (Krehenbrink et al., 2002; Ziegler et al., 2002). Although it is unlikely that this N reserve compound is involved in energy generation, it may be interesting to identify and characterize these N-rich globules considering that cyanophycin dynamics are reported to reflect light conditions and available nitrogen sources, and could thus provide further insights into the physiological adaptations of the purple sulfur bacteria to changing environmental conditions.

Identification of storage compounds *in vivo* without extraction is possible via Raman spectroscopy. Until now, however, detection of biological storage materials using Raman spectroscopy has been a challenge because organic molecules typically exhibit weak normal Raman signals. Our silver-DISH method developed in Chapter 5 can amplify Raman signals of intracellular compounds from targeted microbial cells via the SERS effect and could therefore aid in the identification of this N-rich compound. The application of silver-DISH may allow us to monitor the dynamics of poor Raman scattering compounds like proteins or storage

carbohydrates in individual cells from complex environmental samples for the first time. Moreover, the correlative use of other single-cell instruments like nanoSIMS and SEM-EDS enables us to obtain complementary information from the same sample. The unique information provided by each of these single-cell technologies (i.e. isotopic ratios, elemental composition, and molecular composition) is limited, but their coupled use could provide complementary information with powerful investigative insights in the field of environmental microbiology.

REFERENCES

Abella, C., Montesinos, E., and Guerrero, R. (1980) Field studies on the competition between purple and green sulfur bacteria for available light (Lake Siso, Spain). In *Shallow Lakes Contributions to their Limnology*: Springer, pp. 173-181.

Borisov, V.B., Gennis, R.B., Hemp, J., and Verkhovsky, M.I. (2011) The cytochrome bd respiratory oxygen reductases. *Biochimica et Biophysica Acta (BBA)-Bioenergetics* **1807**: 1398-1413.

Findlay, A.J., Bennett, A.J., Hanson, T.E., and Luther, G.W. (2015) Light-dependent sulfide oxidation in the anoxic zone of the Chesapeake Bay can be explained by small populations of phototrophic bacteria. *Applied and Environmental Microbiology* **81**: 7560-7569.

Fossing, H., Gallardoi, V., Jorgensen, B., Hiittel, M., Nielsenl, L., Schulz, H. et al. (1995) Concentration and transport of nitrate by the mat-forming sulphur bacterium Thioploca. *Nature* **374**: 20.

Guerrero, R., Montesinos, E., Pedrós-Alió, C., Esteve, I., Mas, J., Van Gemerden, H. et al. (1985) Phototrophic sulfur bacteria in two Spanish lakes: vertical distribution and limiting factors. *Limnology and Oceanography* **30**: 919-931.

Halm, H., Musat, N., Lam, P., Langlois, R., Musat, F., Peduzzi, S. et al. (2009) Co-occurrence of denitrification and nitrogen fixation in a meromictic lake, Lake Cadagno (Switzerland). *Environmental Microbiology* **11**: 1945-1958.

Hansel, C.M., Lentini, C.J., Tang, Y., Johnston, D.T., Wankel, S.D., and Jardine, P.M. (2015) Dominance of sulfur-fueled iron oxide reduction in low-sulfate freshwater sediments. *The ISME Journal* **9**: 2400-2412.

Haraldsson, C., and Westerlund, S. (1991) Total and suspended cadmium, cobalt, copper, iron, lead, manganese, nickel, and zinc in the water column of the Black Sea. In *Black Sea Oceanography*: Springer, pp. 161-172.

Heitmann, T., and Blodau, C. (2006) Oxidation and incorporation of hydrogen sulfide by dissolved organic matter. *Chemical Geology* **235**: 12-20.

Joergensen, L. (1985) The methane mono-oxygenase reaction system studied in vivo by membrane-inlet mass spectrometry. *Biochemical Journal* **225**: 441-448.

Jørgensen, B.B. (1982) Mineralization of organic matter in the sea bed-the role of sulphate reduction. *Nature* **296**: 643-645.

Jørgensen, B.B., and Gallardo, V.A. (1999) Thioploca spp.: filamentous sulfur bacteria with nitrate vacuoles. *FEMS Microbiology Ecology* **28**: 301-313.

Jørgensen, B.B., Fossing, H., Wirsen, C.O., and Jannasch, H.W. (1991) Sulfide oxidation in the anoxic Black Sea chemocline. *Deep Sea Research Part A Oceanographic Research Papers* **38**: S1083-S1103.

Kato, S., Hashimoto, K., and Watanabe, K. (2012) Microbial interspecies electron transfer via electric currents through conductive minerals. *Proceedings of the National Academy of Sciences* **109**: 10042-10046.

Krehenbrink, M., Oppermann-Sanio, F.-B., and Steinbüchel, A. (2002) Evaluation of non-cyanobacterial genome sequences for occurrence of genes encoding proteins homologous to cyanophycin synthetase and cloning of an active cyanophycin synthetase from Acinetobacter sp. strain DSM 587. *Archives of Microbiology* **177**: 371-380.

Landing, W.M., and Bruland, K.W. (1987) The contrasting biogeochemistry of iron and manganese in the Pacific Ocean. *Geochimica et Cosmochimica Acta* **51**: 29-43.

Lewis, B.L., and Luther III, G.W. (2000) Processes controlling the distribution and cycling of manganese in the oxygen minimum zone of the Arabian Sea. *Deep Sea Research Part II: Topical Studies in Oceanography* **47**: 1541-1561.

Lovley, D.R., Coates, J.D., Blunt-Harris, E.L., Phillips, E.J., and Woodward, J.C. (1996) Humic substances as electron acceptors for microbial respiration. *Nature* **382**: 445-448.

Milucka, J., Kirf, M., Lu, L., Krupke, A., Lam, P., Littmann, S. et al. (2015) Methane oxidation coupled to oxygenic photosynthesis in anoxic waters. *The ISME Journal*.

Moffett, J.W., Goepfert, T.J., and Naqvi, S.W.A. (2007) Reduced iron associated with secondary nitrite maxima in the Arabian Sea. *Deep Sea Research Part I: Oceanographic Research Papers* **54**: 1341-1349.

Obst, M., and Steinbüchel, A. (2006) Cyanophycin—an ideal bacterial nitrogen storage material with unique chemical properties. In *Inclusions in Prokaryotes*: Springer, pp. 167-193.

Oswald, K., Milucka, J., Brand, A., Littmann, S., Wehrli, B., Kuypers, M.M., and Schubert, C.J. (2015) Light-dependent aerobic methane oxidation reduces methane emissions from seasonally stratified lakes. *PloS One* **10**: e0132574.

Parkin, T., and Brock, T. (1980) The effects of light quality on the growth of phototrophic bacteria in lakes. *Archives of Microbiology* **125**: 19-27.

Pfeffer, C., Larsen, S., Song, J., Dong, M., Besenbacher, F., Meyer, R.L. et al. (2012) Filamentous bacteria transport electrons over centimetre distances. *Nature* **491**: 218-221.

Pitcher, R.S., and Watmough, N.J. (2004) The bacterial cytochrome cbb 3 oxidases. *Biochimica et Biophysica Acta (BBA)-Bioenergetics* **1655**: 388-399.

Preisig, O., Zufferey, R., Thöny-Meyer, L., Appleby, C.A., and Hennecke, H. (1996) A high-affinity cbb3-type cytochrome oxidase terminates the symbiosis-specific respiratory chain of Bradyrhizobium japonicum. *Journal of Bacteriology* **178**: 1532-1538.

Revsbech, N.P., Larsen, L.H., Gundersen, J., Dalsgaard, T., Ulloa, O., and Thamdrup, B. (2009) Determination of ultra-low oxygen concentrations in oxygen minimum zones by the STOX sensor. *Limnol Oceanogr Methods* **7**: 1-381.

Schippers, A., and Jørgensen, B.B. (2002) Biogeochemistry of pyrite and iron sulfide oxidation in marine sediments. *Geochimica et Cosmochimica Acta* **66**: 85-92.

Thamdrup, B. (2000) Bacterial manganese and iron reduction in aquatic sediments. In *Advances in Microbial Ecology*: Springer, pp. 41-84.

Thamdrup, B., Fossing, H., and Jørgensen, B.B. (1994) Manganese, iron and sulfur cycling in a coastal marine sediment, Aarhus Bay, Denmark. *Geochimica et Cosmochimica Acta* **58**: 5115-5129.

Tonolla, M., Peduzzi, S., DeMarta, A., Peduzzi, R., and Hahn, D. (2004) Phototropic sulfur and sulfate-reducing bacteria in the chemocline of meromictic Lake Cadagno, Switzerland. *Journal of Limnology* **63**: 161-170.

Van Gemerden, H. (1968) On the ATP generation by Chromatium in darkness. *Archiv für Mikrobiologie* **64**: 118-124.

Vedamati, J., Goepfert, T., and Moffett, J.W. (2014) Iron speciation in the eastern tropical South Pacific oxygen minimum zone off Peru. *Limnology and Oceanography* **59**: 1945-1957.

Ziegler, K., Deutzmann, R., and Lockau, W. (2002) Cyanophycin synthetase-like enzymes of non-cyanobacterial eubacteria: characterization of the polymer produced by a recombinant synthetase of Desulfitobacterium hafniense. *Zeitschrift für Naturforschung C* **57**: 522-529.

ACKNOWLEDGEMENTS

I would like thank all of the people who have contributed their time, advice, and support to make this thesis possible, including:

Marcel Kuypers- for offering me the opportunity to pursue my doctoral research in the Biogeochemistry Group and for your support, criticism, and advice throughout my time here.

Jana Milucka- who first introduced me to Raman spectroscopy, thank you for your guidance and supervision over the years.

Tim Ferdelman- from whom I have learned so much about iron and sulfur chemistry. Your enthusiasm for solving the many technical difficulties of measuring sulfur species has been inspirational. Thank you for all the helpful discussions.

Kirsten Oswald- I can't believe you are still friends with me after I woke you up at 4:00 AM to row around in circles in the fog. Thank you for always being there to share all my worst moments and for correcting this thesis.

Soeren Ahmerkamp- I might have had too much fun in the office with you, but I still managed to learn German and finish a paper. Thank you for fixing all my technological problems, for your friendship, and most of all for believing in me as a scientist.

Patrick Downes- for all the stories, laughs, and superfoods we shared. You made me look forward to coming to the Jungle office every day.

Cameron Callbeck- Thank you for all your small acts of kindness throughout the years, especially for driving me to Lake Cadagno, but not for the limits on bathroom breaks. I am sorry I was such a neat freak in the lab, so thanks for putting up with my nagging.

Julien Dekaezemacker- merci pour ton aide en tant qu'ami et collègue, surtout pour les centaines d'échantillions mesurées au spectrometre de masse. Je sais que tes efforts sont sous-appréciés.

Daniela Tienken- for your patience and positive attitude on every Cadagno expedition, and the countless hours of silver-DISHing.

Katharina Kitzinger- for the all too short time we shared in the Jungle together, and for the constant supply of snacks which I admit I am surreptitiously eating as I write this. And of course, thank you for translating my thesis.

The remainder of my fellow Biogeo PhD students not yet mentioned- Caroline Buckner, Jon Graf, Philipp Hach, Nadine Lehnen, Clara Martinez-Perez and Niels Schoffelen. I enjoyed my time with you, both during and after work and in various conga lines.

Petra Pjevac- who showed me that it's possible to be a scientist and have a life, thank you for all your help in the foreign world of molecular ecology.

The MarMic Sunshine Class- wherever you are in the world now, thank you all for being like family to me.

Tobias Sommer- thank you for all the hard work organizing field campaigns in Lake Cadagno. Those meals were probably the best in my life.

N a m e : ..... Datum .....

Anschrift : .....

E r k l ä r u n g

Hiermit versichere ich, dass ich

1. die Arbeit ohne unerlaubte fremde Hilfe angefertigt habe,

2. keine anderen als die von mir angegebenen Quellen und Hilfsmittel benutzt habe und

3. die den benutzten Werken wörtlich oder inhaltlich entnommenen Stellen als solche kenntlich gemacht habe.

_____, den .....

(Unterschrift)